

Università degli Studi di Napoli “Federico II”



Dottorato in
Fisica Fondamentale ed Applicata

- 19° ciclo -

Development of calibration techniques for active and
passive radon detectors

Candidato: Venoso Gennaro

Tutor:

Prof. Vincenzo Roca

Coordinatore:

Prof. Gennaro Miele

anno accademico 2006 - 2007

Introduction	4
²²²Rn fundamentals and its measurements techniques	6
1.1 Radon properties	6
1.2 Radon measurement	9
1.2.1 Passive radon detectors	9
Nuclear track detectors	9
Electrets Detectors	12
1.2.2 Active radon detectors	13
Ionization chamber	13
Lucas cell	14
Double Filter Methods	15
Electrostatic chamber	16
The use of ²¹⁸Po+ electrostatic collection for radon measurements	17
2.1 The ²¹⁸Po + electrostatic collection	17
2.1.1. Recombination by small airborne negative ions	18
2.1.2 Electron-scavenging by airborne OH radicals	19
2.1.3 Charge transfer with airborne neutral atoms	20
2.2 Neutralization of ²¹⁸Po ions in air	21
2.3 The ²¹⁸Po ions electrical mobility	24
Development of a facility for the study and the calibration of radon detectors	27
3.1 ²²²Rn standard sources at INMRI	27
3.2. Design and development of a radon calibration facility	30
3.2.1 Apparatus description	30
3.2.2 RaMonA reference monitor	33
3.2.3 Alpha spectrum characteristics	36
3.2.3 Monitor characterization: experimental approach	40
Characterization of radon monitor:experimental and numerical approach.	44
4.1 MonteCarlo simulation approach	44
4.1.1. Electric field calculation inside Ramona	44
4.1.2 ²¹⁸ Po ions transit time distribution	46
4.1.3 The estimation of the collection efficiency	50
4.1.4 The recombination and decay handling	53
4.1.5 Optimization of the algorithm	54
4.1.6 Output of the simulation	55
4.2 Comparison between calculated and measured efficiencies	56
4.2.1 Determination of the neutralization rates	56
4.3 Dependence of efficiency on environmental parameters	59
4.3.1 The influence of the barometric pressure	59
4.3.2 Collection efficiency dependence on temperature	61
4.3.2.1 Mobility dependence on temperature	64
4.3.3 Collection efficiency dependence on humidity	66

<i>Continuous Monitoring in a Radon Chamber: passive detector calibration</i> _____	70
5.1 Radon Chamber _____	70
5.2 Radon monitoring inside Radon Chamber _____	72
5.2.1 Ionization measurements _____	72
5.2.2. Electrostatic ion collection _____	76
5.2.3 Passive detector exposure _____	79
Radon Chamber studies: perspectives _____	82
<i>Conclusions</i> _____	83
<i>References</i> _____	84

Introduction

Since many years radon measurements became customary in a wide-spreading applications. Radon is used as geophysical tracer for locating buried faults and geological structures, in exploring for uranium, and for predicting earthquakes. It is also been used as tracer in the study of atmospheric transport processes and there have been many other application in meteorology, water research and medicine. In any case, the great majority of radon measurements are performed to evaluate the health risk due to radon daughters inhalation in indoor air. Indeed, for many years it is well known that radon and its decay products are the largest source of human exposure to environmental radiations (UNSCEAR, 2000). Since many epidemiological studies confirmed a correlation between lung cancer risk and radon exposure, most of the countries have introduced in their own legislation limits on the ^{222}Rn indoor concentration in particular working places.

Moreover, this specific exposition source shows peculiar mechanisms of dose assessment. In fact, the real responsible of the effective dose are the inhaled radon progeny whose behavior is strictly dependent on different air conditions. Thus, the main topics of investigation are the properties of radon progeny, its interaction with aerosol molecules and its deposition mechanism onto surfaces.

In this contest, it is mandatory to carry out high-quality radon measurements which are guaranteed by calibration facilities, suitable for the determination of calibration in a wide range of variability of all parameters involved and in many different experimental situations.

In fact a large number methods have been developed for the radon measure in different situations and matrices and each of them requires a large variety of sampling technique and appropriate instruments. Thus, calibration procedures have to be settle for each measurements method, that account for the particular sampling and detecting processes. To calibrate correctly radon detectors, it is necessary to refer the instruments response to measurement standards, that are defined in term of different parameters, such as radon activity, radon activity concentration and so on. All of these standards have to be traceable to a reference ^{222}Rn standard developed by the national metrology institute (in Italy ENEA-INMRI).

In this thesis it will be described the procedures involved in the development of a facility able to perform radon detector calibration as well as to carry out experiments for study the radon progeny behavior at controlled radon atmospheres.

The radon sources are produced by emanation from a solid radium source, and an electrostatic cell is used as continuous monitor for the radon exposure determination inside a Radon chamber. This monitor, whose response is highly dependent from environmental air conditions, was characterized studying its response under different values of temperature, humidity and pressure using both an

experimental and a numerical approach. The exposure chamber, equipped by environmental sensors and aerosol particles diameters and analyzer, can be used for the calibration of passive radon detector. Various tests have been carried out to study its reliability.

In the first chapter the radon and its decays properties are described, including some important definitions. It follows a description of its measurements methods, related to the most used passive and active detectors. In the second chapter it will be illustrated the methods of the electrostatic collection for the active radon monitoring, that will be the technique used to control radon concentration in our facility with a suitable instrument (Ramona). In this context it will be described the physical factors that influence the $^{218}\text{Po}^+$ collection as well as the experiments that have investigated the mechanism involved in its neutralizations. In this section we focus our attention on the use of the electrostatic collection technique to measure some important radon progeny physical parameters with both a theoretical and an experimental approach. Some remarks will be done about the importance of the characterization of the radon monitor against climatic parameters.

In the following chapter, we will describe in detail the facility built for the Ramona calibration against temperature, humidity and pressure variation. It was also pointed out the importance of the traceability of the radon measurements to national standard and it will be described our metrology chain that refers to ENEA-INMRI primary radium source.

In the fourth chapter we will illustrate the experimental results and the Monte Carlo methods used for the determination of the neutralization rates and to infer the electrostatic collection dependence on environmental parameters inside the radon monitor.

The description of the radon chamber characteristics will be done in the fifth chapter. Here it will be also introduced new methods for the continuous radon monitoring in a small exposure volume. Conclusion and some perspective on the future radon studies with the developed radon facility will be outlined in the last chapter

Chapter 1

²²²Rn fundamentals and its measurements techniques

1.1 Radon properties

Radon is an **outsider** element in nature because it is the only elements that is a gas in a long chain of radioactive decays. All natural radioactive series contain a radioactive radon isotope. This element, with atomic number 86, is colorless, tasteless and, as noble gas, chemically inert. It can also be soluble in some liquids, such as water or natural gas that can transport it over long distances through the soil . The chemical radon property are summarized in table 1.1

Density at 1 atm pressure and 0 °C	9.73 g L ⁻¹
Boiling point at 1 atm pressure	-62 °C
Density of liquid at normal boiling point	4.4 g cm ⁻³
Diffusion coefficient in air	0.1 cm ² s ⁻¹
Diffusion coefficient in water	10 ⁻⁵ cm ² s ⁻¹
Viscosity at 1 atm pressure and 20 °C	0.229 poise
Solubility in water at 1 atm pressure and 20 °C	230 cm ³ kg ⁻¹
Solubility in various liquids at 1 atm pressure and 18 °C	
glycerine	0.2 cm ³ kg ⁻¹
ethyl alcohol	7.4 cm ³ kg ⁻¹
petroleum (liquid paraffin)	9.2 cm ³ kg ⁻¹
toluene	13.2 cm ³ kg ⁻¹
carbon disulfide	23.1 cm ³ kg ⁻¹
olive oil	29.0 cm ³ kg ⁻¹

Table 1.1 :Chemical radon properties

Radon is produced from the decay of radium isotopes contained in rocks and minerals; the more interesting ones are: ²²²Rn present in the “Uranium series” , ²²⁰Rn (“Thorium series”) and ²¹⁹Rn (“Actinium series”), starting from ²³⁸U, ²³²Th and ²³⁵U, respectively. The radon isotopes occurrence in the environment depends on the local abundance of their respective parents nuclides , on the physical characteristic of the source medium and on their decay mean life. ²¹⁹Rn, because of its short half-life (3.96 s) it has a very limited possibility to migrate into free air. Moreover, the low abundance of ²³⁵U parent nuclide by weight in natural uranium (0.711 %), implies that corresponding radon isotope is also extremely rare in the atmosphere.

A variable fraction of airborne radon daughter can remain unattached and it is referred as the *unattached-airborne fraction*. This fraction, after the inhalation by man, can be deposited in the respiratory tract, in which it releases alpha particles. Also if in minor degree, the *airborne attached fraction* can be inhaled and can improve the dose to the airways, because particles with different size deposit preferentially in different areas of the respiratory tract.

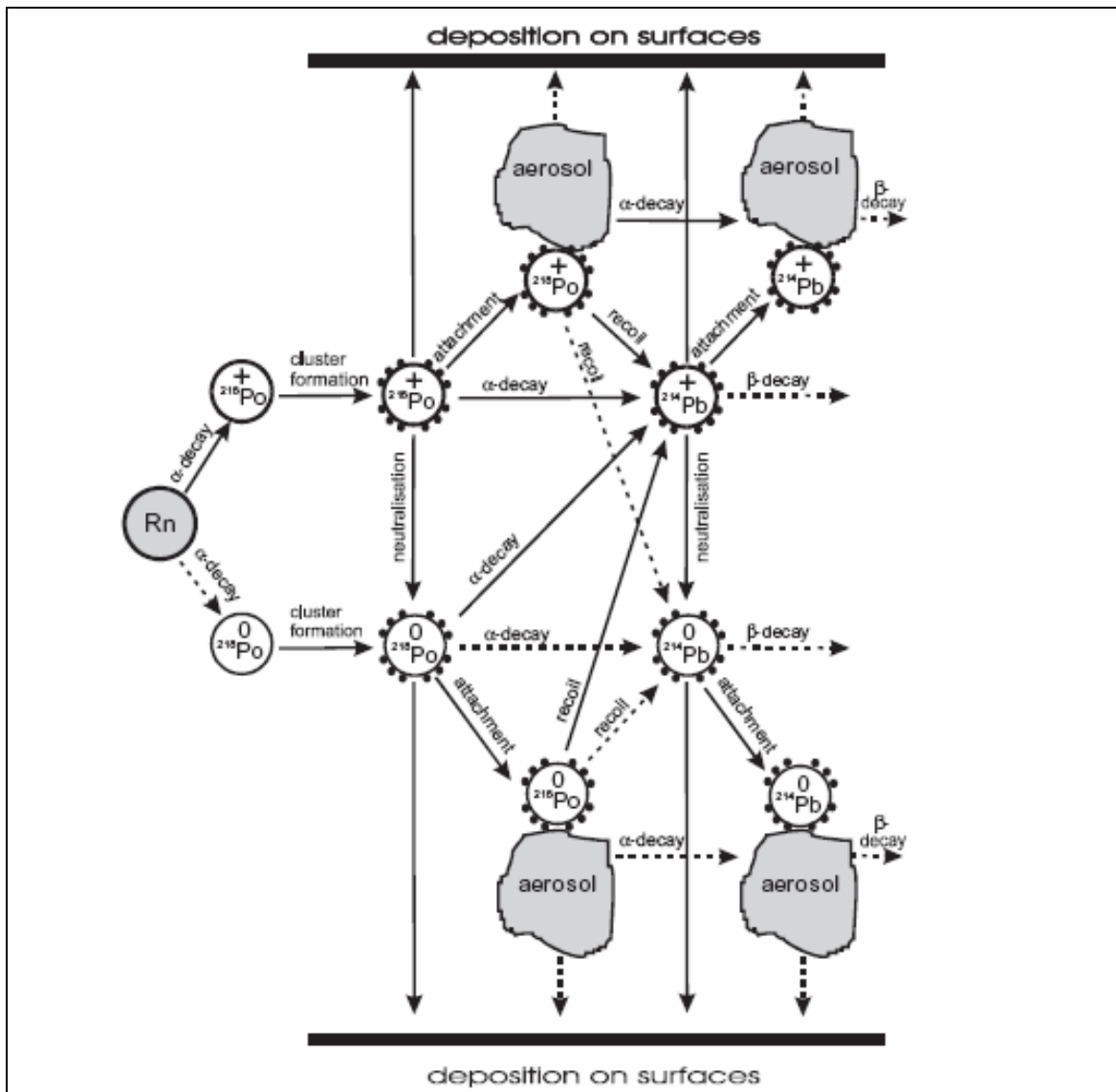


Fig. 1.2 :Radon progeny behavior in air (from Porstendorfer, 2005)

In fact, the alpha emitting radon progeny is entirely responsible for the absorbed dose due to radon exposure. Thus, the most appropriate physical quantity associated with dose estimation is not the radon concentration, but the PAEC, i.e the Potential Alpha Energy Concentration, defined as the total alpha energy emitted during the decay of each radon progeny (present in unit volume o air) up to the end of the radioactive chain. The PEAC is sometimes expressed in term of the so-called radon

equilibrium-equivalent concentration (EEC) that is the radon concentration in equilibrium with its daughters which have the same PAEC as the given non-equilibrium mixture of radon progeny in air. Therefore, the PAEC (or the EEC) are an estimation of the non-equilibrium between radon and its daughter and it is more commonly described in literature by the equilibrium factor:

$$F = \frac{EEC}{C_{Rn}} \quad (1.1)$$

where C_{Rn} is the radon concentration in air.

1.2 Radon measurement

All the techniques to measure radon and its decay products in air are based on the detection of emissions from radioactive decay: most of them are based on alpha and gamma detections. These methods can be grouped in three main categories:

- 1) grab-sample technique, which are based on the sampling of a volume in a short time that can be analyzed successfully;
- 2) Continuous methods, which can provide real-time measurements; this are useful in research application and in testing remedial mitigation action
- 3) Passive or integrating technique, that consists in a time averaged concentration determination over long period (up to one year), used for the estimation of the absorbed dose with appropriate respiratory tract model (ICRP, 65) and suitable also for epidemiological study (Bochicchio, 2005)

Because the radon concentrations are usually very low, the sensibility, accuracy and precision of the measure are essential factors. Being the sources of uncertainty numerous, for every measurements all sources of uncertainty have to be analyzed to reach a good reliability.

1.2.1 Passive radon detectors

Nuclear track detectors

To perform radon measurements any detector sensitive to alpha particles can be used. One of most reliable methods is based on the creation of a latent track due by the passage of an alpha particle in a dielectric material. This situation can be visualized, after chemical treatment, with

optical or electrostatic instruments.. The quantity directly measured is, in this case, the track density ρ per unit exposure time, express in $\text{cm}^{-2} \text{s}^{-1}$). The average radon concentration on the exposure time is calculated from

$$C = k \rho \quad (1.2)$$

where k is the calibration factor, generally expressed in $(\text{kBq h/m}^3)/(\text{tracks/cm}^2)$.

For the radon measurement, the tracks detectors are inserted in a closed diffusion chamber of few square centimeters closed in a polyethylene bag which stops radon progeny, dust particles, water vapor and short living radon isotopes (figure 1.3)

After the radon gas diffuses into the diffusion chamber, radioactive equilibrium is reached between radon and its progeny. But radon decay products can diffuse and deposit on the inner r wall of the chamber, changing the irradiation geometry and the detection efficiency. The first radon descendent, ^{218}Po , has a relatively short half live time (3.05 min) and can partially decay in air and partially be deposited onto the chamber wall. The second alpha emitter, ^{214}Po , that is in radioactive equilibrium with ^{214}Bi whose half life is greater, decays almost entirely after its deposition on the wall. To minimize the deposition, and its sources of uncertainty, a metallic instead of plastic chamber can be used, or a conductive layer can be set on the inner surface with to eliminate the static electricity (Azimi-Garakani, 1988).

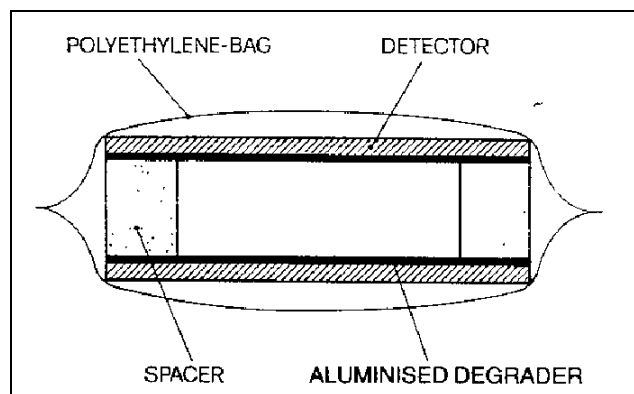


Fig 1.3: Radon gas sampler made of two Lr115 detector enclosed in a polyethylene diffusion bag (from Azimi-Garakani, 1988)

The most used tracks detectors for the radon measurements are the cellulose nitrate (commercial name: LR 115) and particular type of polycarbonate (commercial name: CR 39). These are their some important properties directly affecting measurement reliability:

- 1) The homogeneity and isotropy of the material;
- 2) The transparency, that allows the detection with an optical microscope;
- 3) A reduced fading effect, so that the detector can be analyzed after long time after exposure;

The Lr 115 are thinner than CR39 detectors in such a way that only alpha particles with energy lesser than 4 MeV can leave visible tracks on the film but this limitation can be avoided with a Mylar absorber that reduce the particle energy. For the LR 115 type, another important characteristic is that a chemical treatment reduces the film thickness making the tracks passing through the materials. In this way it is possible to count them with an automatic electrostatic counter (spark counter) than simplifies the scoring respect to the expensive and time consuming technique used for the Cr 39 plastics. In fig 1.4 are visible the tracks generated on the LR 115 detector by the alpha particles emitted by radon and its progeny.

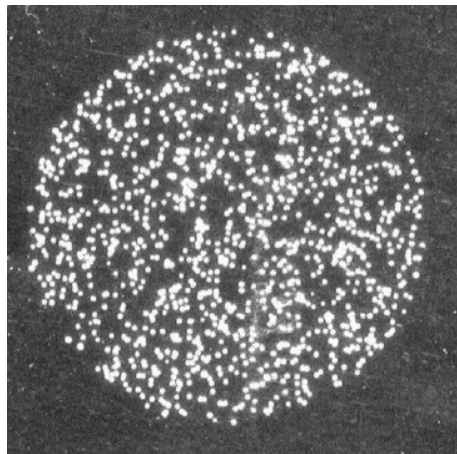


Fig 1.4. Alpha tracks on LR 155 film visible with on optical microscope

This kind of measurements have a complex procedure which highly influence the detectors response and its uncertainties. In particular, the LR 1115 strippable detectors response is dependent on the residual thickness of the micrometric film after the chemical etching and on the background exposure that causes the presences of unavoidable tracks. Because the Lr-115 are the most used technique for long. term radon measurements, in table are indicated all its sources of uncertainties and their relative standard amounts. These values refer to a radon measurements with order of magnitude at least of 100 Bq/m³.

Source of uncertainty	Uncertainty component (1σ) (%)
tracks counting	2%
thickness measure	2%
background	5%
coefficients for thickness corrections	10%
calibration factor	10-15%
Overall uncertainty	20%

Table 1.2. Typical standard uncertainty of radon measurements with the LR 115 technique at annual mean concentration higher than 100 Bq/m^3

Electrets Detectors

An electret detector consists in a charged Teflon disk carrying a stable electric charge mounted at the bottom of a sampling chamber whose air inlet is filtered at the entry. The filter allows only the radon entry, excluding its progeny and dust particles. Radiations coming out from radon and its progeny borns inside the chamber generate ions that can be collected by the electret (Kotrappa et al, 1990). In this case the charged disk is not only a source of the electrostatic field, but also as a radiation sensor (figure 1.5)

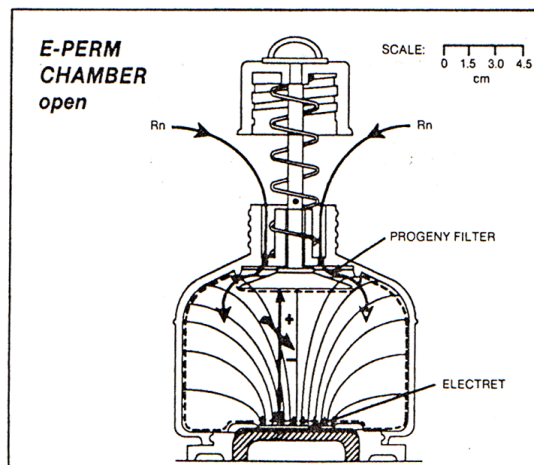


Fig 1.5 Scheme of an E-perm chamber used for short-term radon measurements (from Kotrappa et al, 1990)

The drop in the electret surface voltage is a measure of the time-integrated ionization during the time interval equal to the air sampling time. These measurements can be converted in R_n concentration with an opportune calibration factor.

$$C_{Rn} = \frac{V_i - V_f}{(T) \cdot (CF)} - BG \quad (1.3)$$

Where C_{Rn} is radon concentration in $Bq\ m^{-3}$;

T is the exposure period in days;

$V_i - V_f$ are initial and final voltage on the electret surface;

CF is the calibration factor in unit of $V\ Bq^{-1}\ m^3\ h^{-1}$

BG is the C_{Rn} concentration equivalent of natural γ radiation background. This factors arise from the fact that also γ radiation can ionize sampled air decreasing the electret voltage. This background is minimized with low Z material used for the chamber wall

1.2.2 Active radon detectors

In some cases it is important to perform continuous monitoring of the radon concentration: there are several technique for carrying out this objective. In the following the most used will be briefly described.

Ionization chamber

An ionization chamber is essentially a capacitor, where air between electrodes is the radon carrying medium. The decays occurring in the air provide for the ionization of the air molecules, and the created charged carriers are collected by the electrodes (figure 1.6) The current induced in the electric circuit is a measure of the decay rate inside the chamber

If ionization current is measured immediately after the radon sampling, the current grows with time up to the first 3 hours, that is the time for the radon progeny to reach the equilibrium with radon. If the measure is delayed by this time, the current is proportional to the radon concentration.

The theoretical sensitivity of this instrument is in the order of 10^{-14} Ampere/Bq with typical measuring time of 30 min, but this limit is variable with the volume of the chamber and the measurement time. Typically with 1 liter ionization chamber it is possible to measure $5\ Bq\ m^{-3}$ with an uncertainty of 10%-20%.

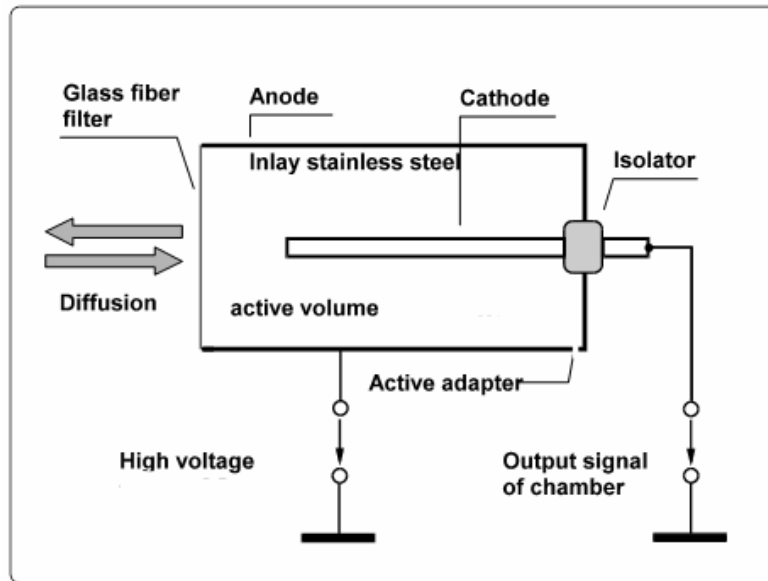


Fig 1.6: Scheme of a ionization chamber suitable for the radon measurements

Lucas cell

A Lucas cell (Lucas, 1957) is a chamber whose internal wall is covered with ZnS(Ag), a scintillation material, with a window transparent to photons. When radon enters in the container chamber, after the alpha particles interaction with ZnS(Ag) in the wall, scintillation photons are generated, which are converted into current pulses with a coupled photomultiplier tube. Finally the pulses can be detected using a scaler.

The theoretical conversion factor is 3 pulses (per Bq), since each alpha particles emitted by radon is followed by two others from the decay of ^{218}Po and ^{214}Po , but the real conversion factor is in the range 2-2.5 pulses per Bq. One of the shortcoming of this method is that each cell has its own calibration factors. Moreover, there is an uncertainty factor arising from the decay of the long-living ^{210}Po present in the radon chain, which is also an alpha emitter and which stay long time on the wall. For this reason, calibration and internal background measurements have to be done every time due to permanent contamination.

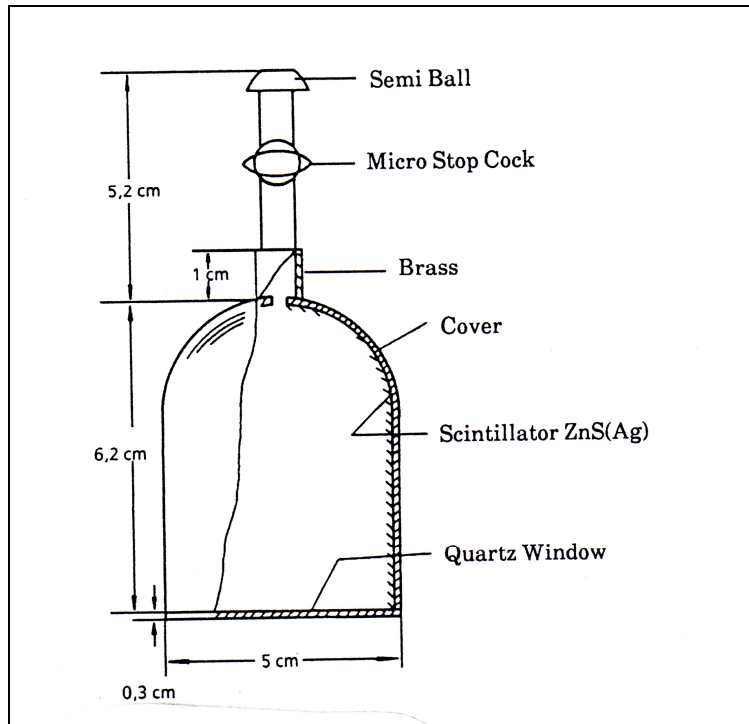


Figure 1.7: Scheme of a scintillation Lucas Cell (Lucas, 1957)

Double Filter Methods

With this technique the air containing radon is pumped through an inlet filter, which stops entry of radon progeny and aerosols in the measurement volume and a second filter is set at air exit. Depending on the flow rate and the volume size, a fraction of radon decay inside the sampling chamber and its decay products can be collected on the second filter, where a detector can allow to count alpha and beta particles emitted from filter surface.

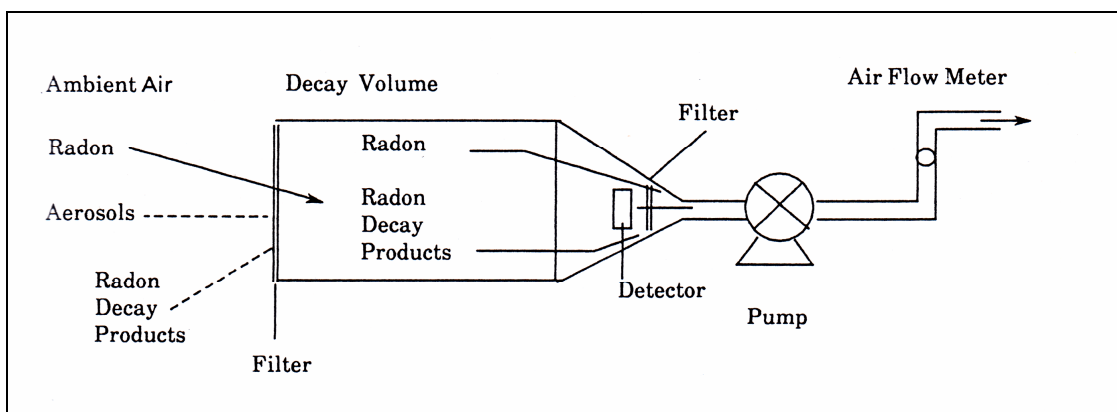


Figure 1.8: Design of a double filter instrument

The efficiency of this method is low since there are plate-out losses, especially of ^{218}Po , inside the chamber. In the just described configuration, but with large volume, the detection limits can be less than 1 Bq.m^{-3}

To avoid or minimize the plate-out losses, an intense electric field can be applied to collect the ^{218}Po ions on a filter, or directly on a surface on a surface barrier silicon detector. With this configuration, a detection limit of $0,2 \text{ Bq}\cdot\text{m}^{-3}$ can be achieved.

Electrostatic chamber

The most suited class of instrument used for continuous radon monitoring is based on the electrostatic collection of ^{218}Po ions. The radon may enter in a collection chamber (by diffusion or pumping) where is placed a detector in the center of one of its wall. The detectors are generally a solid state alpha detector (figure 1.9). After applying an electric field between the chamber wall and the detectors, the positive charged ^{218}Po can be collected upon the detectors where the emitted alpha particle can be measured with a good energy resolution.

The time resolution of this methods is of the order of 10 minutes because it depends only on the half-life of ^{218}Po (about 3 min). Moreover, the electrostatic chamber can detect also the ^{220}Rn and its progeny, when they are present. Since it has been extensively used in this work, many other details about this technique will be done in the next chapters.

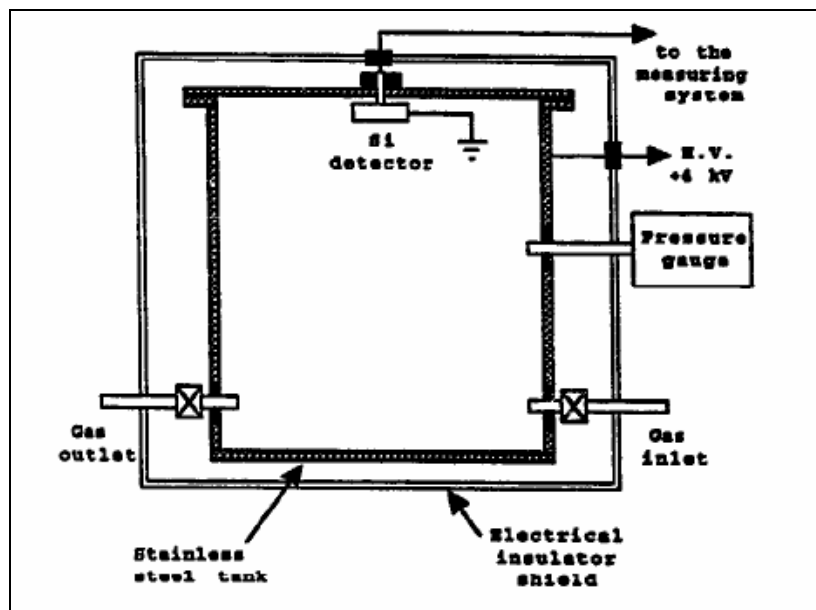


Fig 1.9: Scheme of an electrostatic cell for radon measurements (from De Felice et al, 1996)

Chapter 2

The use of $^{218}\text{Po}^+$ electrostatic collection for radon measurements

The chemical and physical properties of the radon daughters, and in particular of the ^{218}Po nuclide, immediately following its formation from the radon decay, is very important to determine its potential health effect. Moreover, on the electrostatic collection of its ions a great number of continuous radon monitors, such as our electrostatic cell, are based. To upgrade the performances of such kind of detectors, it is very interesting to understand the physical mechanisms involved in the ^{218}Po ions formation and to study the factors that influence their neutralization, a process that can affect the detector responses.

2.1 The $^{218}\text{Po}^+$ electrostatic collection

At birth, ^{218}Po is known to be positively charged from the stripping of orbital electrons by the departing alpha particles in the recoil motion. As the ion slows down toward thermal velocity at the end of the recoil path, it can capture electrons such that at the end of its path, about 88% of the polonium atoms are single charged % (Porstendrofer 79, Dua 83, Chu and Hopke 85) and the remaining are neutral. As it was briefly outlined in the previous chapter, this feature allows its detection with the technique of the electrostatic collection, consisting of the transport of such positive ions on a particle detector, when a voltage difference is set between the detector and the walls of a chamber where radon diffuses in. In this way, since the ^{218}Po is an alpha-emitter nucleus, the high resolution alpha-particle spectroscopy can be performed. It is important to underline that only a fraction of the produced $^{218}\text{Po}^+$ in air is collected on the detector surface. Some alternative processes can occur:

- 1) On flight decay of the $^{218}\text{Po}^+$ ions;
- 2) Recombination with negative ions ;
- 3) Neutralization after interaction with the aerosol particles (attachment);
- 4) Deposition on the walls internal surface (plate-out);

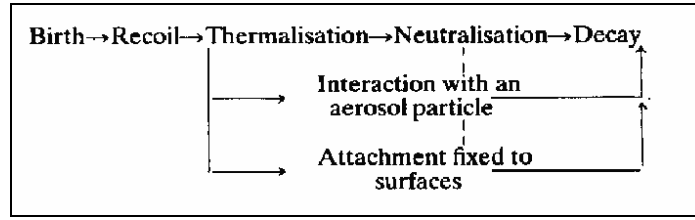


Fig 2.1 Scheme of the ^{218}Po life history

The deposition and the attachment processes are dependent on the electrical charge of ^{218}Po atoms. In fact, it has influence on the mobility of ^{218}Po , characterized by the diffusion coefficient, which controls the formation of the radioactive aerosol and the plateau process on surfaces. From several papers (Goldstein at al 1985, Chu at al, 1988) it is well known that the neutralization mechanism can be described with the following processes, which will be outlined hereafter:

- 1) recombination of the charged ^{218}Po with negative airborne ions;
- 2) charge transfer with neutral molecules present in traces;
- 3) electron scavenging by means of the OH radical formed by the water vapour radiolysis

2.1.1. Recombination by small airborne negative ions

The radon and its daughter emit ionizing radiations producing positive and negative ions in air (including electrons) which can recombine itself, or can neutralize the $^{218}\text{Po}^+$ clusters.

The negative ions production can be expressed by the eq (Busigin, 81):

$$\frac{\partial n_-}{\partial t} = \xi \cdot n_0 - \alpha \cdot n_+ \cdot n_- \quad (2.1)$$

where:

ξ is the ion pair production rate as a result of α -decay of ^{222}Rn ;

n_0 is the ^{222}Rn concentration in units of cm^{-3} ;

α is the ion pair recombination coefficient: $\alpha = 1.4 \times 10^{-6} \text{ cm}^3 \text{ s}^{-1}$ (Chu and Hopke (1988));

n_+ and n_- are the concentration in air of positive and small negative ions respectively

The stationary solution of this equation can be done assuming the same airborne concentration for both positive and small negative ions, $n^+ = n^-$,

$$n_+ = n_- = \sqrt{\frac{\xi n_0}{\alpha}} \quad (2.2)$$

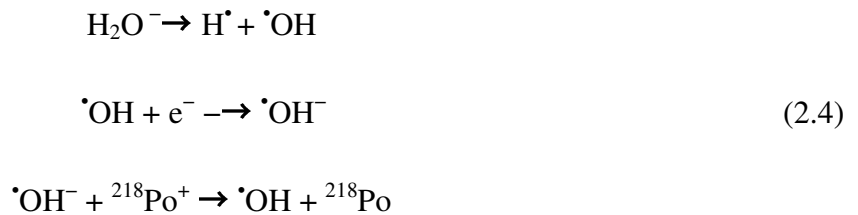
The neutralization rate, K , depends linearly on the airborne negative ion concentration and therefore:

$$K = a \sqrt{\frac{\xi n_0}{\alpha}} \quad (2.3)$$

where the a constant has been estimated to be of the order of 10^{-5} (Busigin et al., 1981; Chu and Hopke, 1988; Shi and Hopke, 1991) suggesting that the neutralization mechanism with airborne small negative ions may be significant only at ^{222}Rn concentration of the order of kBq m^{-3} .

2.1.2 Electron-scavenging by airborne OH radicals

The radiolysis of water vapour, which occurs by means of the radon progeny radiations, produces the hydroxyl radical (OH^\bullet) that are excellent electron acceptors (molecular scavenger) for their high electron affinity (1.83 eV). The scavenging of the electrons by the OH-radicals is responsible for an increased local concentration of negative small ions and enhances recombination rate due to the these ions. The mechanism of electron scavenging by means of water vapour molecules is explained by the following reactions (Chu and Hopke, 1988):



The OH radical concentration can be evaluated from the equation

$$\frac{\partial [\bullet\text{OH}]}{\partial t} = Q[\text{H}_2\text{O}] - k_R [\text{H}] [\bullet\text{OH}] \quad (2.5)$$

where Q is the dissociation constant of the water vapour molecules and k_R is the recombination constant of the radicals $H\bullet$ and $\bullet OH$ with airborne concentrations $[H\bullet]$ and $[\bullet OH]$, respectively. Assuming the same concentration level for the radicals $H\bullet$ and $\bullet OH$, i.e., $[H\bullet] = [\bullet OH]$, the steady-state solution of equation gives:

$$[\bullet OH] = \sqrt{\frac{Q[H_2O]}{k_R}} \quad (2.6)$$

which suggests that the $\bullet OH$ radical concentration in air and, hence, the neutralization rate should be proportional to the square root of the water vapour concentration.

2.1.3 Charge transfer with airborne neutral atoms

The charge transfer mechanism for the neutralization consists in the electrons removal operated directly by colliding neutral molecules. However, since the first ionization potential of polonium (8.43 eV) is lower than that of various airborne molecules, it seems that this mechanism is unlikely or cannot occur (fig 2.2.). Instead, being the $^{218}\text{Po}^+$ unstable, it may react chemically with the air oxygen to form polonium dioxide (PoO_2^+) whose ionization potential is about 10 eV (Busigin et al. (1981)).

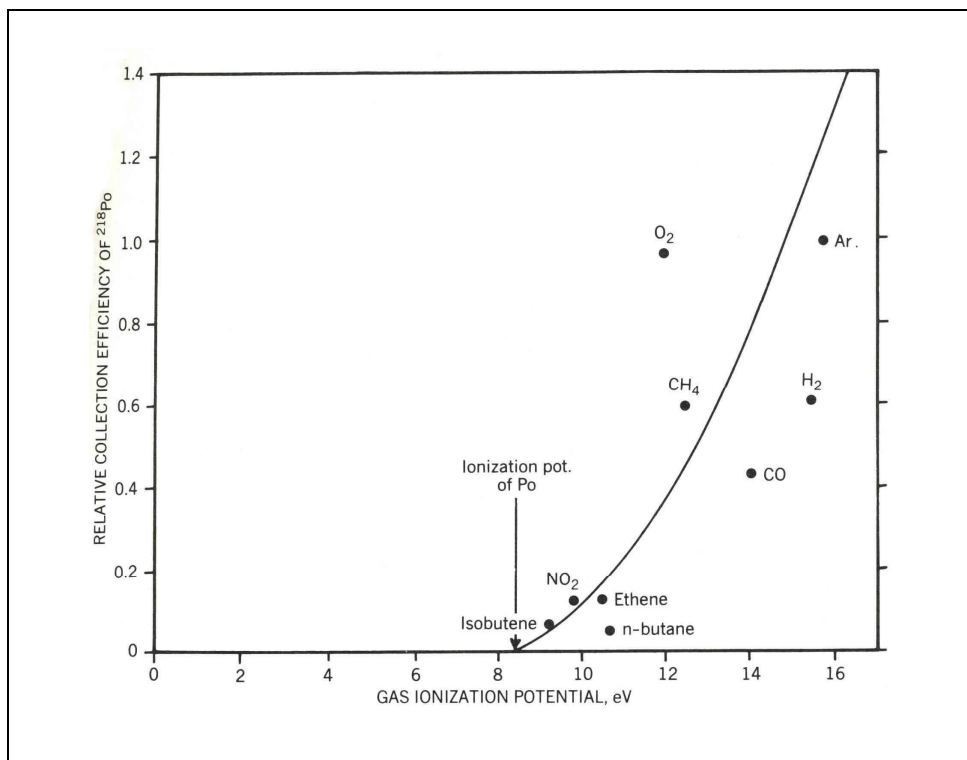


Fig 2.2 Electrostatic collection versus gas ionization potential. The charge transfer mechanism can occur only if the polonium react with oxygen to form PoO_2 , a compound that has an higher ionization potential (Busigin et al, 1981)

In such circumstances, the polonium dioxide, having an higher ionization potential, can be neutralized by removing electrons from water vapour or from trace gases present in air that have lower ionization potential. The charge transfer mechanism is highly dependent on the air ionization potential, on content of gas traces and/or organic vapours and on the concentration of the airborne ^{222}Rn . (Chu and Hopke, 1988). It has to be noted that neutralization rate by means of the charge transfer is faster since the electrons can be transferred directly by a single collision with a donor molecule. The time needed for the polonium neutralisation in air is of the order of milliseconds (Phillips et al., 1988).

2.2 Neutralization of ^{218}Po ions in air

After the description of the three basic mechanisms of the $^{218}\text{Po}^+$ neutralization process, it is important to compare the measured neutralization rate with the average time preceeding the electrostatic collection of Po ions .

Experimental data on the neutralization rate (Dankelmann 2001), are referred to normal environmental air conditions, and they allow to calculate the contribute of each of the three mechanisms described in the previous section. Therefore, the neutralization rate v can be defined as:

$$v = v_{\text{CT}} + v_{\text{IR}} + v_{\text{OH}} \quad (2.7)$$

where v_{CT} is the charged transfer mechanism recombination rate; v_{IR} is the small ion recombination rate; v_{OH} is the neutralization rate due to electron scavenging by OH radicals. As illustrated in fig 2.3, the neutralization rates is linearly dependent on square root of mean radon concentration, that is responsible, with its daughters, for the ions production in air. The moisture content influences the neutralization rate especially in the range of RH between 0 and 30%. For higher values, the influence of the humidity is so small to be considered constant. This humidity dependence can be ascribed only to the electron scavenging mechanism (fig 2.3). In fact, the authors estimated that the neutralization rate by charge transfer v_{CT} has a value of $0,4 \cdot 10^{-3}$ s and it is constant for all the experimental conditions, while for the two other mechanisms, the calculated neutralization rates are expressed by:

$$v_{\text{IR}} \propto 10^{-3} \sqrt{C_{\text{Rn}}} \quad (2.8)$$

$$v_{\text{OH}} \propto f(\text{RH}) \sqrt{C_{\text{Rn}}}$$

where C_{Rn} is the radon concentration expressed in Bq/m^3 and $f(RH)$ is a function of the relative humidity that can be shown in fig 2.2

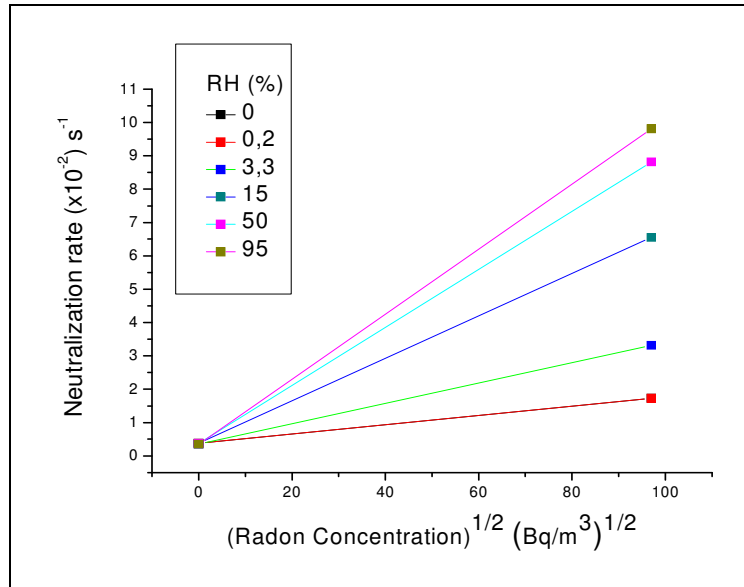


Fig 2.2 Neutralization rate versus radon concentration (adapted from Dankelmann et al , 2001)

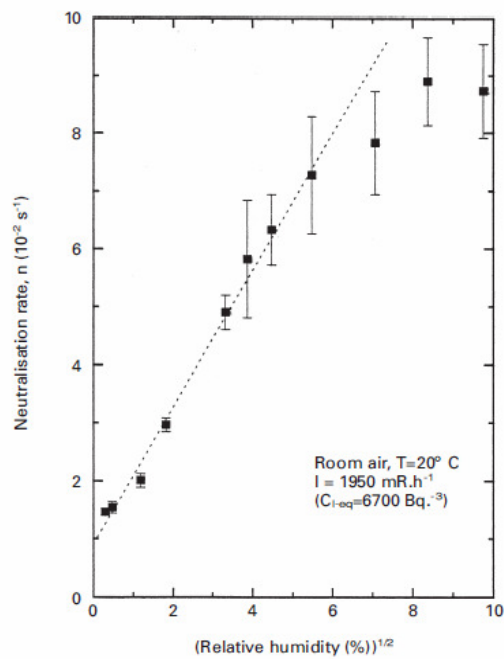


Fig 2.3 The neutralization rate by small ion recombination is a function of the square root of the relative humidity (from Dankelmann, 2001)

In a previous work, Chu and Hopke (1988) found that the neutralization rate (ν) depends on humidity with the following expression:

$$\begin{aligned} \nu &= 1.14\sqrt{[H_2O]} \text{ s for } [H_2O] \leq 1800 \text{ ppm} \\ \nu &= 47,8 \text{ s for } [H_2O] > 1800 \text{ ppm} \end{aligned} \quad (2.9)$$

where the $[H_2O]$ is the water vapour concentration expressed in ppm. At 25°C temperature and 1000 mbar pressure, an absolute humidity of 1800 ppm correspond to a 7% relative humidity. For both the cited works, the functional dependence of the neutralization from the humidity is the same but the characteristic values of the neutralization rates differ by three order of magnitude:

$$\begin{aligned} \nu &\approx 0,05 \text{ s}^{-1} \quad (\text{Dankelmann et al, 2001}) \\ \nu &\approx 50 \text{ s}^{-1} \quad (\text{Chu and Hopke, 1988}) \end{aligned}$$

at 50% RH. This apparent discrepancy can be explained by the different radon concentration used in two different studies. Dankelmann (2001) at al worked with radon concentration less than 10^4 Bq/m³, while Hopke (1988) carried out measurements with radon values higher than at least 2 order of magnitude, where the effect of the small ions recombination increase the neutralization rates. Moreover, these estimations could be affected by the high uncertainty associated to the ^{218}Po ion mobility, a parameter that must to be known for the calculation of the neutralization rate. In any case, it is well established also by some other works that the neutralization rate constant increases with the increasing relative humidity at a given radon concentration in air (Howard at al, 1990) and in argon gas (Leung at al, 1987).

Thus, it is clear that the effect of the humidity on the $^{218}\text{Po}^+$ neutralization is reflected on the response monitor based on the electrostatic collection (fig 2.4)

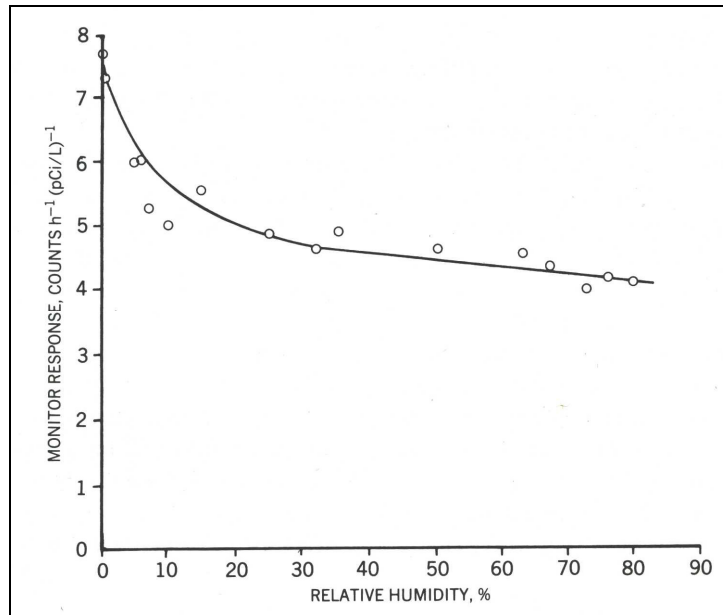


Fig. 2.4 Response of an electrostatic collection monitor at varying relative humidity (George, Breslin, 1977)

For these reasons, for the measurement of the radon concentration with this technique, it is mandatory to evaluate the response dependence on radon concentration and on humidity, both influencing in different way the ^{218}Po ion neutralization rates. To avoid the humidity dependence, it is possible to remove moisture from the sampling air before the entry in the active monitor volume, but these procedure requires a complex modification of the instrument design to attain sufficient humidity control.

In the next chapters we will study the humidity dependence of our radon monitor, to corrected its response at normal air conditions.

2.3 The ^{218}Po ions electrical mobility

In literature does not exist a single value for the mobility of the ionised radon daughters. As illustrated in fig 2.3, the experimental distribution of mobility is bimodal (Philips at al, 1988): the first range of the spectrum probably accounts for the unattached ion fraction, and the second for the attached or clustered one.

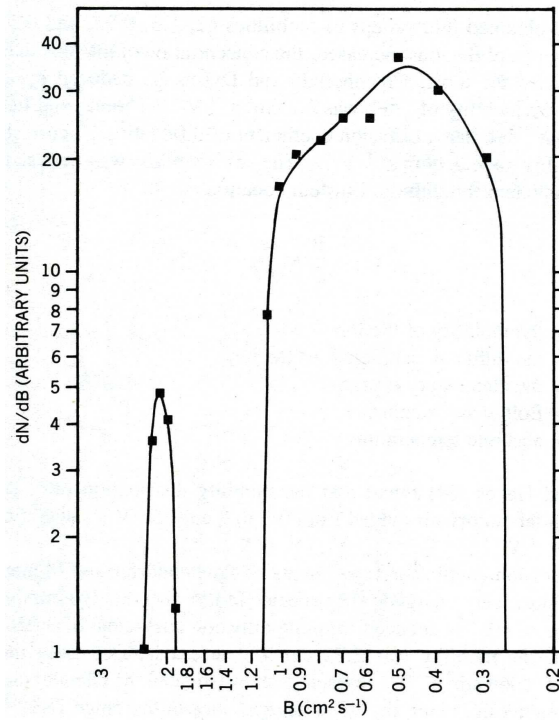


Fig 2.3 The mobility distribution ions in unfiltered air enriched with radon (form Phillips at al, 1988)

In fact, as the age of the ions increases, the concentration of the ions in the highest group decreases (Phillips at al, 1988). Inside electrostatic chamber, only the unattached fraction is collected, because the typical attachment rate are much lower than the neutralization ones. For the unattached progeny the ion mobility measurements probably lie in the range $1,9-2,3 \text{ cm}^2 \text{ s}^{-1} \text{ V}^{-1}$.

The ion mobility μ can be calculated from diffusion coefficient with the Einstein equation:

$$\mu = \frac{eD}{kT}$$

where e is the elementary charge;

D is diffusion coefficient of the ion;

k is the Boltzmann's constant;

T is the absolute temperature.

Moreover, a part of ^{218}Po ions can react with oxygen in the air to form the $^{218}\text{PoO}_2^+$ characterised by a different mobility ($\mu \approx 1,9 \text{ cm}^2 \text{ s}^{-1} \text{ V}^{-1}$) (Chu, 1988; Hopke, 1989; Shi, 1991). These estimated values of mobility can be used for the estimation of the neutralization rates, but care must be taken when the gas temperature changes during the measure. In general, ions mobility spectrum is dependent from the gas temperature (Chanin, 1957) and it has to be investigate about the extent of

this variation for the $^{218}\text{Po}^+$ ions for temperatures in the range (15°-30°C), which can be found in a typical laboratory . In chapter 4, we will calculate this variation using a numerical approach applied to a set of radon concentrations measurement performed with our electrostatic monitor at different temperatures.

Chapter 3

Development of a facility for the study and the calibration of radon detectors

In this chapter it will be described the apparatus which we developed in our laboratory with the purpose to calibrate various kinds of radon detectors at variable air conditions. In this context, it was developed a metrology chain referred to the national standard of radon, which will be reported in details. The experimental apparatus makes us able to characterize our electrostatic cell as reference monitor and allows us to use it for the calibration of passive detectors. It has to remark that the facility will be also useful also for studying the behavior of radon daughter in air.

3.1 ^{222}Rn standard sources at INMRI

The production of radon standard sources is essential for the calibration of radon detectors. Every National Metrology Institute possess a reference ^{222}Rn standard: most of them are based on indirect comparative measurements related to a ^{226}Ra standard, even if in the last years some laboratories developed complex procedures for the absolute methods based on the detection of the alpha particles directly emitted by the ^{222}Rn nuclides (Picolo, 1996, Spring, 2006)

At INRMI-ENEA, the Italian Metrology Institute, the ^{222}Rn standard sources are calibrated against radium standard solution through a Radon Measurements system Facility. The apparatus (figure 3.1), described in De Felice, 1996, is capable to transfer radon gas samples into an electrostatic cell, that is a reference monitoring instruments which detects the alpha particles emitted by the radon progeny after that the equilibrium is reached.

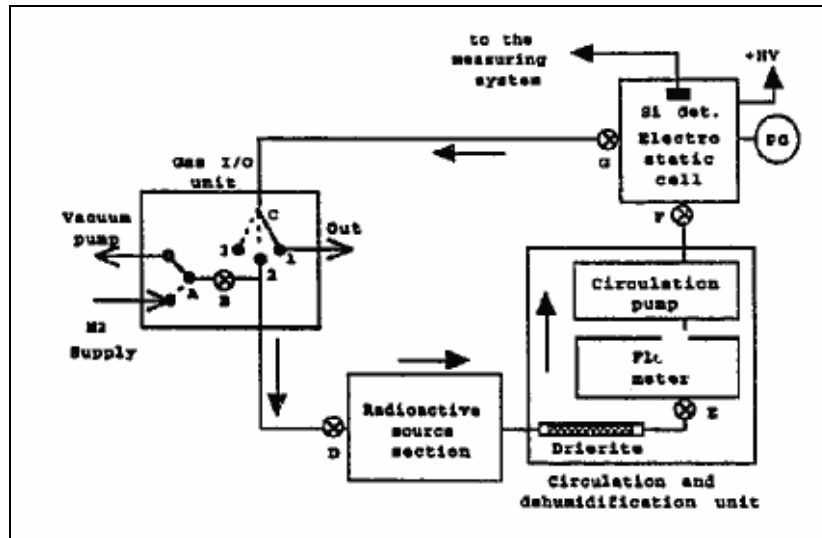


Fig 3.1 Scheme of the ENEA-INMRI ^{222}Rn Reference Measurement System (from De Felice 1996)

From the ^{218}Po count rate it is possible to determine the radon activity in the circuit and to relate it to the radium standard solution. The comparison with radium standard is performed in two steps:

- 1) Calibration of the RMS (Reference Measurements System). In the radioactive section of the facility (fig 3.2), the B2 radon bulb is left empty, while the B3 bubbler is filled with standard radium solution with valve closed until the equilibrium ^{222}Rn and its direct daughter is reached. After that the radon recirculation in the circuit produces its homogeneous distribution, the reference electrostatic cell response is a measure of the radon activity that is the same of the used radium standard. Thus it is possible to determine the efficiency of the facility expressed by :

$$\varepsilon_{\alpha} = \frac{R_{\alpha}}{A_{Ra}} \quad (3.1)$$

where R_{α} is the electrostatic cell response expressed in count per second of the ^{218}Po alpha detected, and A_{Ra} is the reference activity of the radium sources.

- 2) Calibration of the ^{222}Rn gas sample. After the calibration of the system, the glass bulb B2 can be filled with ^{222}Rn , while the B3 bubbler is filled with the same solution of the first step, but without radium content (figure 3.2). The following procedure is the same described before, but now the monitor response, that it is calibrated in first step, is a measurement of the ^{222}Rn gas sample.

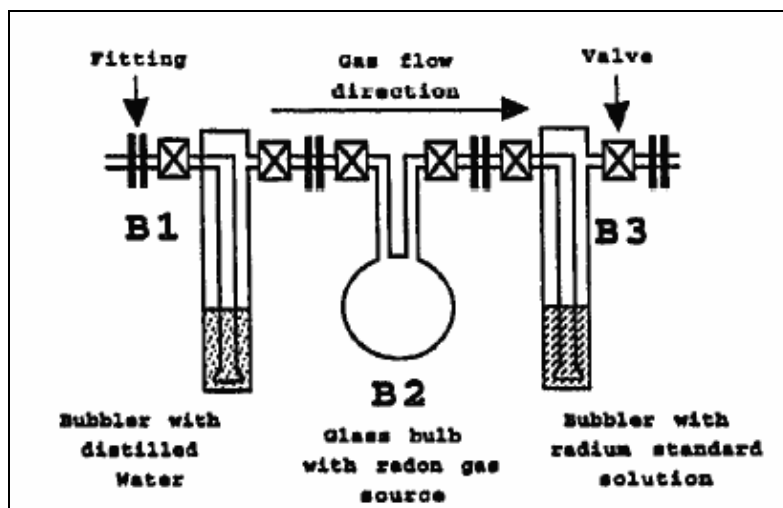


Fig 3.2 Radioactive source section of the ENEA facility (from De Felice, 1996)

The ENEA approach has the advantage to bypass any volume determination since the monitor response refers to the same volume for the calibration procedures described above. Thus, if the circuit volume is kept constant it is possible to obtain reproducible experimental conditions just controlling the temperature and the radium liquid solution amount. For this reason the standard uncertainty of the efficiency of the Reference Measurement System has a low value 1.3 % (1 σ).

The only shortcoming of the procedure is that the ^{222}Rn sample cannot be used after its calibration in the circuit facility, so this is a destructive method. In order to perform non destructive calibrations of ^{222}Rn sources, a Transfer System was also developed, based on the measurement of radon sources in glass ampoule, prepared connecting it to a commercial radium source, by a well-type NaI(Tl) γ detector, before their destructive calibration by the RMS system. The counting efficiency of the detector is

$$\varepsilon_{\gamma} = \frac{R_{\gamma}}{R_{\alpha}} \varepsilon_{\alpha} \quad (3.2)$$

where R_{γ} is the NaI(Tl) response expressed in count per second in a selected γ window of the multichannels and R_{α} is the electrostatic monitor response for the same radon source.

The Transfer system shows also a good reproducibility and the total uncertainty of the efficiency value ε_{γ} is less than 1,2%.

3.2. Design and development of a radon calibration facility

In our laboratory, a calibration facility was developed keeping in mind the procedures of the National Metrological Institute. The apparatus is able to perform calibration of active and passive monitoring using a radon source standard in glass bulb with a well defined geometry. A local radon transfer system based on a HPGe detector was set up and tested, while the reference monitor used is an electrostatic cell (RaMonA), whose collection chamber and its relative electronics was designed and built in our laboratory.

The facility has been used also to study the dependence of the efficiency of the electrostatic cell on temperature, pressure and humidity.

3.2.1 Apparatus description

The scheme of the facility is shown in figure 3.3. It can be divided in two main section. The first is used for the characterization of the monitor RaMonA, and it will be described here in details; the second one is used for the generation of reference atmosphere inside an exposure chamber (Radon Chamber) where it is possible to calibrate passive detectors of radon and its progeny.

The apparatus drawn in section 2 will be described in chapter 5.

Below, a brief description of the components of the first section follows:

1) **Thermo regulator.** It allows to vary the temperature inside the electrostatic chamber (Ramona).

It consists of:

- a 50 x 20 box where the monitor is placed, thermally isolated respect to external environment;

- two Peltier cells allowing to regulate the temperature;

An electronic programmable device controls and set temperature value with a 0.2 °C tolerance in 0-60 °C temperature range.

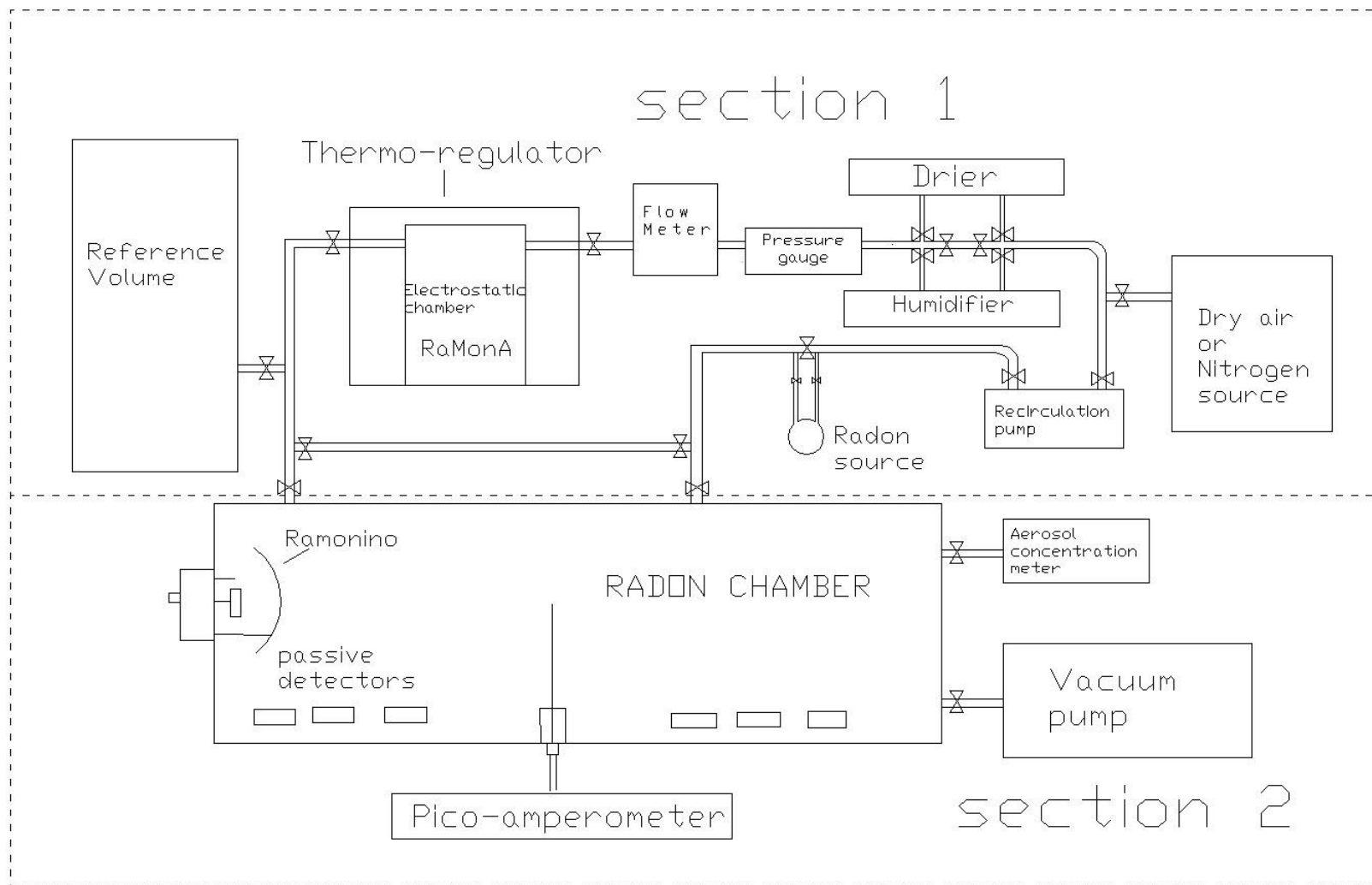


Fig 3.3. Scheme of radon calibration facility designed and tested in our laboratory

2) **humidifier and dryer.** It allows to change the moisture content in the air sampled inside Ramona in a controlled way. Both devices consist on a Nafion tube, semi-permeable for the water molecules, housed within a flexible plastic tube shell (PermaPure MD/MH-110-24F-4). The possibility of the water vapor molecule permeation through the Nafion is due to the difference of the water partial pressure between the internal and external shell of the tube.

In the drying process, the sample gas can flow in the Nafion tube while water vapor is absorbed by the walls of the membrane and is removed with a dry purged gas which flows countercurrent to the sample and whose role is to carry away the moisture permeating the membrane. The dry gas flux is provided by an external gas cylinder filled with dry air. The humidification process has the same physical principle. Instead of a dry gas, in the external Nafion membrane flows hot water and moisture content can be absorbed within the internal tube where the sampling gas pass. Unlike the “classical” Drierite salts, that operate as desiccant trap, these Nafion devices are very useful because they allows to vary the moisture content in active way , that is within shorter times, and with higher precision.

3) An **electronic flux-meter** with relative controller (MKS Mass Flow Controller 1179A) able to vary the air flux up to 2 liter/min with uncertainty less than 0,5%. It was placed at the entry of the chamber to set the inlet air flow rate

4) A **Baratron pressure gauge** (MKS Baratron 626A), able to measure the pressure in the circuit with great precision (uncertainty 0,1% in the 10-1000 mbar) and independently on the gas which circulate in it.

5) **Membrane pump** (KNF model N 726 FTE) able to carry the air gas with a maximum flow rate of 15 l/min; since it has PTFE (Teflon) garnitures, it guaranties radon sealing.

6) **Reference volume.** It is a stainless steel reference volume, known with great precision (uncertainty <0,5%) whose purpose is to measure the effective volume of the circuit, that cannot be easily geometrically determinate since the presence of many valves and other not regular elements.

7) A **glass bulb** fitting channel, where it is possible to connect the glass bulb containing radon sources. The radon loading process and the activity measurements of the reference radon will be described in the next paragraph.

All these components are connected with Teflon tubes with inner diameter of 6 mm and appropriate metallic radon and air leak-free connector. All component are tightly sealed respect to external air.

3.2.2 RaMonA reference monitor

RaMonA, that is the acronym of Radon monitoring and acquisition, is the radon continuous detector that we use as reference monitor of our calibration facility..

The geometry of the collection chamber is designed to include not only a solid state silicon detector, but also a set of environmental sensors and an integrated module for their signal conditioning (see figure). In our laboratory was also realized a control unit that serve the collection chamber and is ultimately able to generate the output alpha spectrum, because it is formed by a compact electronic chain suitable for normal spectroscopic measurements.

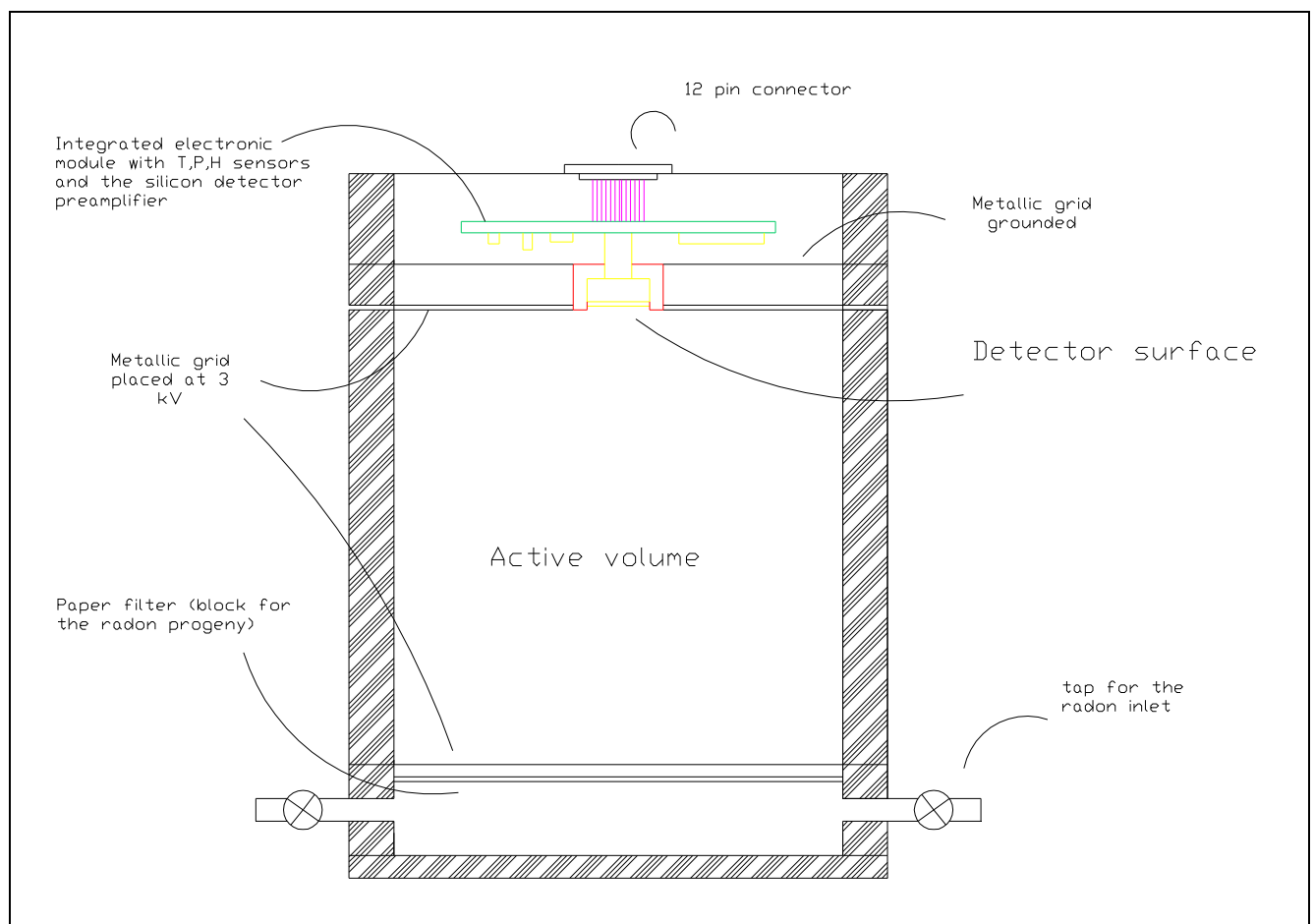


Fig 3.4. Scheme of the RaMona electrostatic cell monitor

The principles of measurements of the electrostatic cell radon detectors were illustrated in the first chapter, so here only the new characteristic of Ramona system will be described

As the prototype chamber that we used for the first continuous radon measurements and extensively described in (Pugliese et al., 2000), the new chamber consist in a aluminum 10x10 cm cylinder , whose walls have two taps for the inlet and outlet of radon containing air (fig 3.4). The new model has its tap gasket in teflon, a material where radon do not diffuse in. Inside the chamber, at the entry of the radon in the active sampling volume, a paper filter is placed, whose function is to block the entry of the radon daughters, allowing the entry of only the radon gas. In this way in the active volume only the decay products that came from radon that is present the sampling volume are detected. For safety reasons, the whole chamber is inserted in a PVC holder which protect the operator on accidental contacts wit the chamber when high voltage in on. As illustrated in figure 3.2 upon one of cylinder basis, in an insulated holder, is positioned a silicon alpha detectors, mounted at the center of an electronic integrated module, also staying in the chamber. By knowing climatic parameters is crucial because the instrument response depend on temperature, pressure and humidity (Roca at al, 2004). On the internal module the preamplifier, three environmental sensors (temperature, pressure, humidity) and the electronics for signal conditioning are mounted; the shielding from the high voltage inside the chamber is achieved by two metallic grids that form a Faraday cup.

A typical spectrum, produced with a mixed radon and thoron source put in the chamber, is shown in **Figure 3.5**

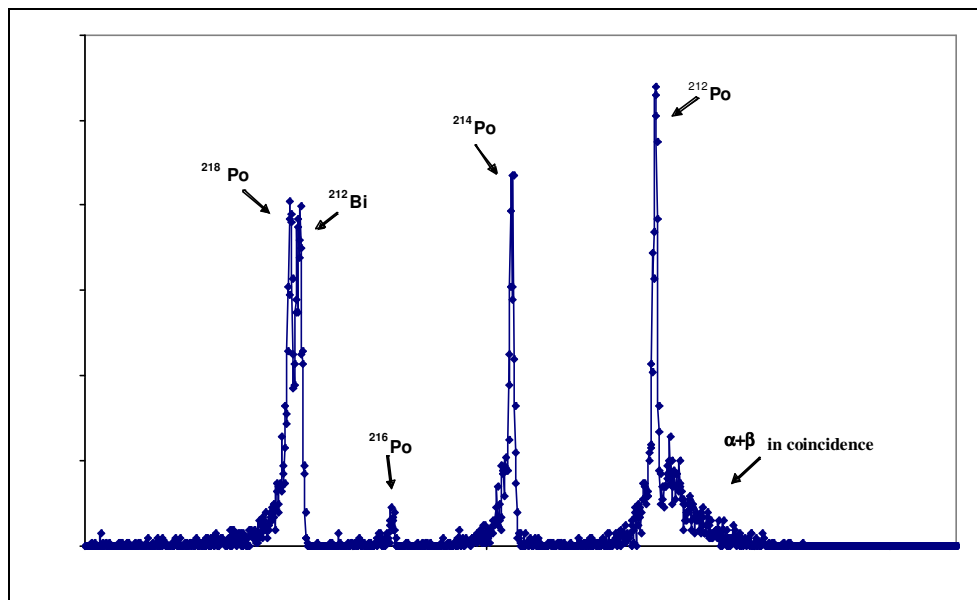


Fig. 3.5 Spectrum of the alpha emitters daughters of ^{222}Rn and ^{220}Rn

As no air layer reduces alpha energy, emitted just on the detector surface, the resolution is generally better than 1%, so the good separation of alpha particles of both isotopes is possible.

The control unit of RaMonA contain three subsections:

- 1) the linear one, that has the aim to form and discriminate the silicon detector signals;
- 2) the control section, that has two logic programmable device (PLDs): one for the stretcher and the trigger control, the second for the multiplexer and dead time control;
- 3) the conversion section, that perform the digital conversion of all the analogical signal from the sensors and from the detector;
- 4) communication section, controlled by a microprocessor Rabbit core 2200 that control the ADC conversion and the external communication through an Ethernet interface using the TPC/IP protocol. This property allows also to control the system by remote, once assigned an IP address to it.

A dedicated software controls the spectrum acquisition and the mode of sending data from its internal buffer.

Via software it is possible:

- a) to start and stop the acquisition;
- b) to set the HV voltage applied to the collection chamber;
- c) to set the region of interest
- d) to initialize and program acquisition cycles;
- e) to visualize variation of environmental parameters versus time
- f) to calibrate energy spectrum and to save to acquired data in text format for off-line analysis.

In the following table the main characteristics of Ramona are showed:

Gross gain amplifier	1x 10x 100x
Fine gain amplifier	with trimmer
Signal formation constant	3 μ s
Total conversion time	20 μ s
Input signal polarity	+/-
HV voltage	from 0 to 4 kV (remotely controlled)
Ethernet interface	10 Mbps
Alimentation	12 V, 6Ah (with buffer rechargeable battery)
Pole zero correction	
Discrimination on the input signal	
Input for other detector (preamplifier output)	

Fig. 3.6 Specification of the Ramona control unit

It has to be evidenced that this control unit can be used as part of a electronic chain for spectroscopy. It gives the opportunity to connect an output from a second detector (for example a NaI(Tl) or a HPGe γ detector) and it is suitable especially for in field measurements.

3.2.3 Alpha spectrum characteristics

As well shown in fig 3.7, the alpha peak shape of the two polonium isotopes has a Gaussian form in the high energy side but introduces a tail on the left side .

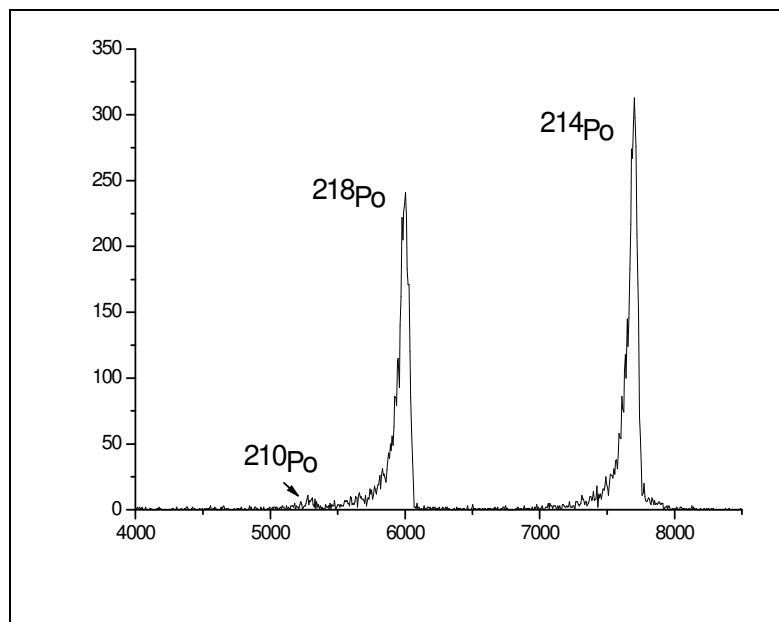


Fig 3.7 Typical alpha spectrum of ^{222}Rn source. It is also shown the ^{210}Po background peak

The most important contribute to this tail is due to the surface dead layer of the silicon detector, 500 Angstrom thick.. In fact, the polonium atoms that are deposited on the detector surface after the electrostatic collection, emit half of their alpha particles toward the sensitive layer over a wide range of angles. Thus, the alpha particles, before entering into the sensible zone, loss an amount of energy ranging on an interval depending on the angular spread (figure 3.8)

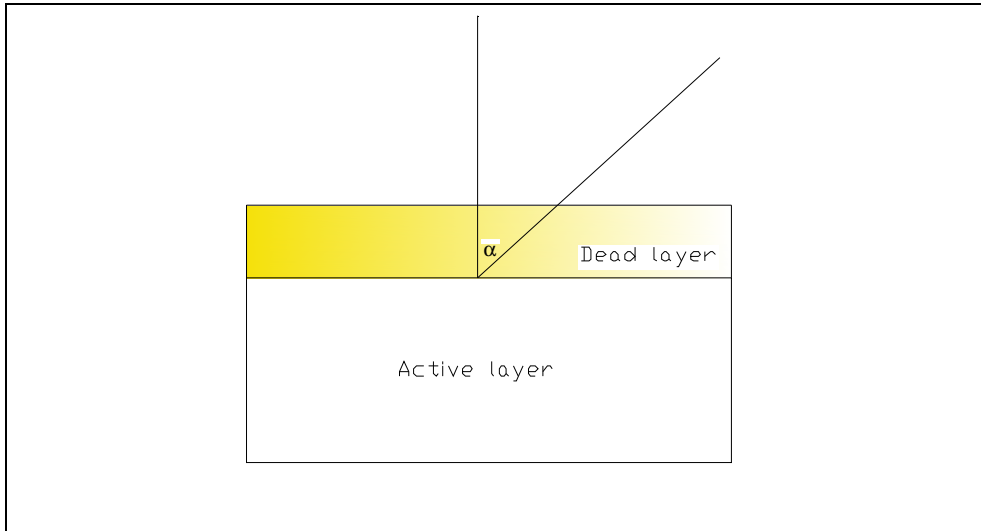


Fig. 3.8 The scheme of the emission from the detector surface

Moreover, the immediate radon descendent, the ^{218}Po , is deposited not only on the detector surface, but also on the upper part of the conductive case of the detector. For this reason the alpha particles coming from the internal vertical fraction of the case surface, before entering in the active volume can lose part of their energy in air (figure 3.9) and, also in this case, depending on the incidence angle.

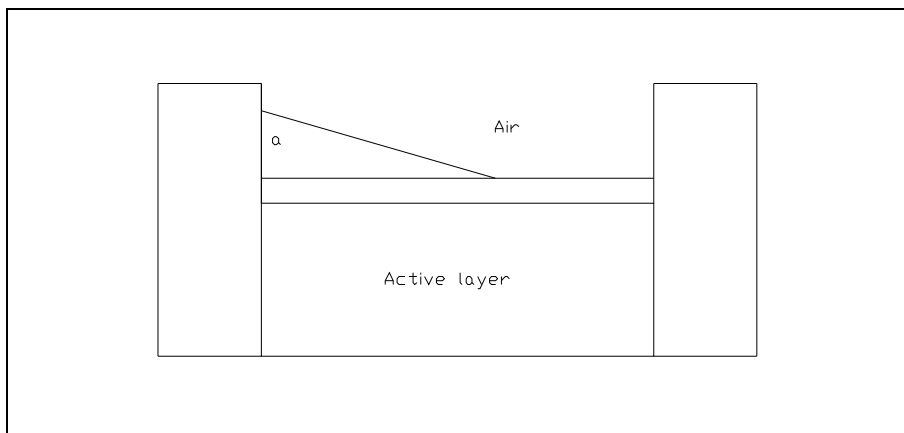


Fig 3.9 Scheme of the emission from the conductive detector edges

A simple calculation confirms these hypotheses. We simulate with a Monte Carlo code the alpha particle emission from the surface of detector and from its conductive edge. We suppose that the geometric efficiency for the alpha emitted from the detector is about 0.5. Regarding the edge emission, we ranged the point of emission along the edge, and the angle of emission toward the detector. In the calculation, we included not only the energy losses in air and in the silicon dead layer, but also the alpha straggling, i.e. the energy spread inside the active layer and we used parameters specified in the detectors Data Sheet, that is: dead layer = 500 Angstrom; straggling = 30 keV.

In the figure 3.10 the 6 MeV peak of the ^{218}Po built following this procedure is showed. . As it can seen the contribute of the alpha emitted from the edge is much lower (about 5%) than the contribute from the detector surface emission.

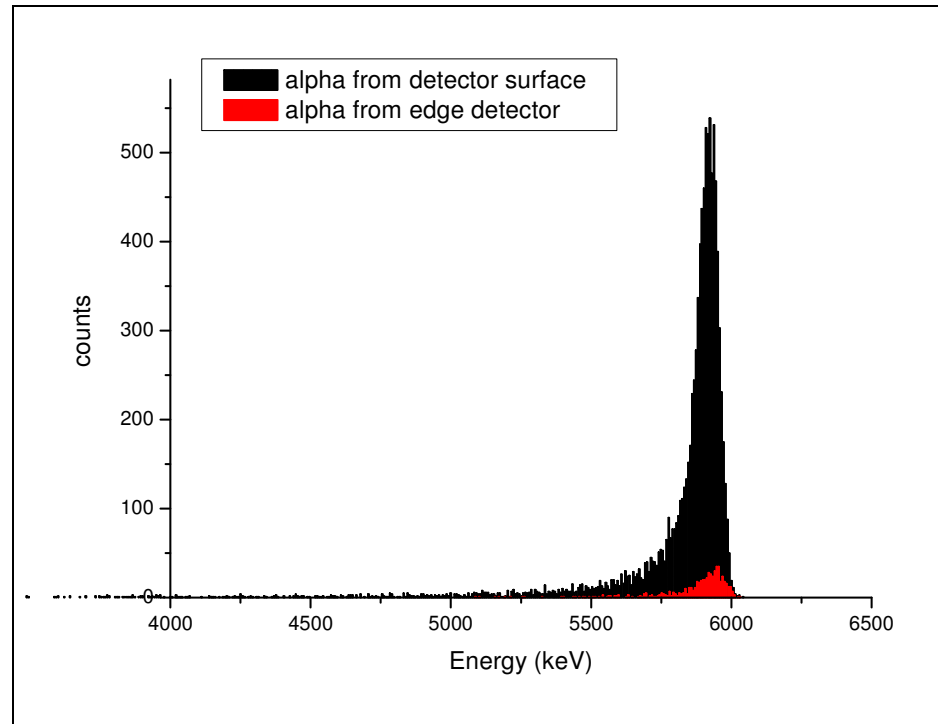


Fig 3.10 Comparison between the spectrum sources of the detected alpha. The alpha emitted from the edge are only the 5% of the total

The comparison between simulated and the experimental spectrum is very good as illustrated in the figure 3.11. The simulated spectrum is the sum of the of two contributes that were described above This reconstruction of the peak suggests to mark, for evaluate the correct value of the polonium count rate, a Region of Interest (ROI) including also the tail, at least up to position of the 5,3 MeV line of the ^{210}Po . It was estimated that the 98% of the total ^{218}Po alpha counts is in a 0.5 MeV range below the peak, thus the latter is used as the ^{218}Po Region Of Interest.

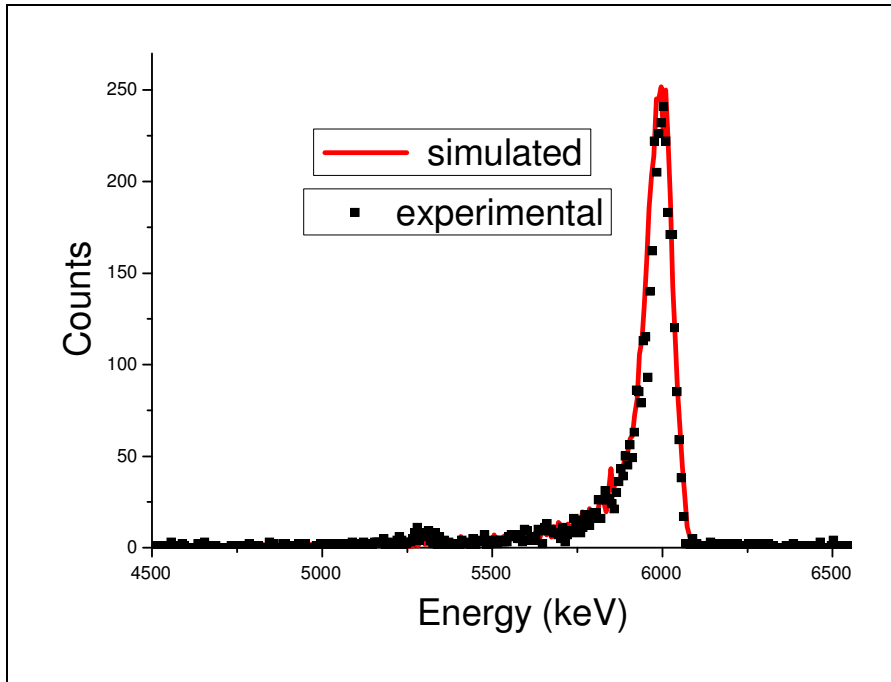


Fig 3.11 Comparison between experimental and calculated ^{218}Po alpha peak. The agree is good

Another characteristic of the spectrum is shown in figure 3.12. The high energy peak shape is different between the two polonium isotopes. In particular the energy cutoff for the ^{218}Po is much sharper than for ^{214}Po .

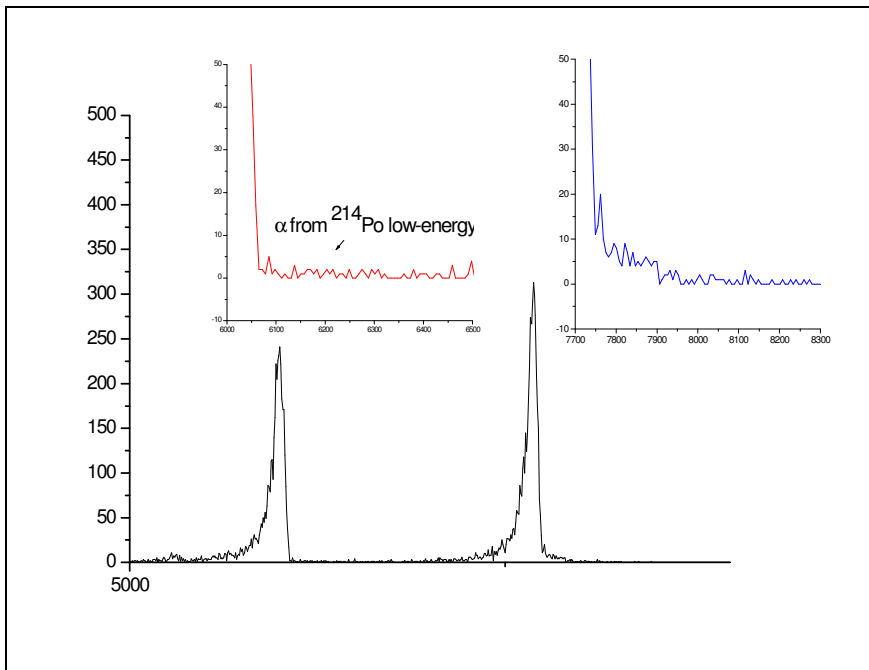


Fig 3.12 The high energy tail of the ^{214}Po is smoother than that of ^{218}Po .

This shape is due to the contribute of the beta particles emitted by ^{214}Bi , the direct ^{214}Po father nuclide, in coincidence with alpha particle of 7.69 MeV. The reason is the short half life of ^{214}Po , only 164 μs , that allows that beta and alpha particles could be frequently emitted within times of the

same order of the shaping time of the electronic chain. In other words, when both alpha and beta particles hit the detector within a time that is comparable with that associated with their electronic formation signals, their energy are summed and falls in a well defined ADC region. Therefore, to correctly evaluated to ^{214}Po contribute, the energy window (i.e. the Region of the Interest) have to be enlarged up to 8.3 MeV, that is the sum hof 7.69 MeV and the 0,61 MeV, i.e. the maximum energy of the beta spectrum emitted by ^{214}Bi .

3.2.3 Monitor characterization: experimental approach

As it was previously said, the radon monitor response is highly dependent on the environmental parameters inside the electrostatic cell. In this section it will be explained the procedure that we set up for studying this dependence with the use of the facility just described. Detailed information about the various phases of the method will be done here.

Phase 1) Cleaning of the circuit

After assuring the correct sealing of the apparatus, the circuit is cleaned pumping its air until a 10 mbar vacuum is reached. Then the volume is filled with dry and aged air (radon and moisture free) taken from a gas bottle previously connected with the circuit. The procedure is repeated for every new measurement cycle

Phase 2) The circuit volume measurement

To measure with a good precision the volume of the circulation system in which radon will be fluxed, we used the isothermal expansion method using a reference box whose volume is known with great precision. To do this, we filled our reference volume with dry air and at the same time pumped air from the rest of the circuit, whose volume is unknown, and measure the initial pressure with our pressure gauge inside the two volumes. After the isothermal expansion, is then measured the final pressure in the total volume and it is possible to calculate its value using the well known continuity equation (conservation of the air mass) $PV = \text{const}$, at T constant, assuming gas as ideal. The measurement of the circuit volume is performed at the beginning of each measurement cycle. and has a statistical uncertainty of 0,2%,

Phase 3) The radon activity measurement

The radon which will be fluxed inside the circuit is provided by a Radium source (Pylon. RNC-RN-1025) with a nominal 100 kBq activity. The source consists on a dry powder ^{226}Ra contained in an

aluminum cylinder box hermetically closed so that it can be in the secular equilibrium with ^{222}Rn . The radon produced by the sources is collected by diffusion in a glass ampoule with a 33 cm^3 volume.



Fig 3.13 Glass bulb with fitting valve used as reference radon source

After that the ampoule reached a desired radon activity, that depends on how much time it is connected to the source, it is hermetically closed and removed from the source. The radon activity is measured with a HPGe γ detector that allows to identify the gamma emitting radon progeny, i.e. ^{214}Pb and ^{214}Bi . To relate the progeny activity to radon activity, a waiting time of least 3 hours needs. If the waiting time reach the 10 hours, the influence on the activity measurement of daughters eventually entered into bulb with radon, is eliminated.

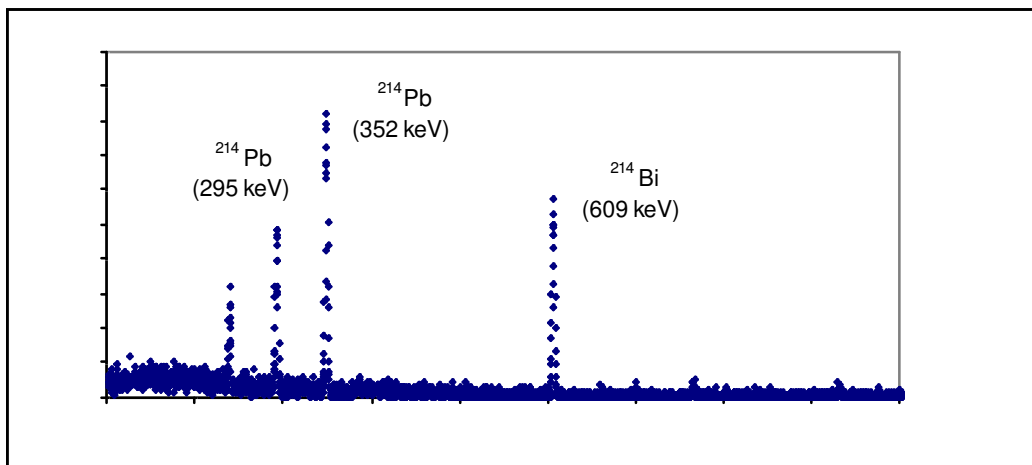


Fig 3.14 : γ spectrum of the radon source in glass bulb

In figure it shown a typical gamma spectrum of radon progeny. The lines used to calculate the activity are the most intense ones, that are $^{295}\text{ keV}$ e $^{352}\text{ keV}$ emitted from ^{214}Pb and 609 keV from ^{214}Bi .

The used gamma detector is HPGe (ORTEC GMX 45P4-ST) with a very good resolution (FWHM =2,16 keV at 1332 keV ^{60}Co peak energy) and a relative efficiency of about 50%. The spectroscopy electronic chain is constituted by a preamplifier (ORTEC A257N), amplifier (ORTEC

mod. 672) and a multichannels card (SILENA mod. 9308) connected to a PC, from which it is possible to visualize the spectrum and to perform peak analysis.

The radon activity measured has to be corrected for the decays during the measurements and then corrected by a decay factor related to a reference date.

Phase 4) The inlet of radon source in the circuit

After the measurements of its content, the ampoule is connected to the fitting of the circuit, previously cleaned as described in section 1 and filled with aged air. Just before the radon intake, the pressure inside the circuit have to be the same of the atmospheric one. After this operation, the ampoule tip can be opened to allow the radon intake in the facility and the membrane pump have to be turned on as long as the uniform radon redistribution can occur. This time interval has to be calculated measuring the radon content inside Ramona and verifying that after this time the radon concentration, corrected for decay, remain constant.

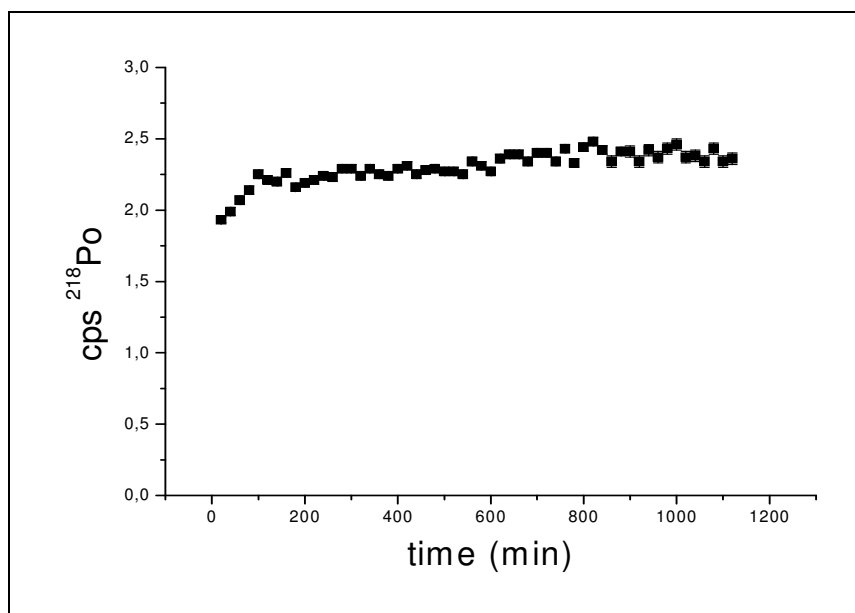


Fig:3.15 After a transient time from the radon intake, the radon concentration reach the equilibrium value

Phase 5) The control of environmental parameters

Before the radon intake, the values of environmental parameters have to be opportunely settled. We planned to study the correlation of the radon detector response respect to one parameter at time; so for example, when we studied the temperature influence we have to vary only the temperature values, taking care to left unchanged the other parameters, i.e. pressure and humidity.

The sensors within Ramona allow to control the variation of the environmental conditions generated by our modification of the setting values. The temperature variations is obtained simply changing

the setting of the thermo-box connected to the apparatus and including the Ramona chamber. On the contrary, the moisture variation is more difficult. It has to be alternatively open and close the dryer and humidifier [taps](#) of the circuit until the desired value is reached.

Phase 6) The alpha spectrum measurement for the efficiency calculation

For every measurements cycle, a 20 min acquisition time is set for each spectrum acquired with Ramona system. For each spectrum the efficiency was calculated using the following relation:

$$\varepsilon = k \frac{r_s}{A_{mis}} \quad (3.5)$$

where:

r_s is the counting rate of the ^{218}Po , that is the integral area under the asymmetric ^{218}Po . This measurement is corrected by a decay factor, the same of the gamma measurement.

k is the effective volume that is the ratio between the collection volume inside the Ramona and the total volume of the circuit previously measured as described in the Phase 2)

A_{mis} is the radon activity (in Bq) measured in the ampoule with gamma spectroscopy;

In the evaluation of the efficiency we use the ^{218}Po peak integral area because this nuclide has a short half life (3.05 minutes), so it reach the radioactive equilibrium with radon after about 20 minutes, that can be considered as the minimum time response of the instrument..

Chapter 4

Characterization of radon monitor: experimental and numerical approach.

The apparatus described in the previous chapter make it possible to estimate how the monitor response is affected by climatic parameters changes. This allows to optimize its efficiency and to normalize it at standard climatic conditions. Moreover, this kind of measurements will be also used to obtain useful information about the neutralization of the $^{218}\text{Po}^+$ ion and its electrical mobility in different air conditions. To this aim we developed a methods to describe the events inside the electrostatic chamber with a MonteCarlo code. The procedure adopted is based on two steps:

the calculation of the electric field strength inside the chamber, followed by the determination of the $^{218}\text{Po}^+$ transport times, i.e. the times that the ions spent in the volume chamber before their collection on the detector surface;

the estimation of the ions collection efficiency with a code that describe opportunely the physics of recombination and the decay processes.

4.1 MonteCarlo simulation approach

4.1.1. Electric field calculation inside Ramona

The Voltage in the active volume chamber obey to the Laplace equation, that is an elliptic partial differential equation (4.1):

$$\partial_{xx}V(x, y, z) + \partial_{yy}V(x, y, z) + \partial_{zz}V(x, y, z) = 0 \quad (4.1)$$

The boundary conditions specified around the chamber are the walls placed at 3,5 kV, the silicon detector surface polarized at 20 V, and the conductive edge of the detector grounded (figure 3.4).

To find the solutions of this equation we use a numerical approach using the finite differences method (see appendix A). To simplify the problem we solve the 2D Laplace equation on a lateral section of the cell because of the system symmetry around its central vertical axis. The chamber

surface section is divided in a grid where voltage was iteratively calculated in each lattice point using an appropriate algorithm.

In figure 4.1 are illustrated the equipotential lines inside the chamber. Knowing the voltage scalar field it is possible to calculate the electric field along the x and y directions using the relation:

$$E_i = -\frac{\partial V(x, y)}{\partial i} \quad \forall i \in \{x, y\} \quad (4.2)$$

The electric field strength (expressed in *Volt/cm*) are then estimated by the module of the x and y components:

$$|E| = \sqrt{E_x^2 + E_y^2} \quad (4.3)$$

The contour plot of electric field strength, calculated for each lattice point, is illustrated in figure 4.2. It can be seen that at the edge of the chamber there are regions with minimum strength.

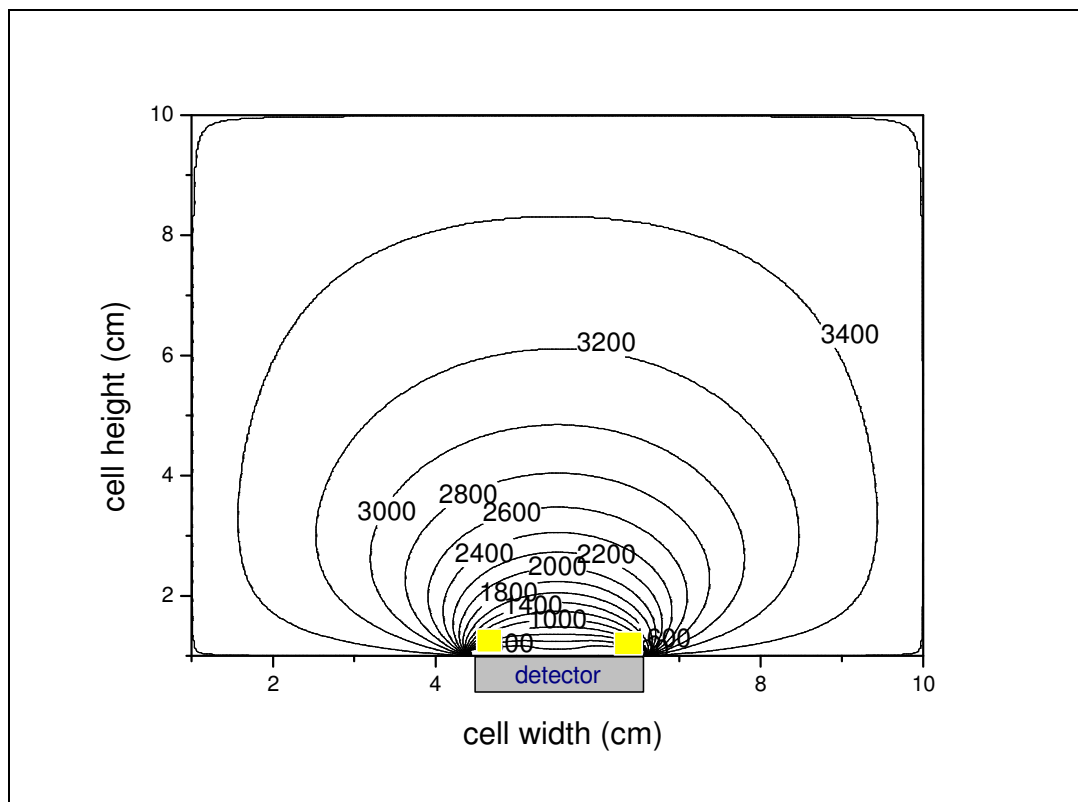


Fig 4.1 Contour plot of the voltage equipotential lines inside the electrostatic chamber drawn in section. The labels of each line are in expressed in Volt

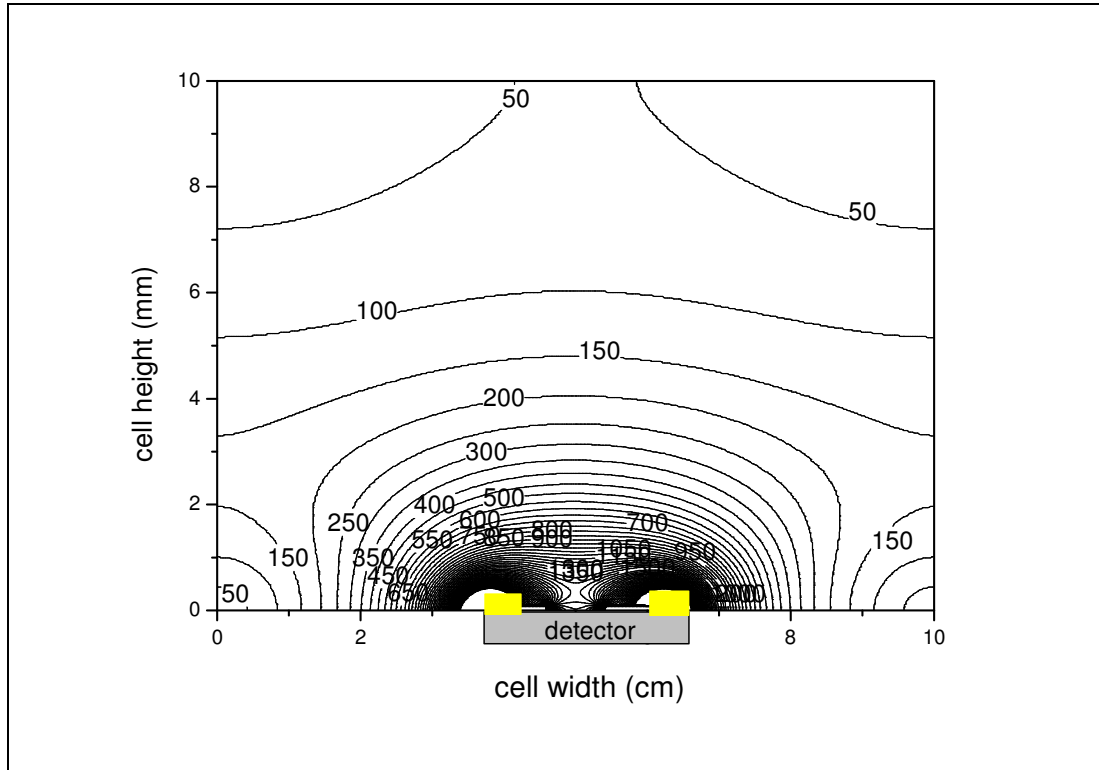


Figure 4.2 : The contour plot of the electric field strength inside the cell. The label of the lines are expressed in Volt/cm

4.1.2 ^{218}Po ions transit time distribution

The time \mathbf{T} occurring to ^{218}Po ions to be collected on the detector surface is an useful parameter for the estimation of the collection efficiency of the electrostatic chamber. Without the neutralization inside the cell, the time spent in air by a $^{218}\text{Po}^+$ freshly generated (i.e. ^{218}Po born charged) depends only on the electrostatic field and on its position inside the chamber:

$$\mathbf{T} = f(\vec{E}, x, y) \quad (4.4)$$

Thus, it is possible to evaluate for each position inside the cell, i.e. for each point of the grid, its corresponding transit time. In next sections the distribution of these times will be used as matrix data in a MonteCarlo code for the estimation of the collection efficiency.

With this aim, we used an algorithm able to calculate the trajectories of the ions immersed in the electric field. Knowing the mobility μ of the ions, the drift velocity in each point of the grid can be calculated by:

$$\vec{v}_d = \mu \cdot \vec{E} \quad (4.5)$$

where \vec{E} is the local electric field. From this relation is possible to calculate the trajectories of the ions from their starting point up to the detector surface. T could be calculated using a the following relation:

$$T = \int_{t_i}^{t_f} dt = \int_{\gamma} \frac{ds}{\mu \cdot E} \quad (4.6)$$

where t_i is the time of the generation of the polonium ions after the radon decay and t_f is the time after which the ions are collected on the surface. The integral has to be calculated on the curve γ , the trajectory of the ion. In a discrete space, as our grid, these trajectories can be approximated by a polygonal whose segments are the distances between the centers of the n grid squares. The direction of these segments is determined univocally by the electric field in correspondence of the same grid points (fig 4.3).

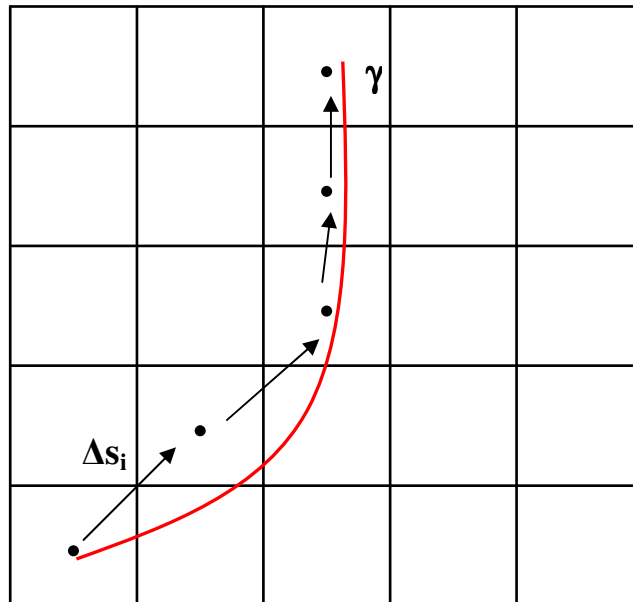


Fig.4.3. Trajectories of the ions drifted by the electric field are approximated by a polygonal in the grid

The estimation of T in the grid can be done making discrete the (4.6), that become:

$$T = \sum_{i_0}^{i_f} \frac{\Delta s_i}{\mu \cdot E_i} \quad (4.7)$$

where E_i is the electric field in the i^{th} grid square and Δs_i is the segment that links the i^{th} with the $(i+1)^{\text{th}}$ square. The sum is extended from i_0 , the initial point of the trajectory up to i_f the final position which is in correspondence of the detector surface.

The application of the (4.7) to each grid point allow to determine the distribution of the times T inside the chamber. In figure 4.4 it is illustrated the times contour plot, that indicates the lines with the same times. In figure 4.5 is shown the total distribution of times. It has to be noted that most of them are shorter than 0.01 s

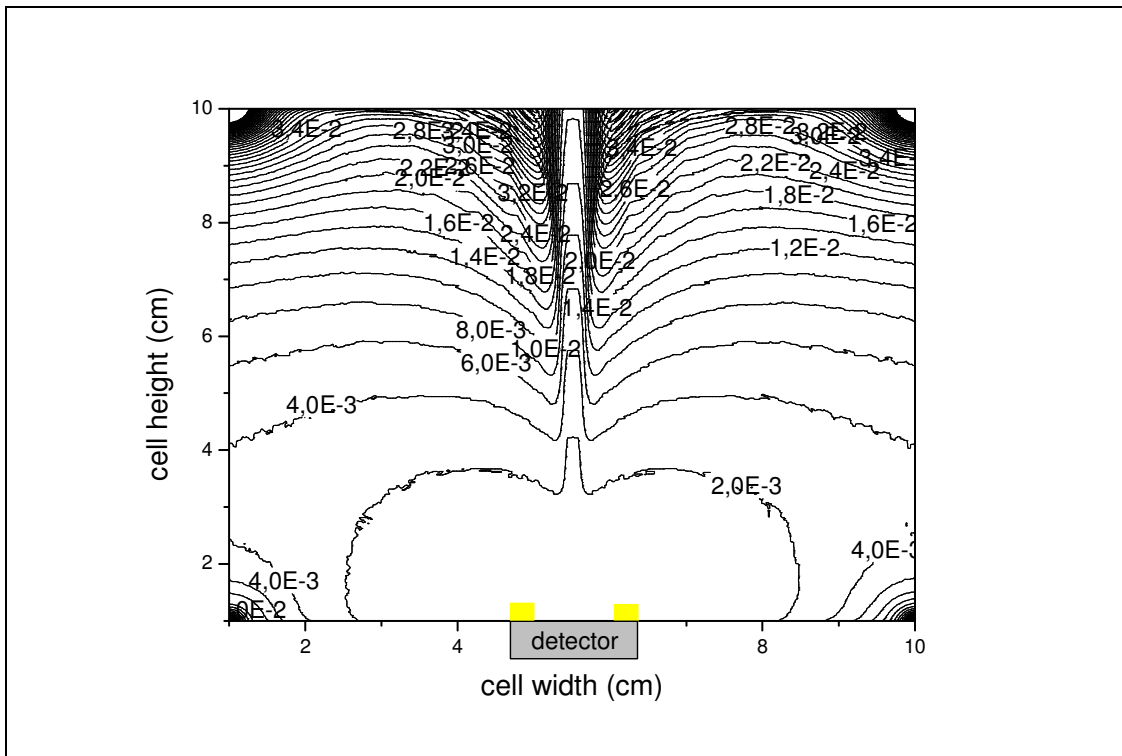


Fig. 4.4 Contour plot of the times for each grid point in the cell.

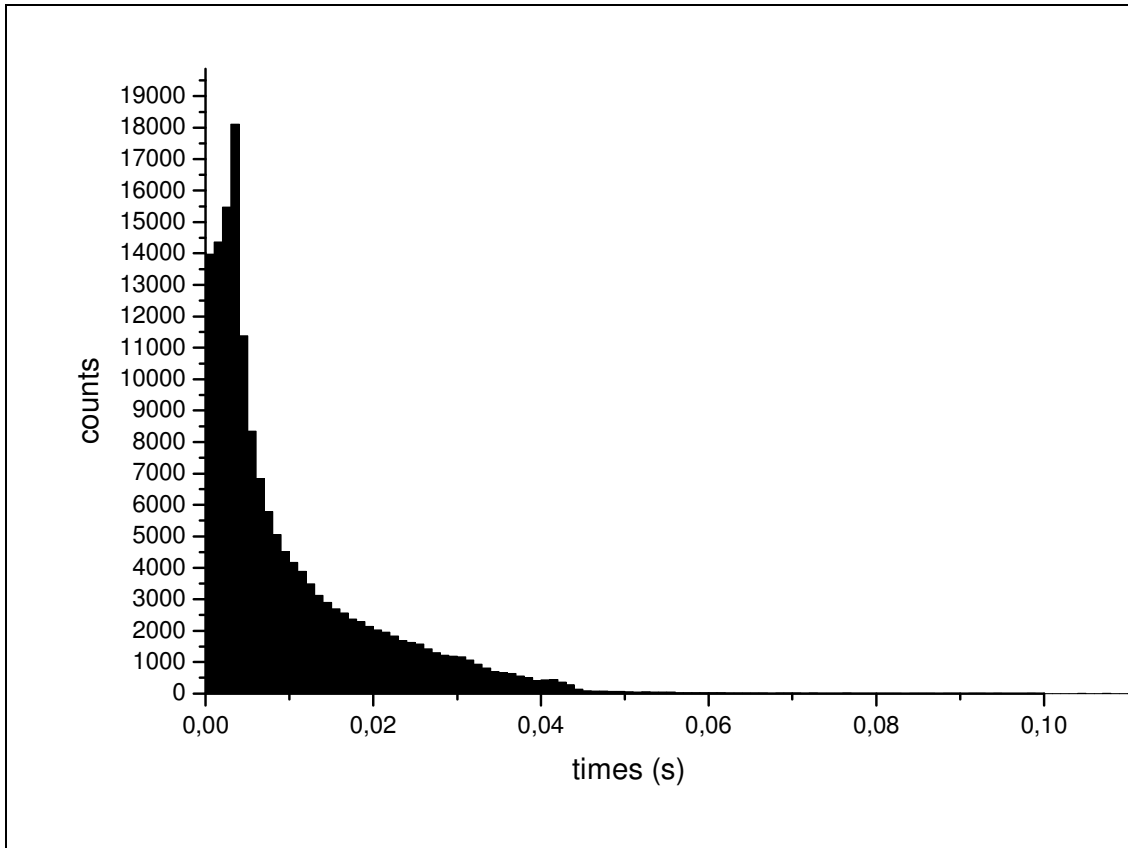


Fig 4.5 The distribution of the times of the polonium ions inside the cell

Finally, knowing the trajectories of the ions, it is possible to estimate if a ^{218}Po ion, generated in a well defined grid point, will be collected on the detector surface or on its conductive edge (fig 4.6). In the last case, the emitted alpha particles cannot be detected .

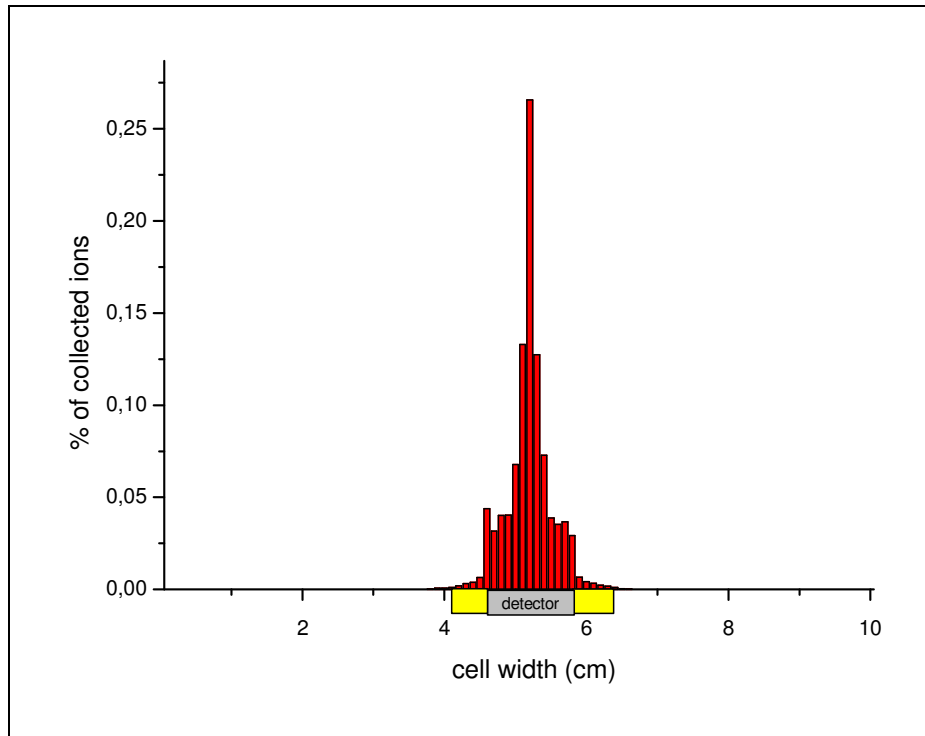


Fig 4.6 Distribution of the collected ions on the detector plane section. The tails of the distribution lie out of the surface detector.

Thus, once fixed the electric field inside the chamber, the fact that an ion can be transported or not on the detector surface depends univocally on its grid position. It has to be remarked that this kind of description of the electrostatic ion collection, up to now has been done neglecting the influence of the decay and recombination. These random processes will be introduced in the next section for the complete characterization of the problem.

4.1.3 The estimation of the collection efficiency

After the determination of the electric field and the time T distribution, we will develop a model in which recombination and decay are taking into account for the study of the collection efficiency of our monitor.

The first model assumption is that the efficiency depends on two main parameters: the electrical mobility μ and the recombination constant τ of $^{218}\text{Po}^+$, that is the mean time that occur for the ion recombination, and sometimes expressed as the inverse of its neutralization rate.

The second assumption is that μ and τ are itself dependent on air conditions inside the chamber. In particular μ depends on temperature and pressure, while τ is influenced by humidity and radon concentration.

So the collection efficiency can be written by :

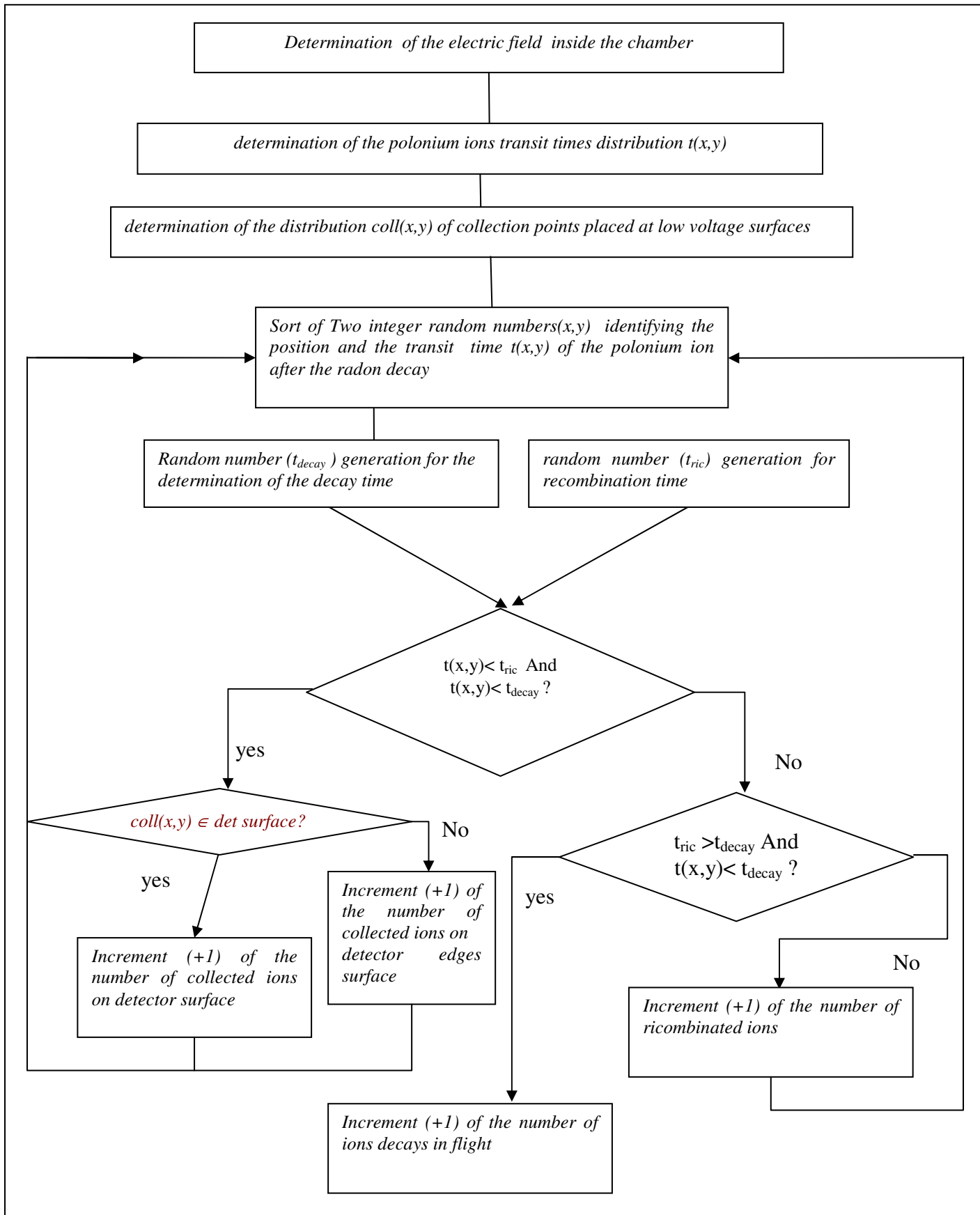
$$Eff(\mu, \tau) = Eff(\mu(T, P), \tau(U, C_{Rn})) \quad (4.8)$$

The main purpose of our approach is to determine how mobility and recombination time air condition take influence from air conditions. To reach this goal we will calculate $Eff(\mu, \tau)$, with the MonteCarlo code, and then we compare it with the experimental efficiency at different temperature, pressure, humidity and radon concentration. Experiments were carried out varying one parameter at a time, with the wariness, to leave constant the others during the measurements.

The procedure adopted for the determination of the collecting efficiency can be described in 4 steps, which are further visualized in the flow chart

- 1 calculation of the electric field inside the chamber for each grid point;
- 2 evaluation of the distribution transit time of the polonium ions through the active volume chamber up to collecting surfaces; we consider that the radon atoms are homogenously distributed inside the electrostatic cell, so the decay probability is independent on its coordinate in the chamber.
- 3 calculation of the distribution of the collecting point ($coll(x,y)$) on the low voltage surface, i.e. the silicon detector and its conductive edges surfaces. This distribution represent the initial positions of the ions in the grid, for which the ions are bounded to be collected on the detector surface by means of the electric fields.
- 4 Generation of the recombination and decay process though a MonteCarlo code. The code take into account the characteristic mean time of recombination (τ_{ric}) and of polonium decay τ_{decay} , generating two random number Tr e Td as described in the following paragraph. In addition, the code “extract” the position of a polonium ion, and so its transit time and its point of arrival on the collecting surfaces.

If one of these numbers Tr and Td is smaller than the collection time previously calculated, then the ion cannot reach the detector surface, and it decay or recombine depending on the which number is the smaller. Otherwise, if both these number are greater than the collecting times, then the ions are collected on the active surface depending on its correspondent collecting point previously calculated.



Flow Chart of the MonteCarlo used for the estimation of the collection efficiency

4.1.4 The recombination and decay handling

In this section, we describe how to take into account the stochastic nature of decay and recombination processes..

Firstly, to correctly simulate the recombination inside the chamber, we treat it as a decay process. Thus the recombination constant τ_{ric} can be considered as the mean elapsed time before a recombination occurs

As for the decay, the law describing the process is:

$$N(t) = N_0 \cdot \exp\left[-\frac{(t-t_0)}{\tau_{ric}}\right] \quad (4.10)$$

where $N(t)$ is the number of ions not yet ricombinated

N_0 is the number of ions at time t_0

τ_{ric} is the mean recombination time.

The ratio $p = \frac{N(t)}{N_0}$ represents the fraction of ions not yet ricombinated at time t and it can be considered as probability function being $\in (0,1)$. The inverse of this function is:

$$t - t_0 = -\tau_{ric} \cdot \ln(p) \quad (4.11)$$

This relation allows to numerically represent the recombination, assigning a random number the argument p . We use the same approach for generate the decay mechanism, using the decay mean time τ_{decay} in the above formula.

4.1.5 Optimization of the algorithm

We calculated the electric field strengths and the distribution times with different mesh values. For each mesh used, in **table 4.1** is indicated the mean and the median time T together with the collection distribution on the detector surface. The mobility adopted in the calculation is $2 \text{ cm}^2\text{V}^{-1}\text{s}^{-1}$.

mesh	transit times (s)		collection on detector surface (%)
	mean	median	
100	0,02	0,01	79,5
200	0,02	0,01	78,2
300	0,02	0,01	74,7
400	0,02	0,01	72,2
500	0,02	0,01	72,2

Table 4.1: the calculation of parameters used in the code at different mesh values

The times are the same for each mesh used in the calculations. We choose for the code calculation the mesh value 400 after which the collection distribution remain constant.

To control the algorithm used for the decay and the recombination mechanism processes, we compare the true decay constant of ^{218}Po (180 s) and the recombination time constant ($\tau_{\text{ric}} = 0,01 \text{ s}$) with mean values obtained from the code run with different number of events.

events	Estimated ^{218}Po mean life	Estimated recombination mean life
10	167,0	0,008
100	177,0	0,010
1000	178,0	0,009
10000	180,8	0,010
20000	180,8	0,010
30000	180,9	0,010

Table 4.2 : Estimated mean life at different numbers of events

It can be seen that from 10000 events the estimated mean life for both the processes is comparable with the real values. In the code, we use this number of events for handling the stochastic processes of decay and recombination.

4.1.6 Output of the simulation

As described in the flow chart figure, the code allows to calculate the percentage of ^{218}Po ion collected on the surface detector, and the percentage of recombination and of in-flight decays. The input data of the code are: the ^{218}Po ion mobility μ , the recombination constant τ , and the voltage applied to the cell. All these parameters affect the collection efficiency, so we vary each of them at a time, fixing the others. The output (Table 4.3 and fig 4.8) is the percentage of ions collected on the detector surface, that it is an estimation of the collection efficiency, the percentage of the total collected ions (on detector surface and on its edges) and of ^{218}Po that decay in flight.

INPUT	OUTPUT		
mobility $\mu = 2 \text{ cm}^2\text{V}^{-1}\text{s}^{-1}$			
Voltage = 3.5 kV			
Recombination time (τ) (seconds)	% collected ^{218}Po ion on detector surface (efficiency)	% total collected ^{218}Po ion	% ^{218}Po on flight decay
0,01	22,3%	42,7%	0,003%
0,02	35,4%	59,1%	0,005%
0,03	43,1%	68,1%	0,005%
0,04	48,2%	73,8%	0,006%
0,05	51,8%	77,8%	0,006%
0,075	57,3%	83,9%	0,006%
0,1	60,5%	87,4%	0,007%
0,125	62,5%	89,6%	0,007%
0,15	64,0%	91,2%	0,007%
0,175	65,0%	92,3%	0,007%
0,2	65,9%	93,2%	0,007%
0,3	67,8%	95,3%	0,008%
0,4	68,9%	96,5%	0,008%
0,5	69,5%	97,1%	0,008%
1	70,8%	98,5%	0,008%
5	71,9%	99,7%	0,008%
10	72,0%	99,8%	0,008%
100	72,2%	100,0%	0,008%

Table 4.3 : A typical output of the simulation program.

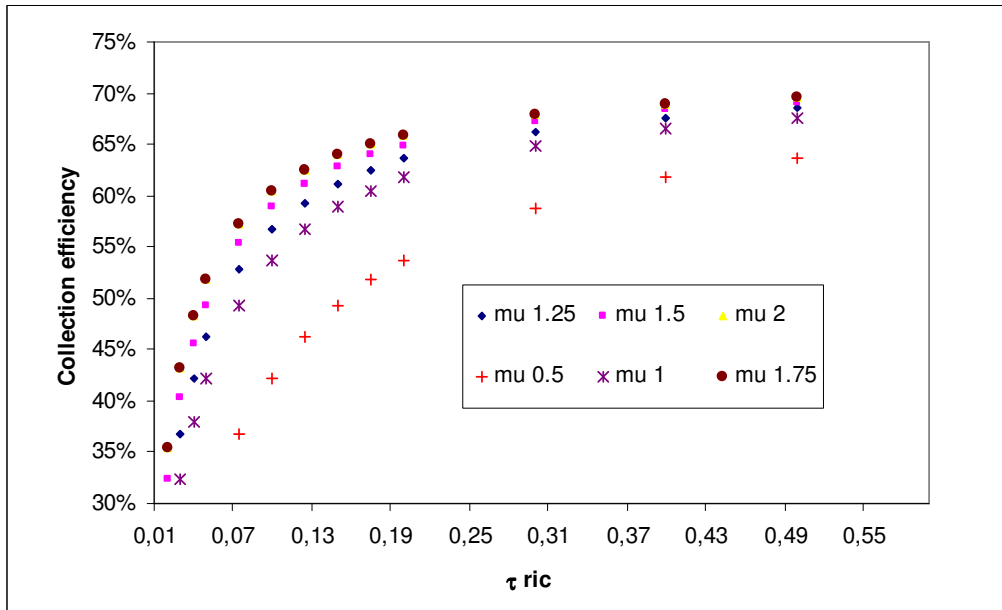


Fig 4.8 Collection efficiency versus recombination time. Data calculated at six different $^{218}\text{Po}^+$ electrical mobility

4.2 Comparison between calculated and measured efficiencies

Hereafter it will be described the experimental results obtained varying the climatic parameters inside the cell. Their comparison with the efficiency calculated with the numerical approach will be useful to estimate the $^{218}\text{Po}^+$ neutralization rates, directly affecting the collection efficiency.

4.2.1 Determination of the neutralization rates

Varying the voltage of the chamber, the calculated ion collection increases up to a constant efficiency value as indicated in **fig. 4.9** The efficiency plateau value depends only on the electrostatic chamber geometry.

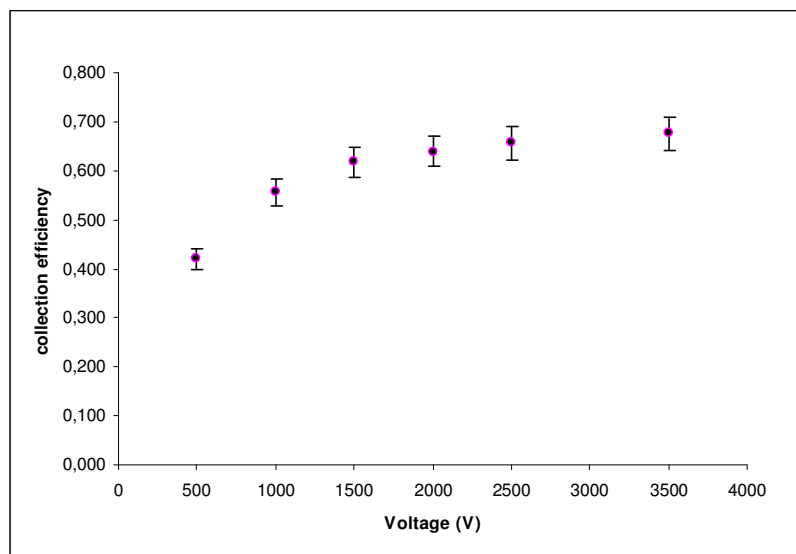


Fig. 4.9 The calculated collection is highly influenced by the voltage at the chamber walls until it reach a constant value

The minimum voltage (V_{plateau}) for which the collection efficiency reaches the plateau is dependent on the neutralization rate: at standard temperature, this value depends exclusively on the recombination rate and can be used as a key parameter to calculate the ^{218}Po neutralization times and studying how they are influenced by air conditions.

However, it has to be noted that at voltage higher than 3500 V there is no stable response of the instrument (figure 4.10), probably caused by some sparks events that occur within the chamber due to the reaching (somewhere in the cell) of the dielectric rigidity: in this case, it is not possible reach V_{plateau} .

Thus, it is important to study the efficiency variation up to 3,5 kV, that was chosen as the higher voltage in our experimental set up. In **fig 4.11** is plotted the calculated collection efficiency variation at fixed recombination times and at fixed mobility $\mu = 2 \text{ cm}^2\text{V}^{-1}\text{s}^{-1}$. As it can be seen, as higher the recombination times as faster the plateau is reached

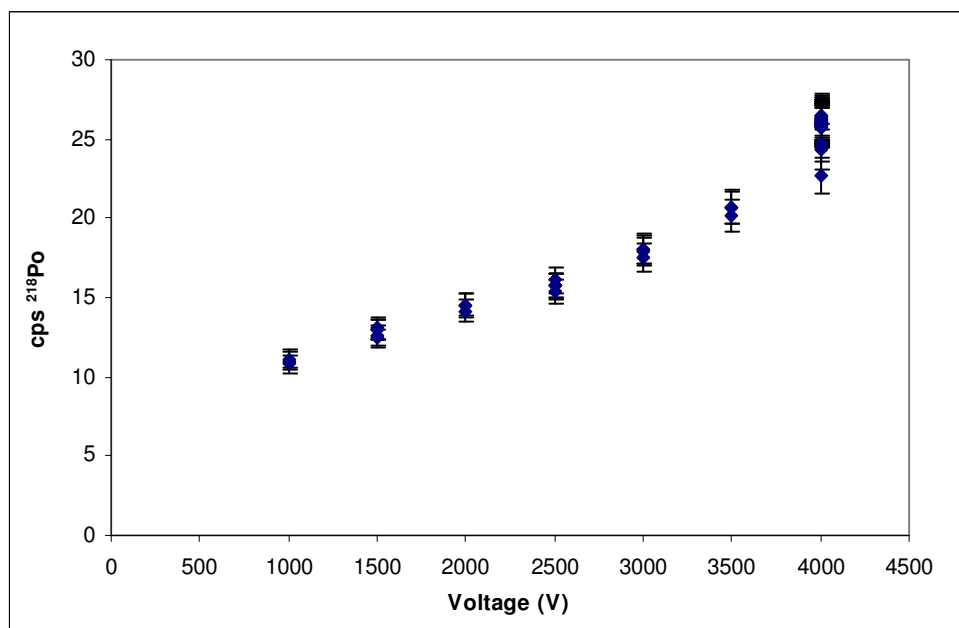


Fig 4.10 The experimental collection efficiency influenced by the applied voltage up to 3.5 kV

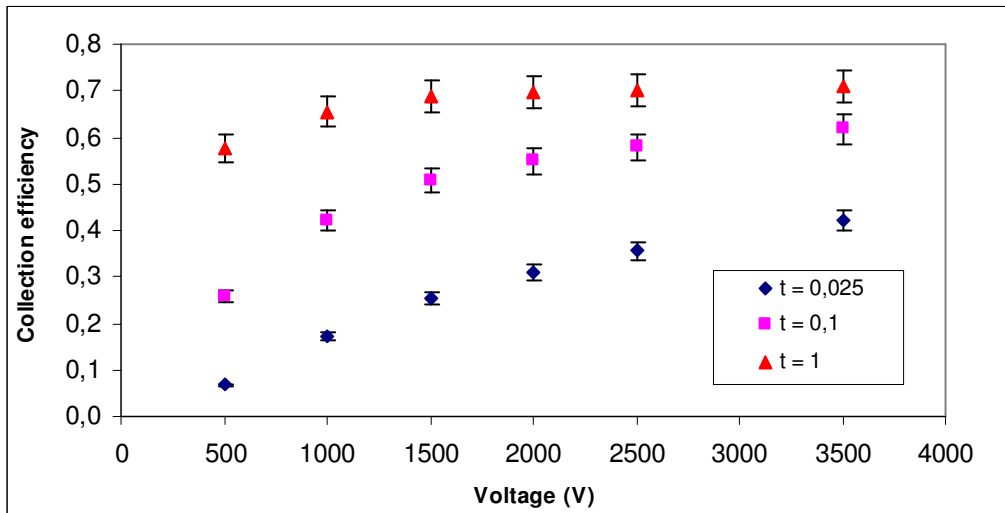


Fig. 4.11 The calculated collection efficiency Vs voltage at different recombination constants

The comparison between the efficiencies allow us to determinate the $^{218}\text{Po}^+$ neutralization rate with a sort of calibration curve. For a set of recombination times τ , we calculate the efficiency dependence on voltage, where the efficiency was normalized respect to maximum voltage, i.e. 3,5 kV.(fig 4.12) For each curve, i.e. for each τ , it is calculated the slope k of the linear fit in semi logarithm scale (fig 4.13).

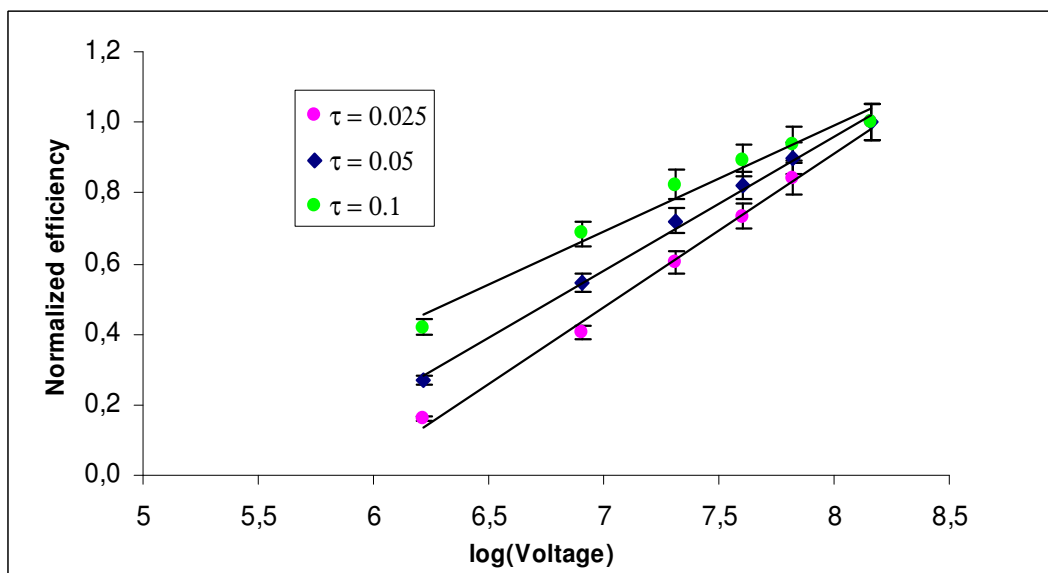


fig 4.12 The slope of the normalized efficiency curves is dependent on the recombination constant

Therefore, the recombination times depends on k in a well defined way, as shown in fig. 4.13

This allows to find out the recombination times from experimental data, after the calculation of the slope k . This procedure will be used in the following sections to calculate neutralization rates in correspondence of the climatic parameters.

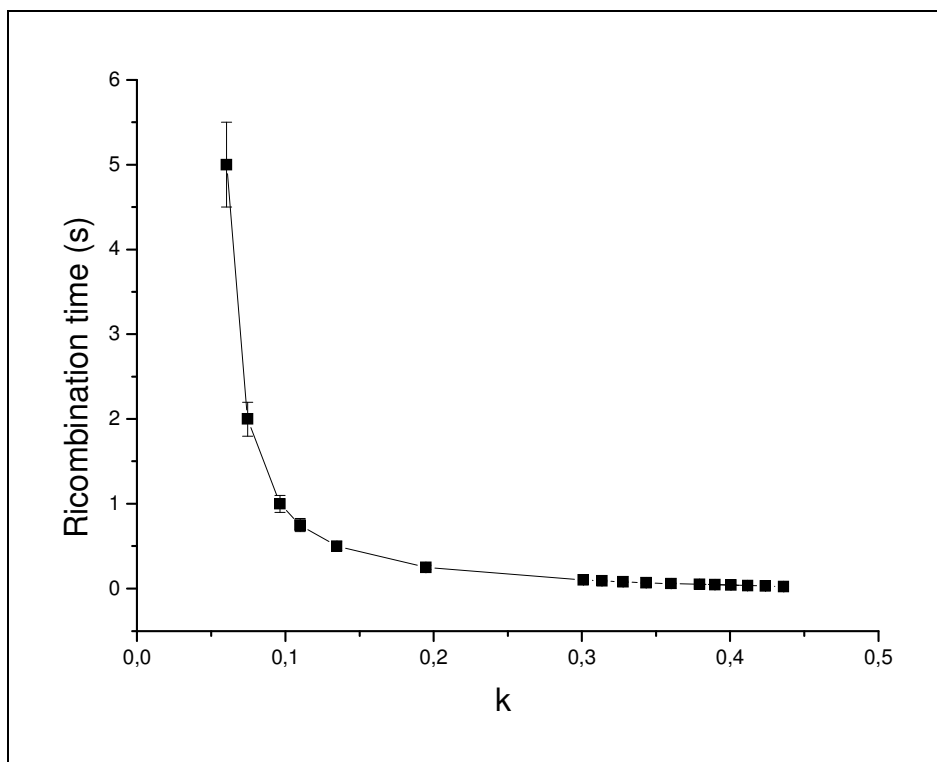


Fig 4.13 .The recombination time can be calculated from the slope k (defined in the text)

4.3 Dependence of efficiency on environmental parameters

Now we illustrate experimental results about Ramona efficiency measured varying the environmental parameters in controlled way using our facility. These results will be useful to correct our monitor response at normal conditions. Moreover they allow us to infer some important information on the neutralization rates and the ions mobility at different environmental air conditions.

4.3.1 The influence of the barometric pressure

The pressure inside the chamber was changed by means of a vacuum pump connected to the cell. To evaluate the reproducibility of the system response, we performed four experiments in the same pressure range (200-1000 mbar), determining the efficiency at different values. In table 4.3, for each experiment are indicated the efficiency variation coefficient and its uncertainty (1 standard deviation)

Experiment Pressure range(200-1000 mbar)	$\frac{d\varepsilon}{dP}$ (cps Bq ⁻¹ mbar ⁻¹)	Relative uncertainty (%)
Exp 1	$(-1,09 \pm 0,02) \cdot 10^{-4}$	3
Exp 2	$(-1,10 \pm 0,06) \cdot 10^{-4}$	5
Exp 3	$(-1,11 \pm 0,06) \cdot 10^{-4}$	5
Exp 4	$(-1,12 \pm 0,05) \cdot 10^{-4}$	5

Table 4.3. Experiments for studying the influence of the pressure on the efficiency

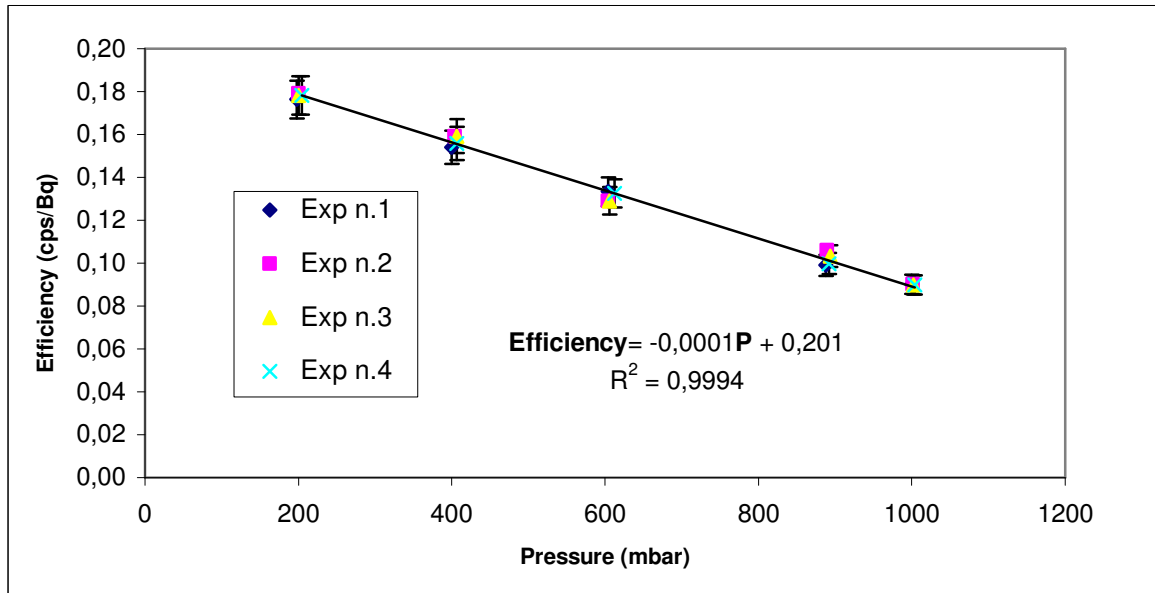


Fig 4.14 The efficiency decreases linearly with the pressure increase

The pressure dependence factor of the detection efficiency is calculated using all the experimental points:

$$\frac{d\varepsilon}{dP} \text{ (cps Bq}^{-1} \text{ mbar}^{-1}\text{)} = (1,10 \pm 0,02) \cdot 10^{-4} \quad (4.12)$$

In addition, the efficiency is normalized at standard atmospheric pressure (1000 bar) (fig 4.15). It can be noted that in the range near the atmospheric pressure (900-1000 mbar), the influence on the monitor response is negligible (<0.2%).

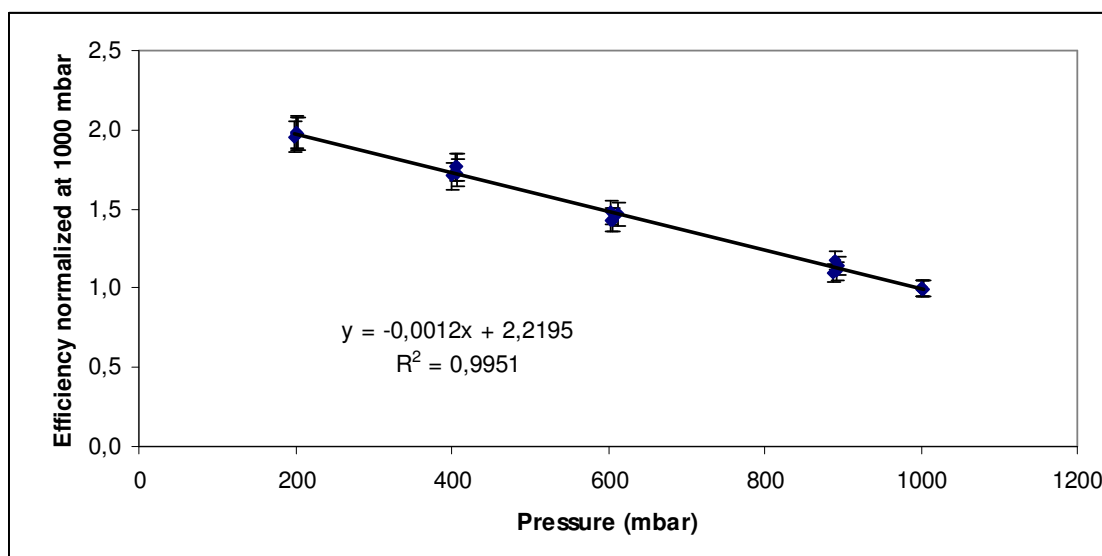


Fig 4.15. Normalized efficiency versus barometric pressure

Finally it has to be noted that the uncertainty associated with the reproducibility of the system response is 0,5%, well below the uncertainties related to each experiments. This assure the reliability of the apparatus for these kind of measurements.

4.3.2 Collection efficiency dependence on temperature

The air temperature inside the electrostatic cell can be changed and controlled by the thermo-regulator in which it was enclosed. The measurements were carried out at different temperatures in the range 15-35 °C. In the following plot (fig 4.16) a typical time variations of all the monitored environmental parameters is shown.

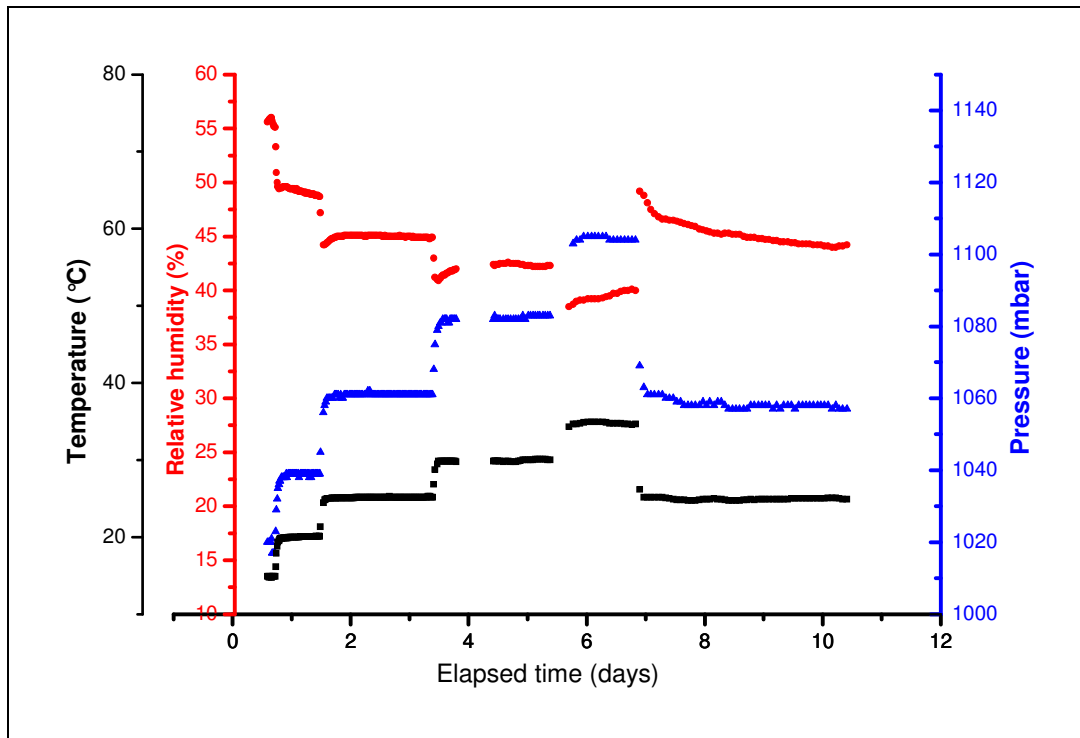


fig. 4.16 The temperature variation influence also the pressure and the relative humidity

It can be seen that the pressure and the relative humidity is dependent on the temperature. The pressure is directly proportional to temperature, so that the air inside the cell can be considered as ideal gas. The influence of the pressure variation, induced by temperature changes, can be neglected for the estimation of the efficiency: as pointed out previously, in the proximity of the atmospheric pressure, the efficiency is almost independent from the pressure. Instead the relative humidity, which is the ratio between the partial water vapor pressure and the saturated water pressure, decreases at higher temperature. The reason of this behavior is that the saturated water pressure increases with increasing temperature, so that the relative ratio decreases. For this reason, to correctly estimate the moisture content in the air, it has to be considered the absolute humidity, expressed in ppm (part per million) that remains constant with increasing temperature since the dew point is well below the range of the temperatures exploited during the experiments.

In **fig 4.17** was shown the temporal variation of the detected polonium ions at various temperatures. It can be noted that the efficiency decreases when the temperature increases.

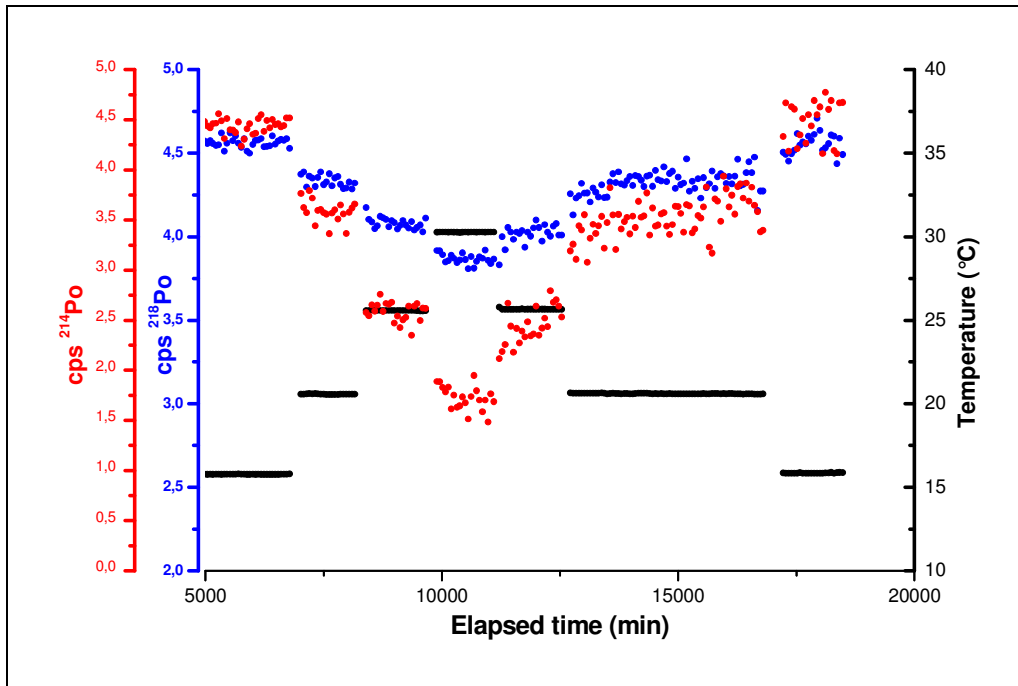


Fig 4.17 The time variation of the ^{218}Po and ^{214}Po count per second in correspondence of various setting temperatures

The experimental results concerning the efficiency at different temperature are shown in figure, where is indicated how the efficiency normalized at $T=25^\circ\text{C}$ depends on temperature. Also for this kind of study, we carried out a series of experiments at the same conditions, that verify the repeatability of the results.

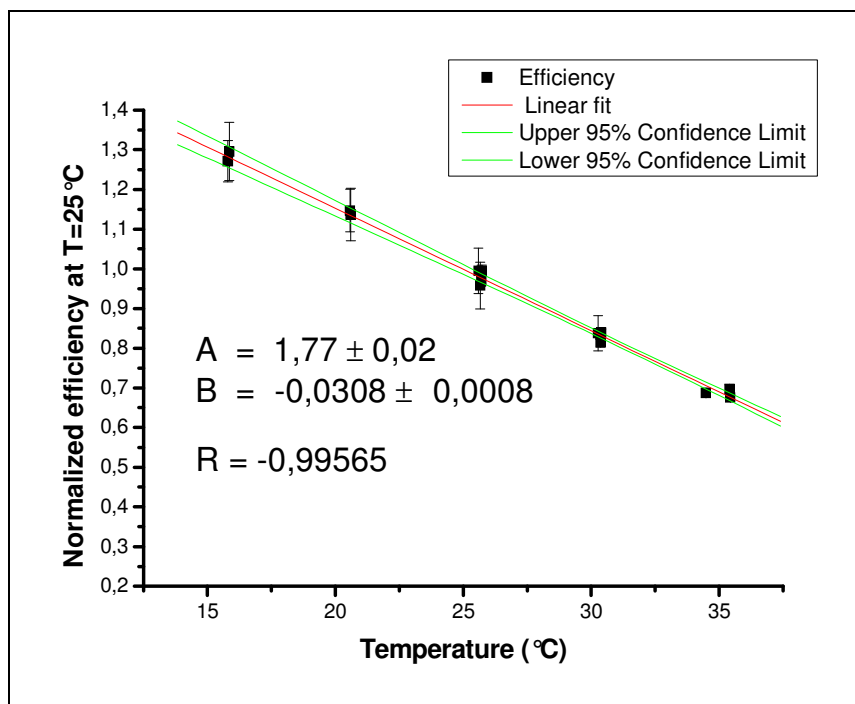


Fig. 4.18 Normalized efficiency at $T=25^\circ\text{C}$ versus temperature. At higher temperature the efficiency linearly decreases.

Thus the efficiency dependence on temperature is linear:

$$Eff_{NORMALIZED}(T) = \frac{Eff(T)}{Eff(T = 25^{\circ}C)} = a + bT \quad (4.13)$$

with:

$$a = 1.77 \pm 0.02$$

$$b = (-0.0308 \pm 0.0008) \text{ }^{\circ}C^{-1}$$

It has to remark that this relation was calculated at normal air condition, that is: 50% relative humidity, estimated at $T = 25^{\circ}C$ and at atmospheric pressure in the range 1000-1100 mbar. In these ranges we have already demonstrate that the pressure influence can be neglected and the same is true form the humidity as we will find out in the next paragraph.

4.3.2.1 Mobility dependence on temperature

The code described in the previous section would be a tool to study how the mobility depends on the temperature changes. In fact the efficiency dependence can be written, decoupling the influence of the environmental parameters on the mobility and recombination time:

$$Eff(\mu, \tau) = Eff(\mu(T), \tau(U)) \quad (4.14)$$

where τ depends essentially on air humidity, while radon concentration and pressure influences can be neglected in normal air conditions and at low radon concentrations used for the experiments.

Calculated the characteristic τ at normal air condition with the method described in section 4.7 , it is possible to estimate $Eff(\mu, \tau)$ with the MonteCarlo code. In **fig 4.19** is shown this calculated collection efficiency normalized at $\mu = 2 \text{ cm}^2 \text{ V}^{-1} \text{ s}^{-1}$, assumed to be the characteristic ^{218}Po ion mobility at $25^{\circ}C$ (*Phillips et al, 1988; Howard at al, 1990*).

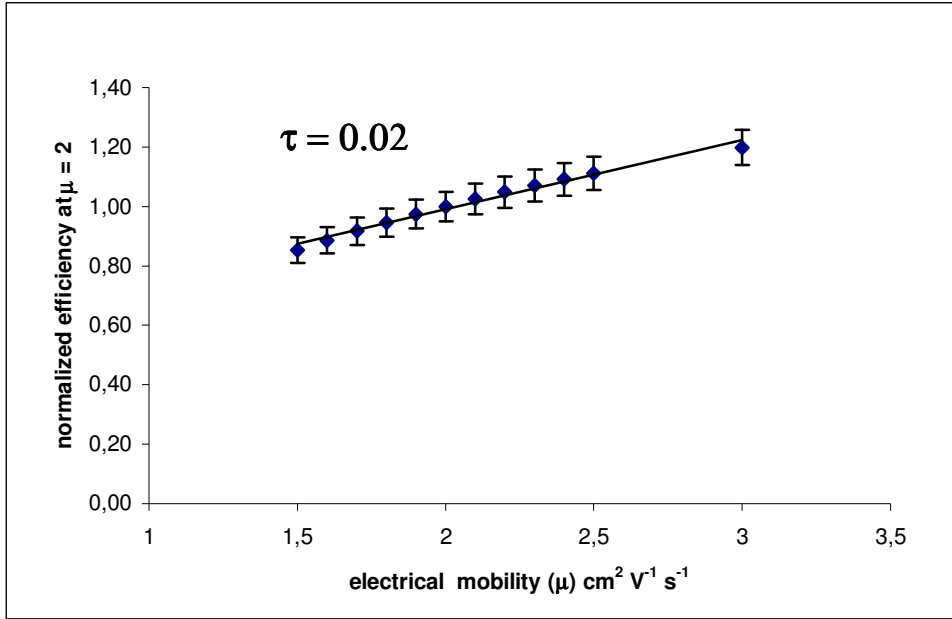


Fig 4.19 Calculated efficiency versus electrical mobility

From the relation (4.14), (4.13) we have:

$$Eff_{Norm}(\mu(T)) = a_{\mu} + b_{\mu}\mu(T) = Eff_{Norm}(T) = a + bT$$

$$\mu(T) = \alpha + \beta T$$

(4.15)

$$\alpha = \frac{a - a_{\mu}}{b_{\mu}} = 5.3 \pm 0.3$$

$$\beta = \frac{b}{b_{\mu}} = -0.132 \pm 0.007(^{\circ}C^{-1})$$

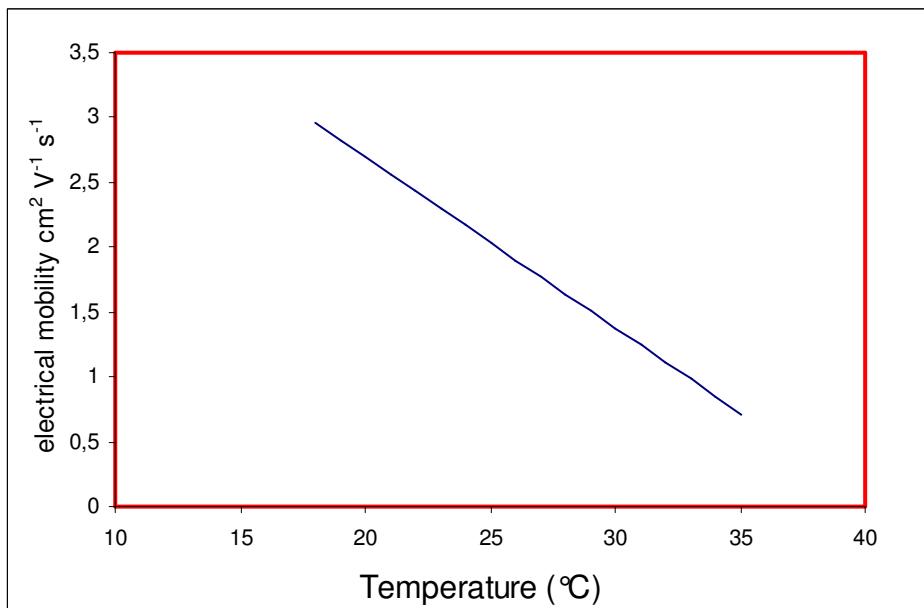


Fig 4.20 The electrical mobility depends linearly on temperature

4.3.3 Collection efficiency dependence on humidity

The efficiency dependence on humidity was estimated (fig 4.21) varying the air moisture content inside the electrostatic cell in the range 15-18% RH. While the measurements were carried out the other parameters were fixed at standard values. Moreover, the measurements were also carried out at low radon concentration to avoid its effect on the efficiency (Chu and Hopke, 1988).

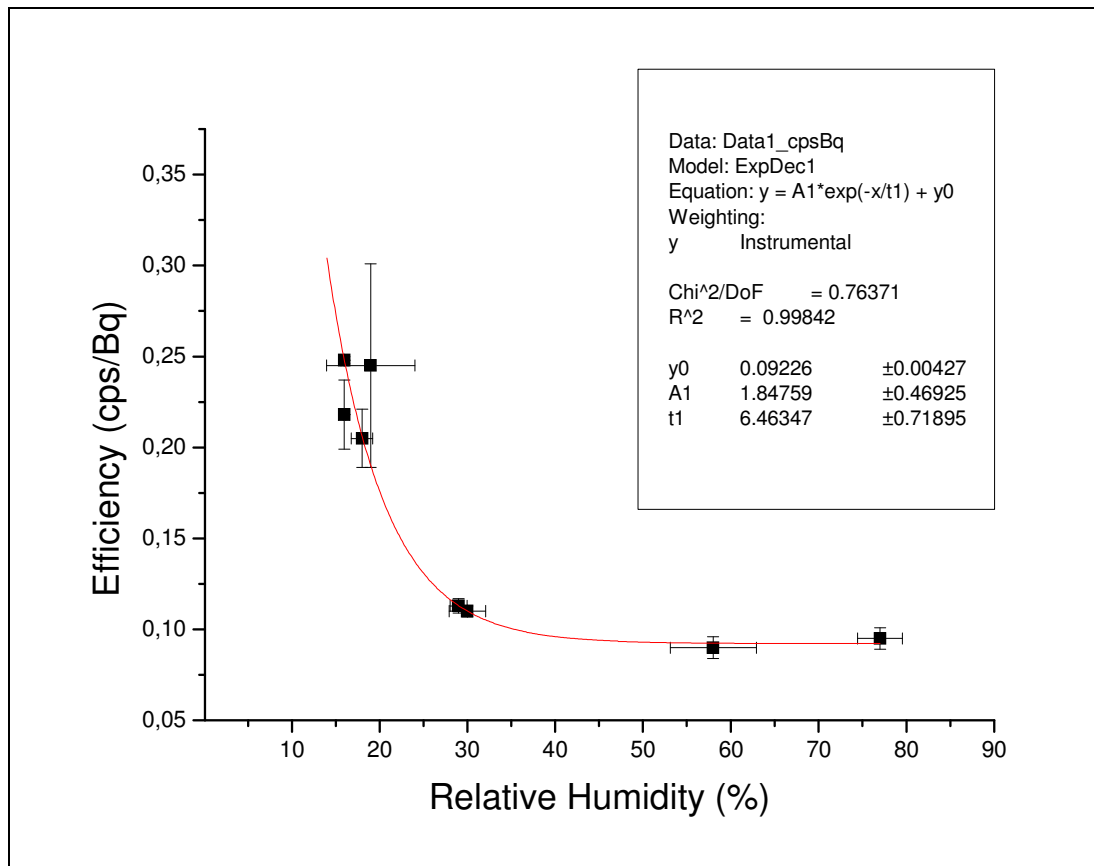


Fig 4.21: The efficiency dependence on the relative humidity

All the points plotted in the graph, as for the previous set of experiments, are the average on different experiments and the uncertainties are the respective standard deviations.

The efficiency is highly dependent on humidity at least up to 50% RH. At higher humidity, it seems to reach a constant value.

From the comparison between experimental and calculated values, it is possible to infer the dependence of the neutralization rates and on the moisture content. With this aim, it was calculated the $^{218}\text{Po}^+$ neutralization rate at 50% RH, with the method described in section 4.7, that remains constant also for the higher humidity values, because the cell efficiency does not change. Its value is

:

$$v_{218P_0} = 50 \pm 4 \text{ s}^{-1} \quad (4.16)$$

In fig 4.22 it is illustrated the collection efficiency versus the characteristic recombination times (τ), up to the $\tau = 0.02 \text{ s}$ that is the inverse of the neutralization time previously estimated (4.16).

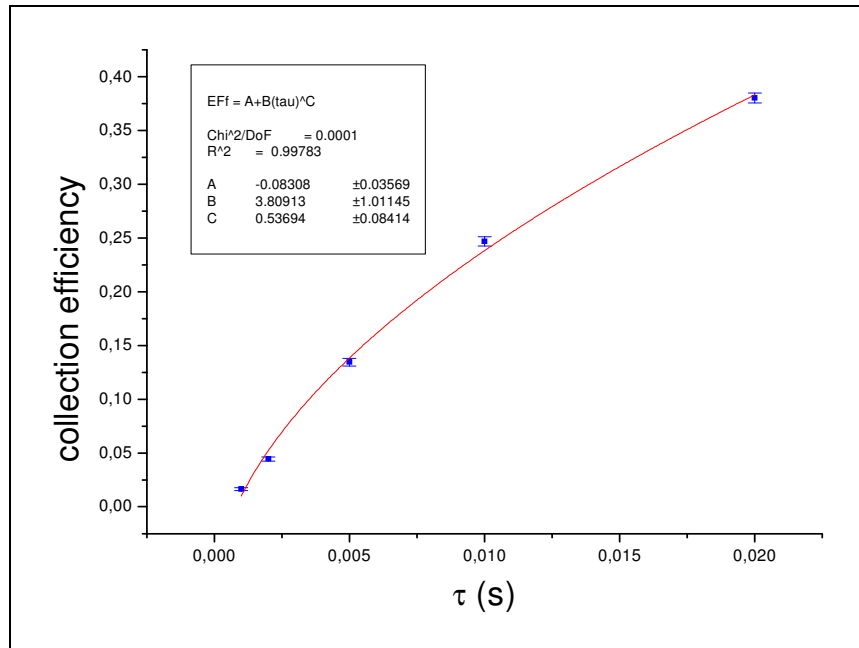


Fig 4.22: The MonteCarlo calculated collection efficiency versus recombination times. The efficiency was calculated at fixed electrical mobility ($2 \text{ cm}^2 \text{ V}^{-1} \text{ s}^{-1}$).

To find out how the neutralization rate depends on the relative humidity we have to compare the absolute (fig 4.21) with the collection efficiency (fig 4.23), that are proportional to each other. The factor of proportionality can be estimated considering that the collection efficiency calculated at $\tau = 0.02 \text{ s}$ correspond at the absolute efficiency measured at 50% relative humidity.

In fig 4.23 and 4.24 it is illustrated the relationship between humidity and neutralization rate.

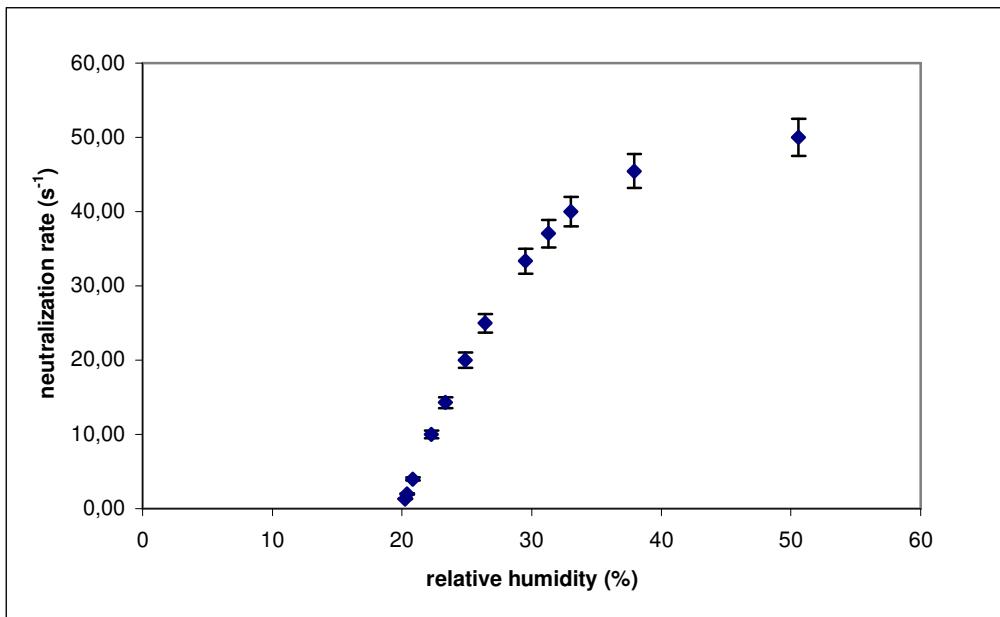


Fig 4.23: Neutralization rate versus relative humidity

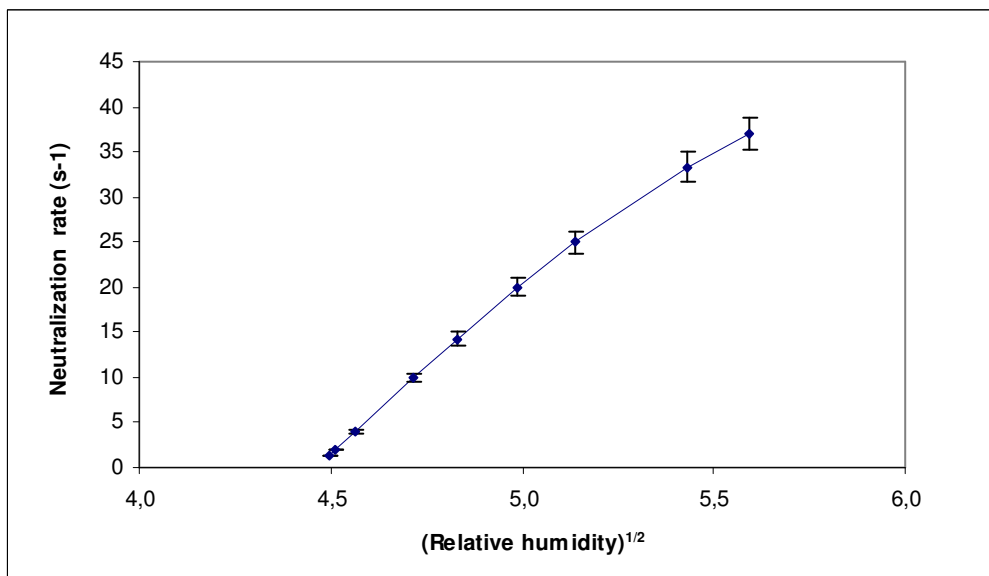


Fig 4.24: Neutralization rate versus relative humidity square root

As expected (Chu, Hopke et al 1988), the neutralization rate increase linearly with the square root of the relative humidity. The relation found in figure 4.24 is:

$$v(s^{-1}) = 33,30\sqrt{RH} - 147,5$$

That confirm the validity of the model outlined in chapter 2 (ref) of the processes involved in the recombination mechanism

In conclusion, we have studied the influence of the environmental parameters on our radon monitoring system (Ramona). The efficiency dependence will allow us to normalize the monitor response to standard air conditions and offers a methodology to calculate the neutralization rate and to find out how these are affected by the moisture content in air.

After the characterization of the monitor, Ramona can be used as reference monitor in a typical radon exposure chamber to control in continuous way the radon concentration. This kind of use will be exploited in the next chapter where it will be also outlined a series of experimental calibration of passive radon detectors.

Chapter 5

Continuous Monitoring in a Radon Chamber: passive detector calibration

Radon Chamber is a basic element for radon detectors calibration, but it is also a very useful apparatus for studying radon and its progeny behaviour in different conditions. The possibility to varying and monitoring the air conditions inside the chamber volume makes the system reliable to study radon and its daughter behaviour and to verify theoretical models designed to describe it

In this chapter both applications in metrology field and in the wider area of the radon behaviour studies. will be described.

5.1 Radon Chamber

In the metrology field, it has to be considered that the large variety of the techniques for the radon measurements and sampling in air imply the use of different calibration procedures, that match well with experimental equipments. For example, the calibration of a real time instruments, based on continuous sampling (in air or in water), should be based on a reference radon monitor capable to perform accurate real time measures with an opportune reference measurement systems. Instead, passive detectors, used for the integrate radon concentration, should be related to the radon exposure, i.e. time integrated radon activity concentration, which can be monitored inside a Radon Chamber with a reference active monitor. The Radon Chamber is equipped by a series of probes useful to monitor the internal air parameters, such as temperature, humidity and pressure, because the detector responses could be influenced by these factors.

The exposure chamber consists on a stainless steel cylinder of about 33 liter volume having an height of 15 cm .and a diameter of 50 cm. It was chosen metallic instead of plastic material to avoid radon diffusion or adsorption through the wall surfaces. The cylinder presents a series of flanges, equipped with *passing connectors* and tube fittings for the inlet of radon with its gas carrier.

The Radon Chamber has a system for the air conditioning, that allows to change and control relative humidity, pressure, aerosol distribution and the type of gas carrier. These parameters are controlled by a series of gauges inside the chamber that allow to monitor their range of variability. In the figure(5.1) some active detectors used to control the radon activity concentration are showed. Two of these are present inside the chamber. They are characterized by small dimensions and so they takes just a negligible part of the available volume. The third one, that is an electrostatic cell,) is placed outside the chamber, connected to one of its flange through a Teflon tube fitting. The radon flux inside this last monitor is assured by a mini-fan.

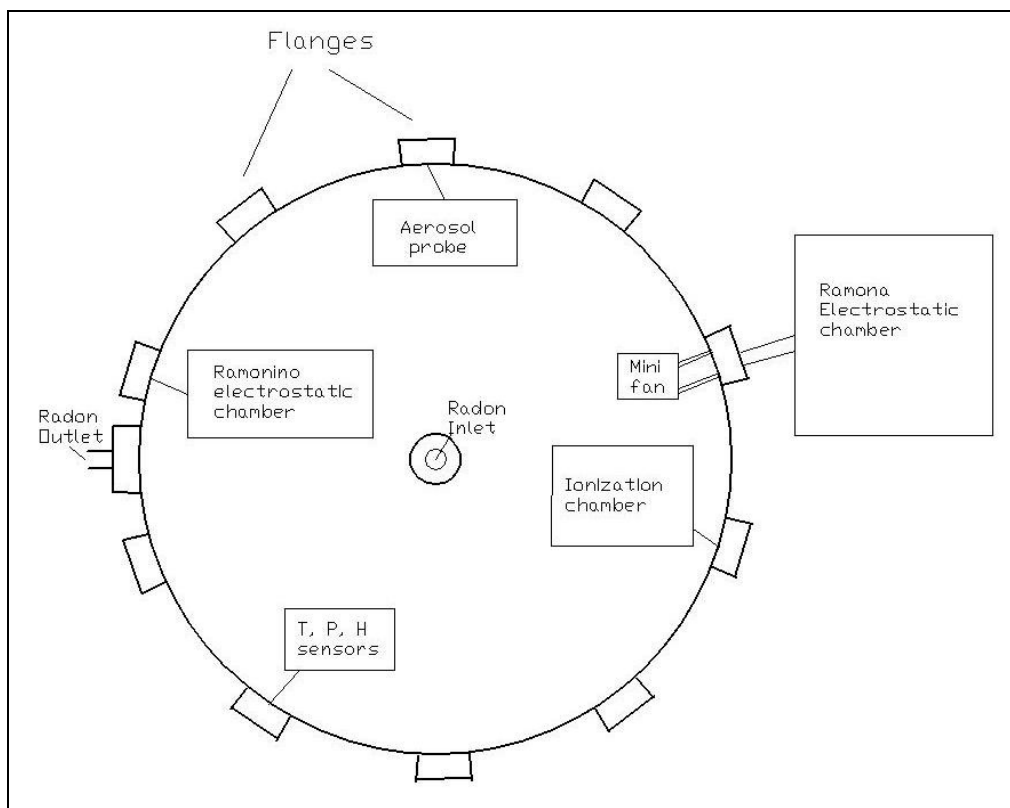


Figure5.1 Scheme of monitoring gauges mounted in the Radon Chamber

The radon inlet of the radon is provided by a recirculation pump which assures the uniform gas distribution from a radon source. The radon flux comes from the upper wall through a circular tube with a series of regularly distributed holes from which radon can escape and diffuse homogenously inside the volume (fig 5.2). Another concentric tube provides for the radon outlet assuring an uniform flux.

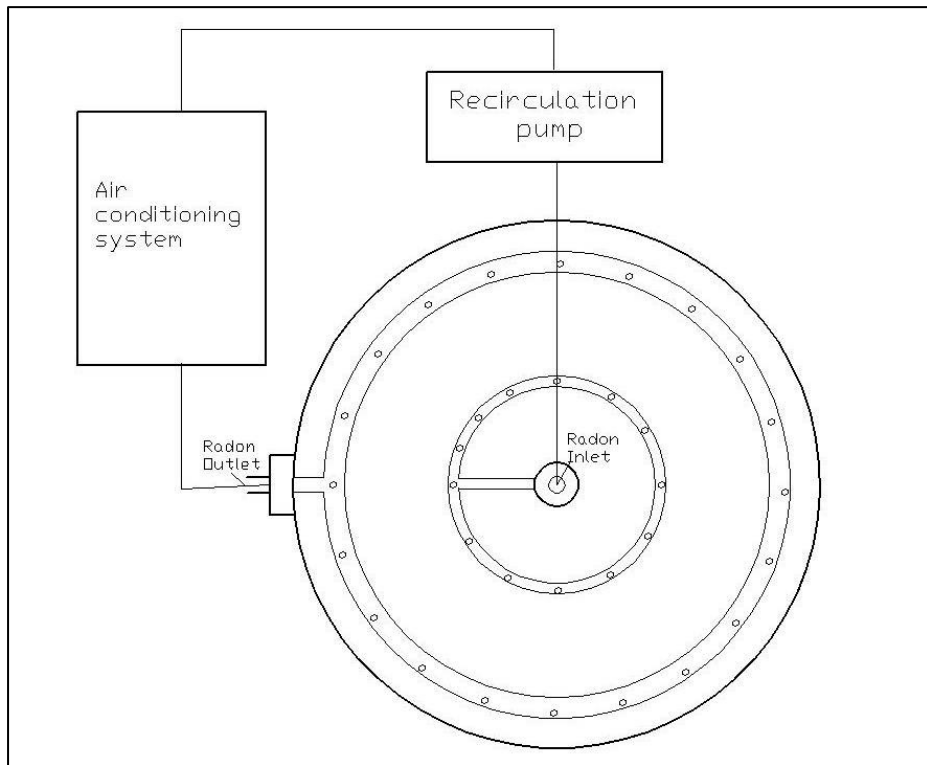


Figure 5.2 Scheme of radon inlet inside the Radon Chamber

If we want to study the radon exposure in environmental air, it is possible to provide for the radon entry directly through a suitable fitting flange directly linked to the Radon Chamber. The radon gas can flow inside by diffusion or by means of a pressure gradient created between the radon source and the chamber previously evacuated by a vacuum pump.

5.2 Radon monitoring inside Radon Chamber

The active radon monitoring inside the chamber can be provided by instruments that utilize the principles of the electrostatic collection or which use the measurement of the ionization in air due to alpha particles emitted by radon and its decay products. We designed a couple of these detectors minimizing their dimension in order to reduce their influence inside the exposure volume

5.2.1 Ionization measurements

Most of the detectors commonly used for the real time radon activity measurements are affected by low detection efficiency. One of the methods used to obtain higher time is to use ionization proportional counter for the continuous radon monitoring in air. Moreover, if the aim of the measurements is to assess the sudden radon concentration variations during short times, it is useful

to count the alpha emitted by the ^{222}Rn decays, without waiting for the radon progeny to be in equilibrium with the father nuclide.

The cylindrical ionization gauge used in our exposure chamber is schematically illustrated in figure(5.3)

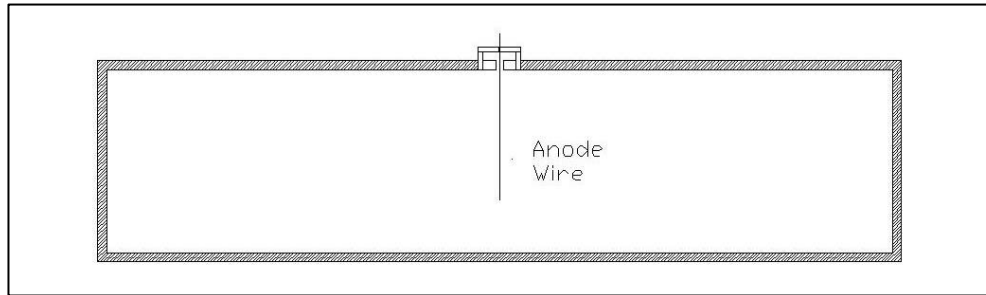


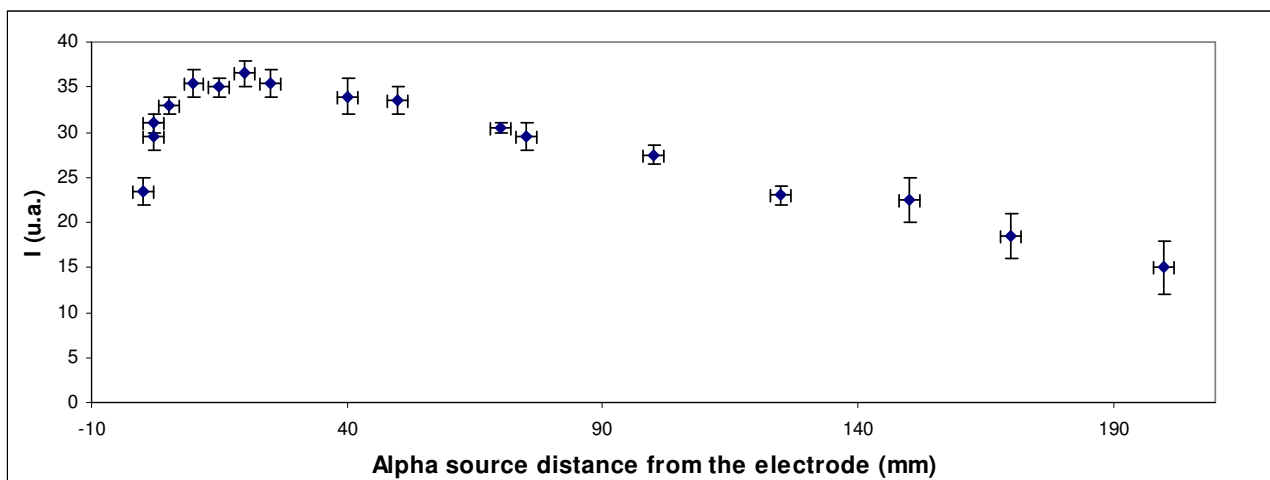
Figure 5.3 Ionization chamber scheme. It is shown a Radon chamber section

At the centre of the chamber it is placed an electrode consisting in a wire 1 mm thick that occupy a negligible volume respect to the whole chamber. Thus, the entire volume of the Radon Chamber can be considered the active volume of a ionization chamber (fig 5.3)

This electrode is positively polarized, so than it can collect the negative ions and/or the electrons produced by radon and its progeny radiations in the chamber.

To test this monitoring system, a series of measurements as been carried out, starting with the study of the response of the instrument to alpha particles of ^{241}Am point source moved around in the chamber.. This kind of measurements was able to confirm the goodness of this approach.

The first results were obtained by varying the source distances from the electrode (fig 5.4)

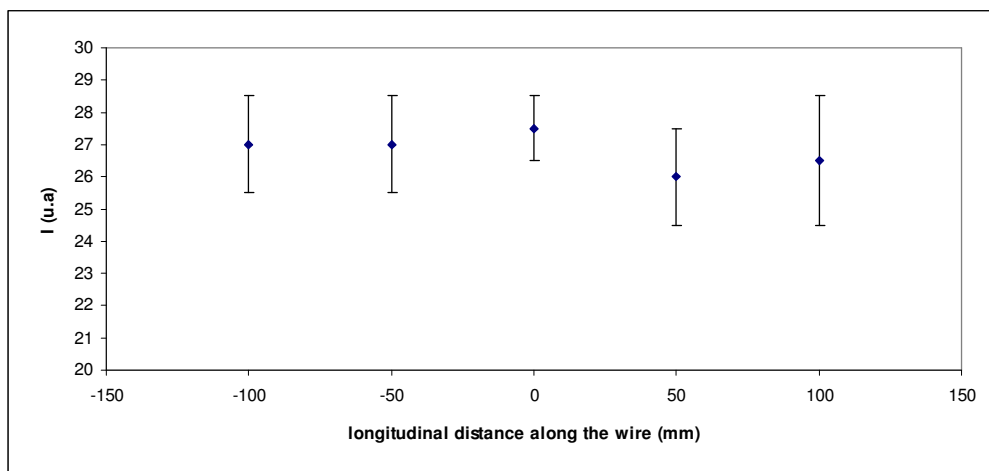


Figure(5.4) Ionization current produced by a point alpha source *versus* source - electrode distance.

We note that the ionization current initially increases in the region near the electrode and then, after reaching a maximum at distance of about 30 mm, slowly decrease at higher distances up to the chamber wall. This trend can be explained in the following way:

- 1) the behaviour near the wire can depend on the space charge effect due to the dense ionization in the nearness of the positive electrode whose net effect is the screening of the nominal potential. Thus the collection of electrons and negative ions is reduced by the reduction of the electrostatic field.
- 2) The slow decrease at higher distances from the wire is due to the recombination mechanism and to the electron attachment from electronegative gases (as oxygen) that can act effectively because the collection times are lower at higher distances.

To demonstrate that the edge effects are negligible, and that the electric field depends mainly on the radial distance, we made a set of measures varying the distance of the alpha sources along the wire, i.e. moving the source in the longitudinal direction respect to the wire (Fig 5.5)



Figure(5.5) Ionization current produced by a point alpha source *versus* distance along the wire. Zero distance is set at the middle of the wire.

The experimental results, within their uncertainties, confirm that the edge effect of the electric field generated around the wire is negligible. So the ratio between the measured current and activity of the source depends on the efficiency of the monitor. This has been measured introducing in the chamber a known activity of radon. The response of the wire has been tested to different polarization values and results are shown ion figure (5.6).

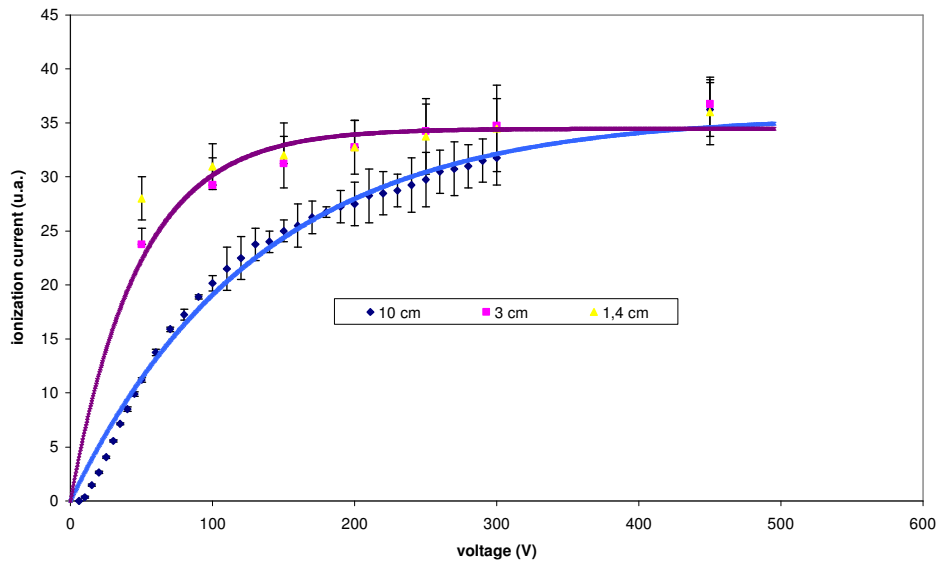


Figure 5.6 The voltage plateau at two different distances of the alpha sources from the wire

The behaviour of the wire current is well described by the well known ionization chamber characteristic in the Townsend region until the plateau is reached (Knoll, 1989). It can be noted, as expected, that the plateau is reached earlier when the source is closer to the wire.

A set of measures was carried out to study the response of the system at different radon activity concentrations. In the studied range (10 – 450 Bq) the response results adequately linear with the radon activity (fig 5.7)

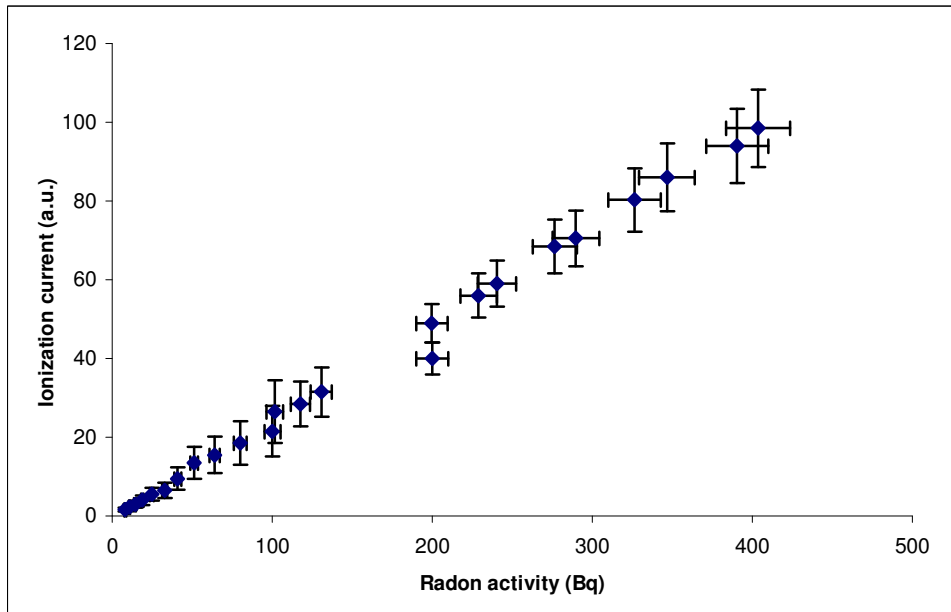


Figure 5.7 Ionization chamber as radon monitor: The ionization current has a linear trend *versus* radon activity concentration

5.2.2. Electrostatic ion collection

For radon monitoring inside our Radon Chamber it was also realized a device, which consists on miniaturized electrostatic collection detector. At the centre of one flange of the chamber was mounted a charged particles silicon detector , placed at the centre of semi-spherical metallic grid. The grid was set to high voltage to allow to charged radon progeny collection on the silicon detector surface. The connectors for the silicon power supply and for the grid polarization, passed through the flange and the sealing was guaranteed by two O-ring placed between the flange and the connectors. A scheme of the apparatus is shown *in figure. (5.8)* .while the figure(5.9) shows a typical alpha spectrum of Ramonino, that has the same characteristic of that of Ramona, but a smaller efficiency due to its reduced sampling volume

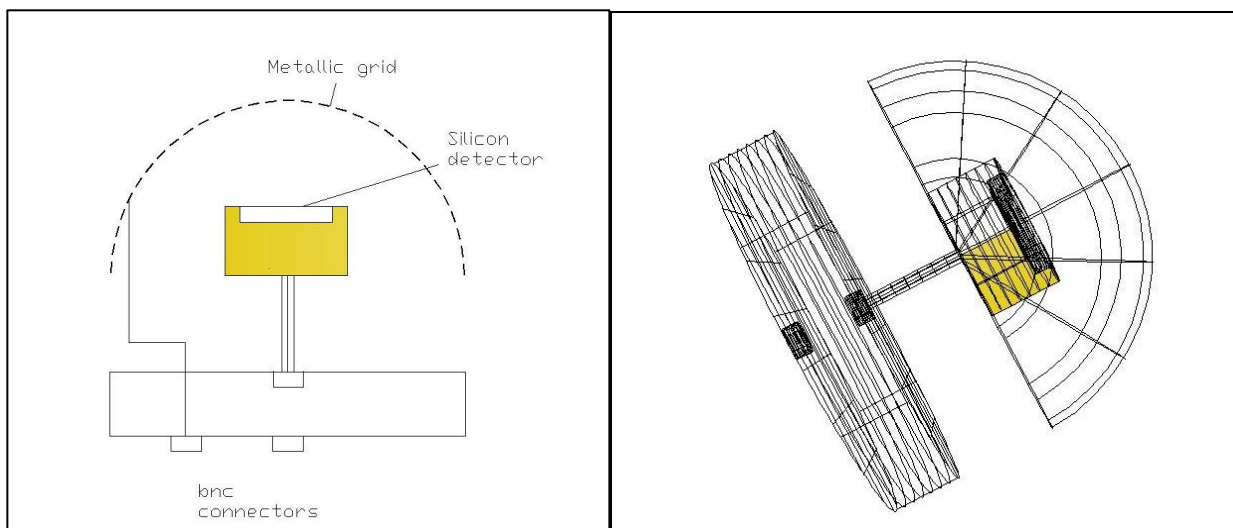


Figure5.8 Scheme of Ramonino detector in section (in the left) and in 3D view (in the right)

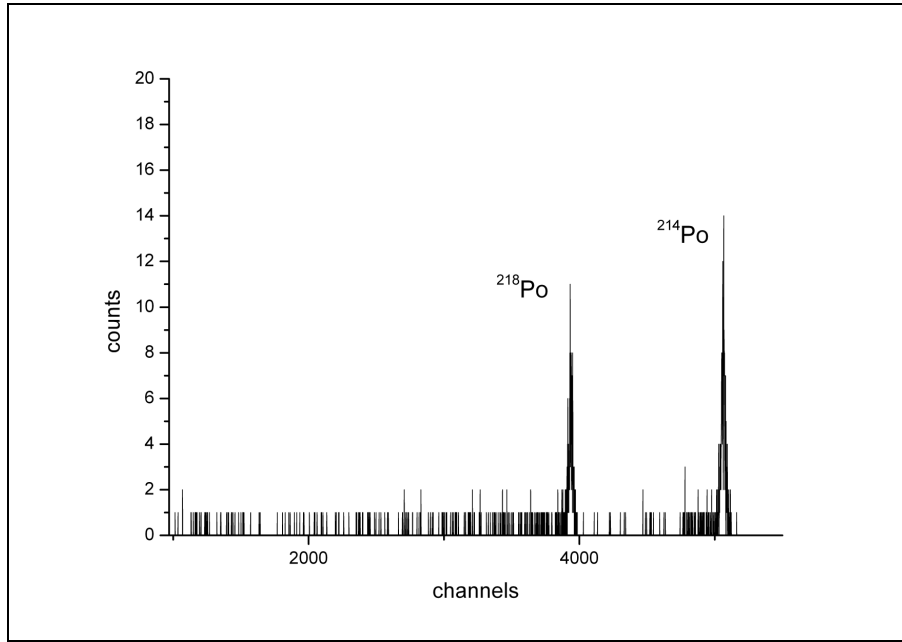


Figure5.9:Ramonino alpha spectrum

As for Ramona, test was carried out for optimizing the radon charged fraction collection. The grid was placed at different voltages to choose the optimal operation value. As expected, the collection efficiency goes up linearly with the polarization voltage. Values higher than 1.5 kV produce a lot of sparks inside the chamber, due to low air dielectric rigidity and little distance between grid and detector case (≈ 1 cm) To avoid detector damage, we retain the best choice the voltage setting at 1 kV. At this value we carried out a series of test measurements.

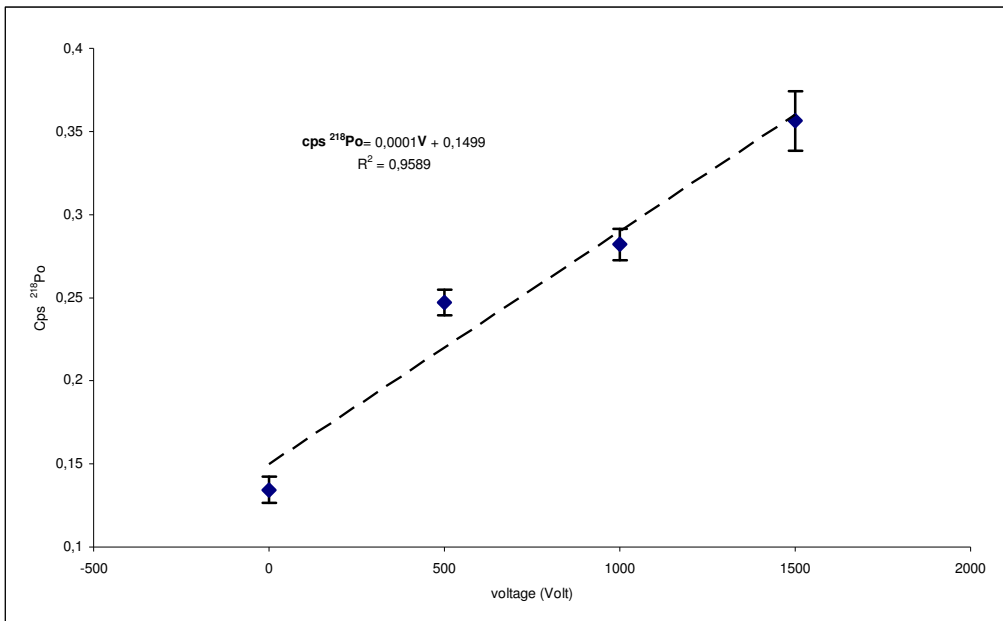


Figure5.10: 218Po counting rate versus grid voltage

To study the detector response, the Radon Chamber was filled with different radon activity, ranging from 500 to 3000 Bq. To analyze spectrum with good statistic 2 hours spectra were collected. As it is shown in the figure 5.11, the linearity of the detector response is quite good ($R = 0,99$) in the observed activity range.

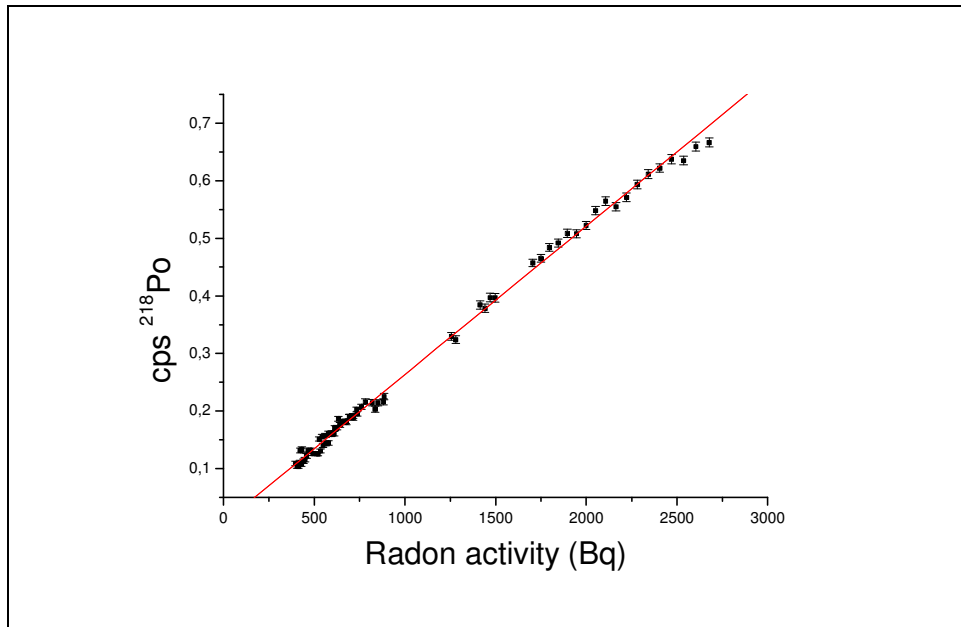


Figure 5.11 ^{218}Po counting rate *versus* radon activity concentration

The calculated efficiency is $eff = (2,6 \pm 0,1) 10^{-4} \left(\frac{\text{cps}^{218}\text{Po}}{\text{Bq}} \right)$

This monitor is useful also to find eventual radon leakages . In fact, s it is shown in figure 5.12 there is a negligible leakage during the measurements.

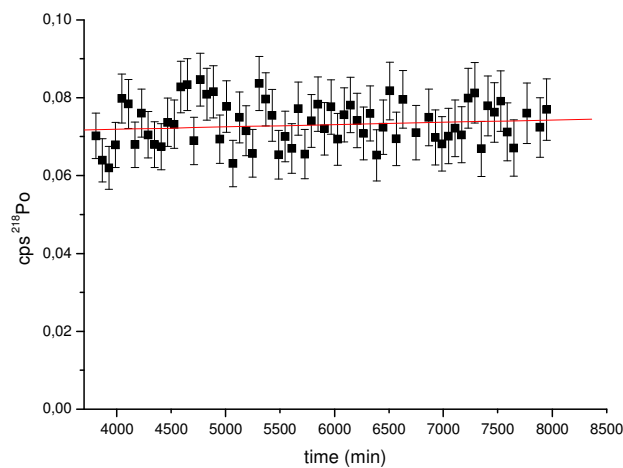


Figure 5.12 Ramonino has a good probe for testing radon leakage

5.2.3 Passive detector exposure

The exposure chamber has been tested with a group of passive detectors to observe the homogeneity of radon distribution on the volume and to determine their calibration factors. From the known activity concentration, that is monitored by one of the previously described probes, it is possible to determine the detector efficiency; the readings of the single detectors, placed in different positions inside the chamber, will allow to test the exposure uniformity. For testing the homogeneity of the exposure, electrets and SSNTD detectors (Ir-115 films) have been used.

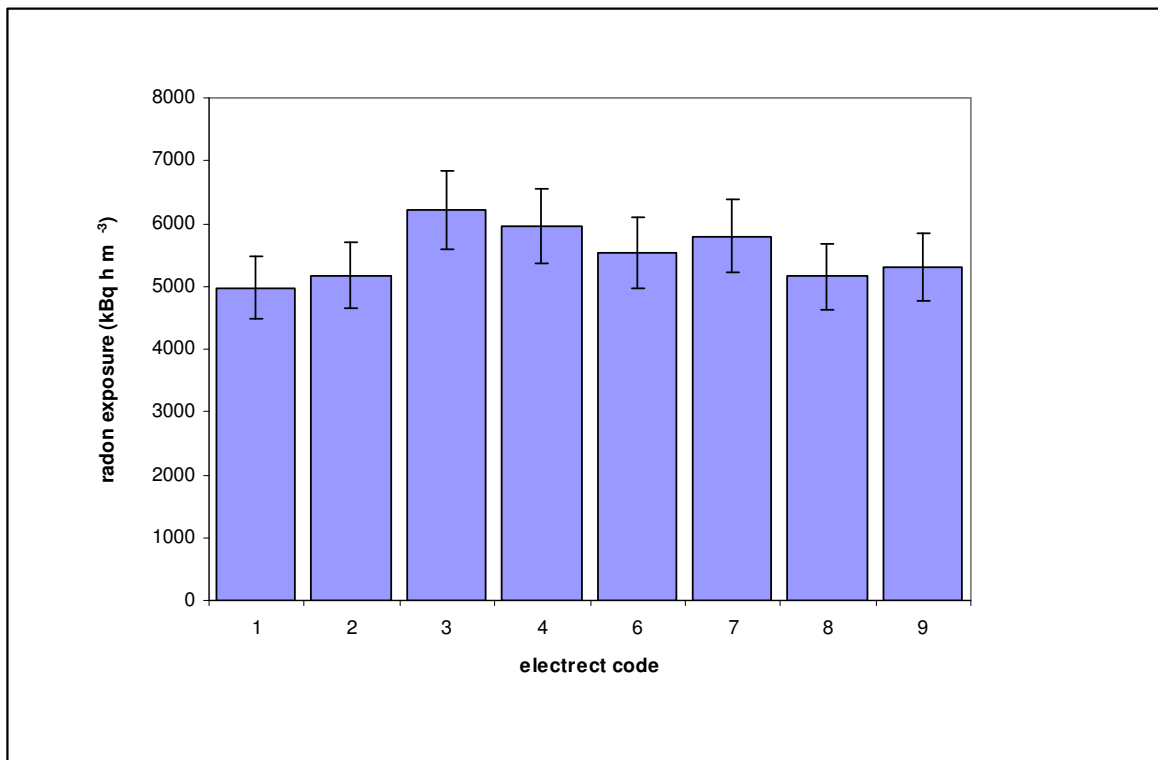


Figure 5.13 Electrets exposure inside our Radon chamber. The measures are comparable with each other (CL 95%)

In fig (5.13) results of measurements performed using electrets are showed. This kind of detectors presents a typical uncertainty (1σ) of 5%. All the measurements are comparable with each other within 2σ standard errors (confidence level of 95%), indicated in the fig. 5.13 as error bars.

The same kind of measurements have been done with SSNTD detectors, which where exposed in air condition with different radon concentrations. The detectors responses were compared with each other and with a set of background measurements.

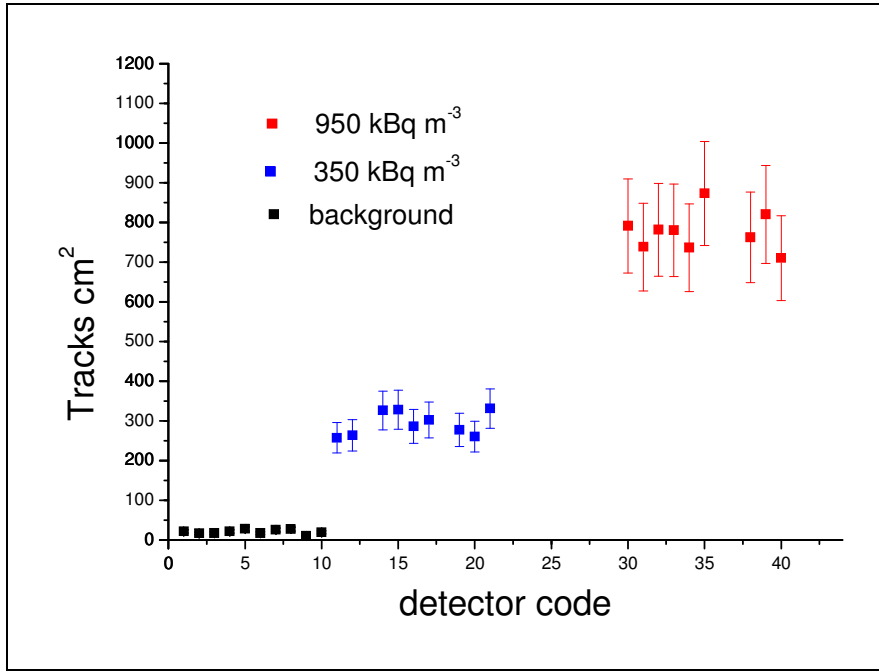


Fig 5.14 Study of radon distribution in the RC using Lr15 films. Track density is reported per each detector.

The figure(5.14) shows that the three groups does not intersect to each other, so that it possible to discriminate the different exposures. Moreover, it can be shown that for each set of detectors, the tracks detected are not dependent on the position inside the chamber (Fig 5.15). This is a check of the uniform radon distribution inside the chamber.

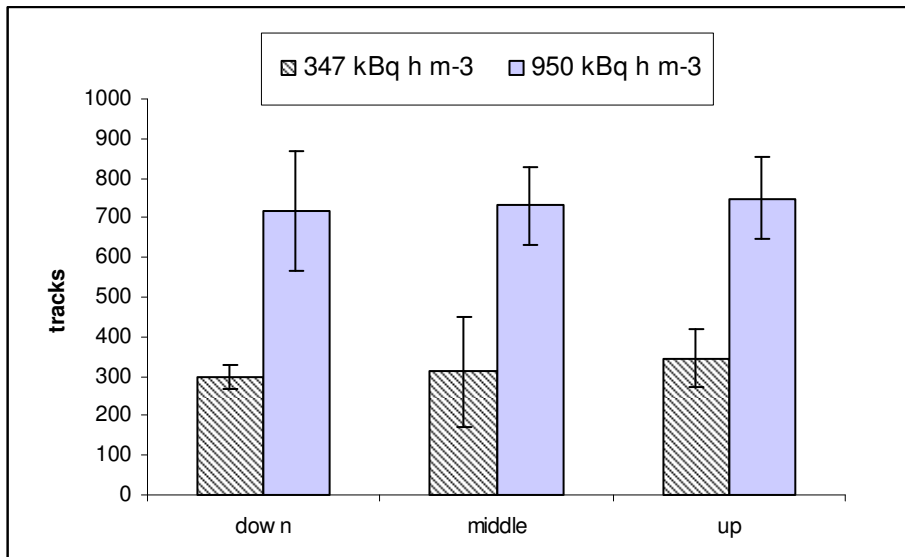


Fig 5.15 Radon measurements carried out at different exposures and positions inside the Radon Chamber. For each position the average of a set of measurements is indicated

The efficiency of the detectors, has been calculated by the formula:

$$Efficiency = \frac{Tracks}{Exposure} \quad (\text{tracks Bq}^{-1} \text{ h}^{-1} \text{ m}^3) \quad (5.1)$$

In figure 5.16 are indicate the efficiencies estimated at different exposure conditions. The difference between the mean of the two experimental distributions is statistically significant ($p < 0.007$, two tail t-test).

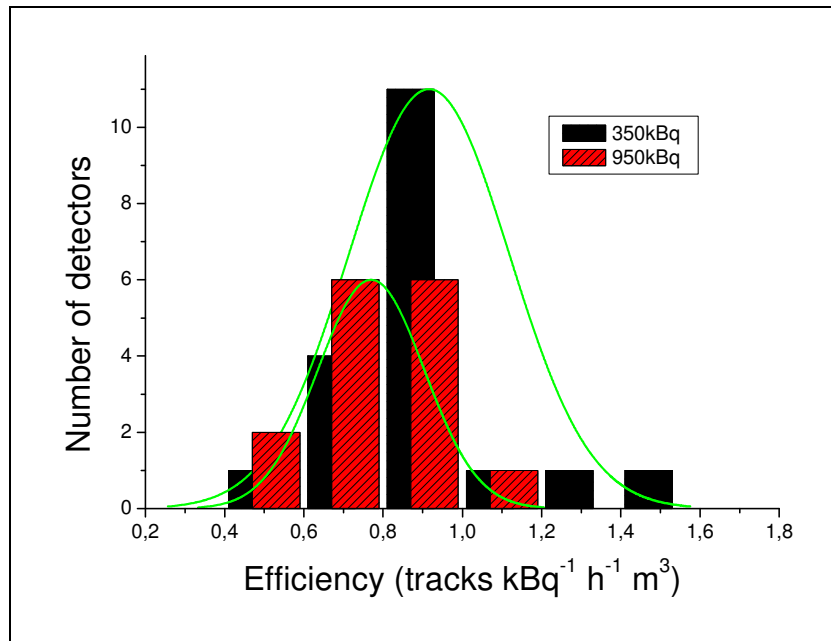


Fig 5.16 experimental distribution of detectors efficiencies at different exposure conditions.

Probably, this discrepancy can be attributed to the procedure used for the reading of this type of detectors, that needs more accuracy to reduce the uncertainties associated to each step of their measurements (table 2, chapter 1). Further investigation needs to be done on these type of detectors and the calibration facility will be used to carried out other measurements at controlled reference radon atmospheres. Finally, our preliminary measurements are enough satisfactory. Our exposure chamber can be used to measure the efficiency of passive detectors, being acceptable the homogeneity of the radon concentration inside the chamber. Further studies will be necessary to improve the efficiencies of the active radon probes inside the Radon Chamber, even if the reliability of these instruments is quite good. Attention has to be paid about the “intrinsic” uncertainties of some passive detectors, i.e. to the anomalous width of some measurements distributions carried out at the same exposure conditions.

Radon Chamber studies: perspectives

The possibility to vary and control the air conditions inside the chamber makes the system reliable to study radon and its daughter behaviour and to verify theoretical models designed to describe it.

Up to now radon facility was used as a tool for the characterization of electrostatic monitor and as exposure radon chamber. But instead of radon, its progeny concentration are the responsible of the health hazard from their inhalation. In fact, for a correct assessment of radon effective dose, it needs to measure radon progeny concentrations, often expressed as equilibrium factor. (1.1). Our apparatus can be also used to estimate the equilibrium factor F and its dependence on environmental parameters. The F factor in radon chamber can be monitored using active grab sample techniques. As indicated in fig 5.1, our exposure chamber is equipped with a series of flanges, some of them can be used as seats for filter where radon progeny can be collected on. The progeny activity deposited on these filters can be detected using alpha or gamma spectrometry techniques and can be related to the F factor if the radon concentration inside the Radon Chamber is known.

With our apparatus we can carry out experiments to study how the F factor is influenced by different air conditions and aerosol concentration. Indeed, we can also vary the aerosol concentration inside the Chamber, using a set of micrometric filters placed in correspondence of the radon inlet, and measure its distribution with a aerosol meter.

Moreover, we can also test the new methods for determining mean integrating F factor (Yu, 2005) using nuclear tracks detectors. This parameter is of crucial importance in the fields of radon dosimetry and epidemiology, because it allows to evaluate a mean radon progeny concentration, more directly related to the dose respect to the mean radon concentration.

Conclusions

Radon measurements are carried out worldwide in many scientific fields and are very important for the evaluation of the health risk due to radon and its progeny inhalation. It is important that this kind of measurements was carried out with accuracy and that their reliability is assured by well defined calibration procedures.

In this framework, we developed a facility that allows to calibrate the most commonly used radon detectors. It consists of an exposure chamber (Radon Chamber), of a radon reference monitor, and of an apparatus suitable for the radon circulation and that provides also for the air conditioning and control within the system. A well defined metrological radon chain allows to refer our radon measurements to a radon standard certified by the National Metrological Institute.

The continuous measurement of radon concentration inside the exposure volume is assured by a device based on the electrostatic collection of the ionized radon progeny on a silicon detector (Ramona). This instrument, also designed and tested in our laboratory, can be used not only as radon probe, but also as powerful tool to study some aspects of radon behaviour. In particular, it helps us to study how the processes involved in the neutralization of the ^{218}Po ions are influenced by humidity and how the electrical mobility of these ions depends on the air temperature. To find out these kind of dependencies we use both an experimental and a numerical approach. The comparison between measured and calculated data allows us to infer that: i) the electrical mobility increases linearly as temperature decreases, at least in the range 15-35°C; ii) the neutralization rate increases as the humidity square root, at least up to 50% RH. Instead the barometric pressure has a negligible influence on the monitor response in the range 900-1100 mbar. The characterization will be completed with the study of the interdependence between the various parameters involved in the Radon daughters transport and the influence on the efficiency of radon activity concentration.

As it has been showed in the description of the whole facility, Ramona will be the external monitor of the radon concentration inside Radon Chamber. In our work two different internal monitors have been tested, which common characteristic is the little dimension and therefore a negligible influence on the chamber volume. Each of them showed a linear response versus radon concentration, that makes feasible their use as radon probes.

The features of the facility described in this work make it a suitable tool to study some problems typical of this field of interest, as for instance the study of the air condition influence on the radon progeny concentration, and consequently on the equilibrium factor.

References

UNSCEAR (United Nations Scientific Committee on the Effects of Atomic Radiation), 2000. Sources and effects of ionizing radiation. 2000 Report to the General Assembly, with Annexes. United Nations, New York.

Decreto Legislativo 26 maggio 2000, n. 241 “Attuazione della direttiva 96/29/Euratom in materia di protezione sanitaria della popolazione e dei lavoratori contro i rischi derivanti dalle radiazioni ionizzanti”. Gazzetta Ufficiale n. 203 Suppl. Ordinario, 31 agosto 2000

J. Porstendorfer, P. Pagelkopf, M. Grundel, 2005. Fraction of the positive ^{218}Po and ^{214}Pb clusters in indoor air. Radiation Protection Dosimetry, 113, No.3, 342-351

ICRP Publication 50 (1987). Lung Cancer Risk from Indoor Exposures to Radon Daughters, vol 17, No.1

ICRP Publication 65 (1993). Protection Against Radon-222 at Home and at Work, Vol 23 no.2

V. A. Nikolaev, R. Ilic, Etched track radiometers in radon measurements: a review. Radiation Measurements 30 (1999) 1-13

F. Bochicchio, 2005. Radon epidemiology and nuclear track detectors: Methods, results and perspectives. Radiation Measurements 40, 177-190

D. Azimi-Garakani, B. Flores, S. Piermattei, A.F. Susanna, J.L Seidel, L. Tommasino, G. Torri, (1988). Radon gas sampler for indoor and soil measurements and its applications. Radiation Protection Dosimetry 24, 269-272

P. Kotrappa, J.C. Dempsey, R. W. Ramsey, L. R. Stieff (1990). A practical E-PERM (Electret passive environmental radon monitor) system for indoor ^{222}Rn measurement. Health Physics 58, 461-467

H. F. Lucas, 1957. Improved low-level alpha scintillation counter for radon. *Review of Scientific Instruments* 28, 68

M. Urban, J. Schmitz, 1993. Radon and radon daughters metrology: basic aspects. *Proceedings of the Fifth International Symposium on the Natural Radiation Environment*, 153-183.

EUROMET, 2005. Comparison of calibration facilities for radon activity concentration. Euromet Project 657, Final Report-2005-02-01.

Busigin A., Van Der Vooren A. W., Babcock J. C. and Phillips C. R. (1981). The nature of unattached RaA(²¹⁸Po) particles. *Health Phys.*, 40, pp. 333-343.

Chu K. D. and Hopke P. K. (1988). Neutralization kinetics for Polonium-218. *Environmental Science and Technology*, 22, pp. 711-717.

Shi B. and Hopke P. K. (1991). Study of neutralization of ²¹⁸Po ions by small ion recombination in O₂, Ar and N₂. *Health Physics*, 61, pp. 209-214

George A. C. and Breslin A. J. (1977). Measurements of environmental radon with integrating instruments. Atomic Industrial Forum Uranium Mill Monitoring Workshop, Albuquerque, New Mexico.

Goldstein S. D. and Hopke P. K. (1985). Environmental neutralisation of polonium-218. *Environmental Science and Technology*, 19, pp. 146-150. 147

Phillips C. R., Khan A. and Leung H. M. Y. (1988). The nature and determination of the unattached fraction of radon and thoron progeny. in: *Radon and its decay products in indoor air*, eds. Nazaroff W. W and Nero A. V., John Wiley & Sons, pp. 203-256

Dankelmann V., Reineking A., Porstendorfer J. (2001). Determination of neutralisation rates of ²¹⁸Po ions in air. *Radiation Protection Dosimetry* 94, No.4, 353-357

Hopke P.K (1989). Use of the electrostatic collection of ²¹⁸Po for measuring Rn. *Health Physics* 57, 39-42.

Howard, A.J., Carroll E., Strange W.P (1991) A simple system for radon-in-air concentration determinations. *American Journal of Physics*. 59(6)

Leung H. M. Y, Phillips C.R. (1987). The electrical and diffusive properties of unattached ^{218}Po in argon gas. *Radiation Protection Dosimetry*, 18, 3-11

Chanin L.M, Biondi M.A (1957). Temperature Dependence of Ion Mobility in Helium, Neon, and Argon. *Physical Review*, 106, 473-479

De Felice P., Myteberi Xh., (1996). The ^{222}Rn reference measurements system developed at ENEA. *Nucl. Instr and Methods A* 369, 445-451

Piccolo J L (1996) Absolute measurement of radon 222 activity *Nucl. Instrum. Methods Phys. Res. A* 369 452–7

Spring P, Nedjadi Y, Bailat C, Triscone G and Bochud F (2006) Absolute activity measurement of radon gas at IRA-METAS *Nucl. Instrum. Methods Phys. Res. A* 568 752–9

Evans, 1935. Ionization Current Produced by Radon, RaA and RaC' in Cylindrical Ionization Chambers. *Physical Review*, 48, 177-186

G. Curzio, D. Mazed_, R. Ciolini, A. Del Gratta, A. Gentili (2005). Effect of air on gas amplification characteristics in argon propane (1%)-based proportional counters for airborne radon monitoring, *Nuclear Instruments and Methods in Physics Research A* 537 (2005) 672–682

Knoll G (1989). *Radiation detection and measurements*, John Wiley and Sons.

Yu, K.N., Nikezic D., Ng F.M.F, Leung J.K.C (2005) Long-Term measurements of radon progeny concentrations with solid-state nuclear track detectors, *Radiation Measurements* 40, 560-568